uOttawa

L'Université canadienne
Canada's university

FACULTÉ DES ÉTUDES SUPÉRIEURES ET POSTOCTORALES

uOttawa

L'Université canadienne
Canada's university

FACULTY OF GRADUATE AND POSDOCTORAL STUDIES

Madlena Rabaev
AUTEUR DE LA THÈSE / AUTHOR OF THESIS

M.Sc. (Chemistry)
GRADE / DEGREE

Department of Chemistry
FACULTÉ, ÉCOLE, DÉPARTEMENT / FACULTY, SCHOOL, DEPARTMENT

Unimolecular Dissociations of Ionized Azo-tert-butane and Acetone azine

TITRE DE LA THÈSE / TITLE OF THESIS

P. Mayer
DIRECTEUR (DIRECTRICE) DE LA THÈSE / THESIS SUPERVISOR

CO-DIRECTEUR (CO-DIRECTRICE) DE LA THÈSE / THESIS CO-SUPERVISOR

EXAMINATEURS (EXAMINATRICES) DE LA THÈSE / THESIS EXAMINERS

D. Bryce

R. Burk

Gary W. Slater
Le Doyen de la Faculté des études supérieures et postdoctorales / Dean of the Faculty of Graduate and Postdoctoral Studies

Unimolecular Dissociations of Ionized Azo-tert-butane and Acetone azine

By

Madlena Rabaev

Thesis submitted to the

Faculty of Graduate and Postdoctoral Studies

In partial fulfillment of the requirements of

the degree of Master of Science

In the Ottawa-Carleton Chemistry Institute

Department of Chemistry, University of Ottawa

Ottawa, Ontario, Canada

September 2008

Candidate

Madlena Rabaev

Supervisor

Dr. Paul M. Mayer

Your file Votre référence
ISBN: 978-0-494-48623-8
Our file Notre référence
ISBN: 978-0-494-48623-8

I dedicate this thesis to all the people

who love and support me,

because without love you can not go on.

Abstract

This M.Sc. thesis presents an experimental and a theoretical study of azo-tert-butane and acetone azine ions which belong to the azo and azine class of compounds, respectively. The experimental study involves an investigation of the fragmentation reactions using tandem mass spectrometry and TPEPICO (threshold photoelectron photoion coincidence) spectroscopy. The theoretical study involves *ab initio* calculations of neutral and ionized azo-tert-butane, acetone azine and their dissociation products. RRKM theory was used to probe the nature of the unimolecular dissociations by comparing theoretical fits to TPEPICO breakdown curves.

Due to an impurity in the sample of acetone azine, only one dissociation channel was studied, namely, methyl radical loss. Contrary to the original hypothesis, that this unimolecular dissociation occurs by a simple bond cleavage reaction, it was found that a rearrangement process takes place.

The unimolecular dissociations of ionized azo-tert-butane that were investigated were formation of species corresponding to m/z 57, m/z 85 and m/z 56. Fragment ions m/z 57 and m/z 85 are competing channels, since their formation occurs by the same C-N bond cleavage. However, it was observed that formation of m/z 57 dominates over m/z 85 at higher internal energies. This observation was explained by the difference in the entropy of activation ($\Delta S^{\ddagger}$) for the two dissociation channels. Formation of m/z 56 is an isomerization reaction; due to its low significance, the mechanism of this reaction was not studied in depth.

Acknowledgments

First and foremost, I would like to express my gratitude to my supervisor, Dr. Paul M. Mayer, for his guidance, support, and patience which make him a truly unique Professor. A student's performance and success is highly dependant on the supervisor's input. Dr. Paul M. Mayer has all the great qualities which made this graduate experience successful and memorable. I enjoyed working on this project and am grateful for having this wonderful opportunity to work with him.

Special thanks to Anne-Marie Boulanger, a former Ph.D. graduate student who welcomed me to the research group, guided me in the first six months of my Masters degree and helped immensely with the theoretical work. She also gathered experimental data used in this thesis work, which made it possible for me to graduate faster than expected.

Words can not describe my gratitude towards all the past and present members of the lab group: Clement Poon, Yawei Lin, Abdul Alhazmi, Anne-Marie Boulanger, Justin Renaud and Brandon Ferrier. We have created together a fun, inviting and warm atmosphere to work in. We laughed, talked, supported each other and created wonderful memories that I am so grateful for. I am truly lucky for having such an amazing lab group, without them this would be a forgettable experience.

I would also like to thank the following three Professors: Dr. John Holmes, Clem Kazakoff and Dr. Tom Woo for creating and conducting great courses, namely, gas phase ion chemistry, introduction to analytical mass spectrometry and introduction to computational chemistry. I have learned a lot of interesting and useful information which I have implemented in my research in one way or another.

Thanks to Dr. Sander Mommers for all his computer and technical help and for sponsoring Trent conference. His wonderful taste in music and food has made those conferences more enjoyable.

Thanks to my family for their constant support and care. Thanks to Dr. D.K. Bohme (supervisor for fourth year Honours project) for helping me select the right supervisor. Finally, thanks to Dr. Yu for his generous scholarship for graduate students with financial need, which I have received.

Table of Contents

List of Figures

List of Tables

List of Abbreviations

AA	Acetone azine
AE	Appearance Energy
ATB	Azo-tert-butane
B3LYP	Becke 3-parameter Lee-Yang-Parr method
B3PW91	Becke 3-parameter Perdew-Wang method (1991)
BHandHLYP	Becke–half and half–Lee–Yang–Parr method
C1	Cell 1
C2	Cell 2
C3	Cell 3
C4	Cell 4
CC	Coupled Cluster
CGF	Contracted Gaussian Function
CI	Chemical Ionization or Configuration Interaction
CID	Collision Induced Dissociation
CIDI	Collision Induced Dissociative Ionization
DE	Deflector Electrode
DFT	Density Functional Theory
DMH	Dimethylhydrazine
EI	Electron Ionization
ESA	Electrostatic Analyzer

ESI	Electro-Spray Ionization
FAB	Fast Atom Bombardment
FFR	Field Free Region
FWHM	Full Width Half Maximum
G1	Gaussian-1 theory
G2	Gaussian-2 theory
G3	Gaussian-3 theory
G4	Gaussian-4 theory
GC	Gas chromatography
GTO	Gaussian Type Orbital
HF	Hartree Fock
HOMO	Highest Occupied Molecular Orbital
ICP	Inductively Coupled Plasma
$I.E._a$	Adiabatic Ionization Energy
$I.E._v$	Vertical Ionization Energy
K.E.	Kinetic Energy
L.C.A.O.	Linear Combination of Atomic Orbitals
MALDI	Matrix Assisted Laser Desorption Ionization
MH	Methylhydrazine
MI	Metastable Ion
MIKES	Mass Analyzed Kinetic Energy Spectrometry
M.O.	Molecular Orbital
MP	Moller Plesset

MW	Molecular Weight
NIST	National Institute of Standard and Technology
P.E.	Potential Energy
PES	Photoelectron Spectrum or Potential Energy Surface
PI	Photoionization
ROVGF	Restricted Outer Valence Green's Function
RRKM	Rice-Ramsperger-Kassel-Marcus theory
RT	Room Temperature
STO	Slater Type Orbital
SP	Single Point
TMH	Tetramethylhydrazine
TOF	Time Of Flight
TPEPICO	Threshold Photoelectron Photoion Coincidence
TPES	Threshold Photoelectron Spectrum
TS	Transition State
UV	Ultra Violet
VTST	Variational Transition State Theory
ZPE	Zero Point Energy
E_0	Activation Energy
E_{xc}	Exchange-correlation functional
m/z	Mass-to-charge ratio
$\Delta S^{\ddagger}$	Entropy of activation
ΔH_f	Enthalpy of formation

Chapter 1

Introduction

Summary

This thesis presents the investigation of the unimolecular dissociations of ionized azo-tert-butane and acetone azine (Figure 1.1) which is part of a larger project that involves studying the fragmentation of N_2 containing ions. The fragmentation was studied by two experimental techniques: threshold photoelectron photoion coincidence (TPEPICO) spectroscopy and tandem mass spectrometry. Rice-Ramsperger-Kassel-Marcus (RRKM) theory was used to model the kinetics of the ions dissociating and produce theoretical fits to the breakdown curves generated from threshold photoelectron photoion coincidence (TPEPICO) spectroscopy data. Ab initio computational methods were used to deduce stable structures and energies of each ion and their corresponding fragmentation products. The entropy of activation ($\Delta S^{\ddagger}$) and activation energy (E_0) extracted from the fits were combined with the experimental and computational results to form the final conclusions.

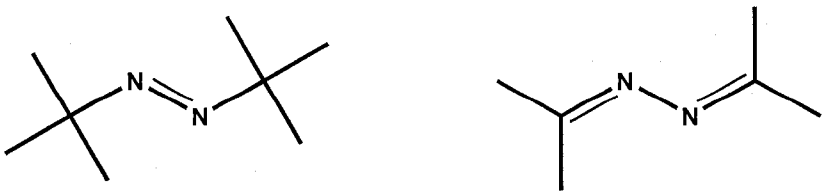

1 **2**

Figure 1.1. General unoptimized structures of azo-tert-butane (1) and acetone azine (2).

1.1 Introduction

Understanding the dissociation of ions under various conditions in the gas phase is of fundamental importance. Mass spectrometry allows one to study the nature of fragmentation reactions at the molecular level. Coupled with a theoretical study, important physico-chemical properties can be extracted. Consequently, these calculations give insight to the dissociation channels occurring in the gas phase that would have otherwise be undetermined.

1.2 Background on N_2 containing molecules

N_2 containing molecules fall into several classes of compounds, such as azines, azo, hydrazines, and hydrazones, Figure 1.2. Each class of compounds has unique properties and different applications. Azines have an interesting structural property, conjugation between C-N and N-N bonds that allows them to act as photoreceptors [1-2]. This property is enhanced when the R groups are phenyl rings. Azo compounds can be similar in structure to azines (depending on the R group) that also have conjugation effects that allow for electron delocalization [3]. They are used as dyes and pigments which may lead to surface and ground water contamination in close proximity to their production [3]. Hydrazines are highly reactive compounds that are used as rocket propellants, fuels, chemical reactants and in boiler water treatments [4]. The hydrazines that are used as rocket propellants and fuels are toxic substances that may leak and evaporate to the atmosphere causing further environmental problems or present a risk to ground and space workers [5]. The biological properties that have recently been discovered in hydrazones present them as potential drug candidates [6]. Also, their nucleophilic nature

(depending on the R groups) enables them to take part in various organic reactions, such as formylation and cyanation [7]. All four classes of compounds (Figure 1.2) have interesting properties that make them applicable in optical materials, textile dyeing, combustion, pharmacokinetics and organic synthesis. Therefore it is worthwhile studying them, as new insights can be gained on their chemical and physical nature.

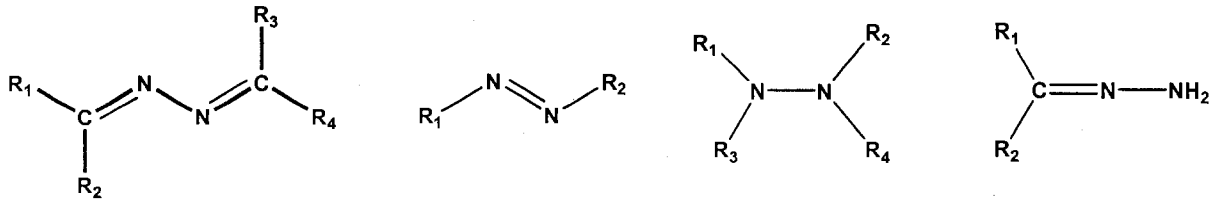

1 2 3 4

Figure 1.2. General structures of four class of compounds: azine (1), azo (2), hydrazine (3) and hydrazone (4).

1.3 Past projects

The larger project that involves studying the fragmentation of N_2 containing ions started with a former Ph.D. graduate student, Anne-Marie Boulanger. The research work comprised of examining the fragmentation of hydrazine molecules, namely, methylhydrazine (MH), 1,1-dimethylhydrazine (DMH) and tetramethylhydrazine (TMH), Figure 1.3 [8]. It is evident from the figure, that the size of the hydrazine molecules is smaller than azo-tert-butane and acetone azine, Figure 1.1. Azo-tert-butane and acetone azine represent the next step up in molecular size from the three hydrazines. A.M. Boulanger has investigated these hydrazine molecules experimentally through tandem mass spectrometry (EI coupled to a three sector mass analyzer) and TPEPICO spectroscopy and theoretically using variational transition state theory (VTST) and *ab initio* calculations. VTST proved to be a suitable theory for fitting the experimental

breakdown curves for the dissociation channels of the three hydrazine molecules. Consequently, activation energies (E_0) and entropies of activation ($\Delta S^{\ddagger}$) have been determined for each dissociation channel studied. *Ab initio* calculations coupled to VTST and the experimental results helped to form an overall picture of the fragmentation reactions for the three hydrazine molecules, including gas phase structures and energetics.

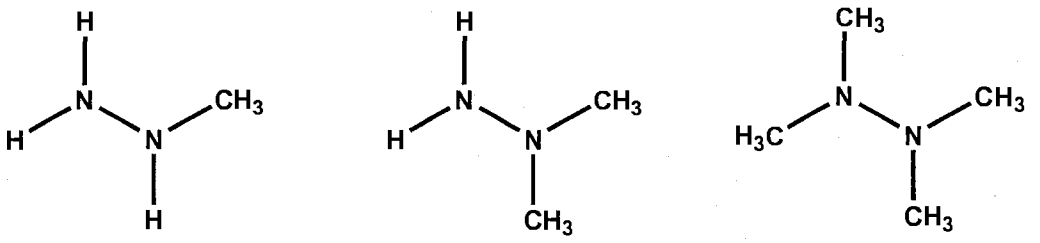

MH **DMH** **TMH**

Figure 1.3. General structures of methylhydrazine (left), 1,1-dimethylhydrazine (middle) and tetramethylhydrazine (right).

A major conclusion derived from Anne-Marie's thesis work was that the entropy of activation ($\Delta S^{\ddagger}$) has a significant effect on the dissociation reactions. VTST allowed her to locate up to ten transition states for the methyl radical loss from MH, DMH and TMH. Each transition state corresponds to a range of internal energy, entropy of activation value and a specific bond length leading to methyl loss (N-C bond cleavage). For each value of R (N-C bond length), the $\Delta S^{\ddagger}$ value for TMH was found to be higher than for MH and DMH. As one of the methyl groups starts to seperate, the rotation of the other three methyl groups become less hindered.

The VTST fits also allowed for deriving thermochemical data for the fragment ions that were studied. The activation energy (E_0) values obtained from the fits were applied in

calculating enthalpies of formation for various ions. They were then compared to enthalpies of formation derived from G3 calculations and a good agreement between the two was found.

1.4 Applications of Azo-tert-butane and Acetone azine

Azo-tert-butane (ATB) is widely used in different applications and therefore it is valuable to understand its various dissociation channels. Azo-tert-butane is used in the formation of silicon containing organic films which have a wide range of applications, from microelectronics to biosensing [9]. The reaction between ATB and the Si layer occurs through the azo (N=N) group and may involve fragmentation upon high temperatures. ATB is also used as a free radical initiator in the formation of polymers (e.g. poly(vinylidene fluoride)) and immobilization of gas chromatography columns [10-12]. In the case of polymerization, ATB generates tert-butyl radicals upon loss of N_2 which occurs under high temperatures (160 ^{o}C) [12].

Acetone azine (AA), in particular, does not have direct applications but rather indirect. For example, it is used in the determination of hydrazine in water by gas chromatography (GC) [13]. Hydrazine, a well known compound used as rocket fuels is converted to AA prior to analysis in GC.

1.5 Goals

The goals of this thesis are

1. To derive accurate thermochemical (ΔH_f and $\Delta S^{\ddagger}$) information for ions and neutrals that result from the unimolecular dissociation of ionized azo-tert-butane and acetone azine.
2. To gain insight on the nature of gas phase fragmentations of N_2 containing molecules.

References

[1] R. Glaser, G.S. Chen, M. Anthamatten and C.L. Barnes, J. Chem. Soc. Perkin Trans. 2 1995, 7, 1449-1458.

[2] G.S. Chen, J.K. Wilbur, C.L. Barnes, R. Glaser, J. Chem. Soc. Perkin Trans 2 1995, 12, 2311-2317.

[3] T. Joshi, L. Iyengar, K. Singh, S. Garg, *Bioresour. Technol.* 2008, 99, 7115-7121.

[4] Agency for toxic substances & disease registry, Website: http://www.atsdr.cdc.gov/tfacts100.html

[5] D.F. Doerr, *Acta Astronaut.* 2001, 49, 463-468.

[6] P. Kovarikova, Z. Mrkvickova, J. Klimes, *J. Pharm. Biomed. Anal.* 2008, 47, 360-370.

[7] A. Ros, E. Diez, E. Marques-Lopez, E. Martin-Zamora, J. Vazquez, J. Iglesias-Sigueenza, R.R. Pappalardo, E. Alvarez, J.M. Lassaletta, R. Fernandez, *Tetrahedron: Asymmetry* 2008, 19, 998-1004.

[8] a) A.M. Boulanger, E.E. Rennie, D.M.P. Holland, D.A. Shaw, P.M. Mayer, *J. Phys. Chem. A* 2008, 112, 866-879.

b) A.M. Boulanger, E.E. Rennie, D.M.P. Holland, D.A. Shaw, P.M. Mayer, *J. Phys. Chem. A* 2007, 111, 5388-5398.

c) A.M. Boulanger, E.E. Rennie, D.M.P. Holland, D.A. Shaw, P.M. Mayer, *J. Phys. Chem. A* 2006, 110, 8563-8571.

[9] M.D. Ellison, J.S. Hovis, H. Liu, R.J. Hamers, *J. Phys. Chem B* 1998, 102, 8510-8518.

[10] Q. Tang, Y. Shen, N. Wu, M.L. Lee, *J. Microcolumn Sep.* 1999, 11, 415-420.

[11] R.C. Kong, S.M. Fields, W.P. Jackson, M.L. Lee, *J. Chromatogr.* 1984, 289, 105-116.

[12] J. Guiot, B. Ameduir, B. Boutevin, *Macromolecules* 2002, 35, 8694-8707.

[13] S. Selim, C.R. Warner, *J. Chromatogr.* 1978, 166, 507-511.

Chapter 2

Theoretical Concepts and Techniques

2.1 A Unimolecular process

A unimolecular process is defined as any species evolving as a consequence of an excitation step [1]. There are several ways in which a system can become excited; some examples are: photo-excitation, thermal-excitation, chemical-excitation and collision-excitation. The mechanism for each type varies but the overall reaction can be written in the following way:

$$A \rightarrow \text{Products} \qquad (2.1)$$

This corresponds to a decompostion reaction; however, at times an excitation can lead to a rearrangement reaction prior to dissociation.

To fully understand a unimolecular process, the rate constant (k), the internal energies and the structures of the initial system (A) and the products have to be calculated theoretically and/or measured experimentally. Several theories have been developed for the calculation of a rate constant (k), namely, Rice-Ramsperger-Kassel-Marcus (RRKM), transition state theory (TST) and variational transition state theory (VTST). RRKM is the theory employed in modeling the fragmentation of azo-tert-butane and acetone azine.

2.2 RRKM theory

2.2.1 Theory

RRKM theory was progressively developed over 25 years, starting in 1927 by Rice and Ramsperger, continued in 1928 by Kassel and ended in 1952 by Marcus [1]. In the first two years, Rice, Ramsperger and Kassel developed RRK theory which can be summarized by the following equation:

$$k(E) = \upsilon \left(\frac{E - E_o}{E} \right)^{s-1} \tag{2.2}$$

where k(E) is the rate constant as a function of internal energy, υ is the vibrational mode responsible for the dissociation, E is the internal energy, E_0 is the zero K activation energy and s is number of oscillators (vibrational modes).

Since the above equation failed to predict accurate dissociation rate constants, RRKM/QET (Rice-Ramsperger-Kassel-Marcus quasiequilibrium theory) equation was developed:

$$k(E) = \frac{\sigma N^{\ddagger}(E - E_o)}{h\ \rho(E)} \tag{2.3}$$

where $k(E)$ is the dissociation rate constant as a function of internal energy E, E_0 is the activation energy, σ is the reaction degeneracy, h is Planck's constant, $N^{\ddagger}(E\text{-}E_0)$ is the transition state sum of states from 0 to $E\text{-}E_0$ and $\rho(E)$ is the parent ion density of states. The definition of reaction degeneracy is vague and can have two interpretations: the # of possible ways to get from the reactants to the products or the # of the point group symmetry. For example, *n*-butane

($CH_3CH_2CH_2CH_3$) according to the first definition can lose a CH_3 radical in two ways, thus $\sigma=2$. But if the point group symmetry is C_1 then $\sigma=1$. The sum of states represents all the possible ways to arrange the internal energy of an ion among its vibrational modes [2]. An example of a state is (0, 0, 0, …. , 0), where all the oscillators are in their ground state. As the internal energy goes up some oscillators may be in excited states, e.g. (0, 0, 2, …. , 0) where the third oscillator is excited the second vibrational level. The density of states represents the number of states per energy interval (E to E + δE) [2]. For a reaction to take place, the transition state must be at a specific state in order to get to the products. In a highly dense system, there are more accessible states, so the internal energy has a higher probability of getting lost among the internal degrees of freedom and not find its way into the reaction coordinate than in a lower density system. In general, the sum and density of states increases with the energy. The sum of states is a unitless number while the density of states has a unit of E^{-1}.

So, while the sums and densities of states are used in RRKM theory, they can be difficult to conceptualize. Therefore, $\Delta S^{\ddagger}$ (entropy of activation) is introduced and is used as a parameter to further describe the nature of the reaction [2]. It is calculated by the following equation:

$$\Delta S^{\ddagger} = k_B \ln\left(\frac{\prod Q_{rv}^{\ddagger}}{\prod Q_{rv}}\right) + \frac{U^{\ddagger} - U}{T} \qquad (2.4)$$

where k_B is Boltzman's constant, Q_{rv} is the rotational-vibrational partition function, $U^{\ddagger}$ and U is the internal energy for the TS and ion, respectively. The partition function, Q_{rv} is simply the Laplace transform of the density of states [3]. Both parts of the partition function, namely, Q_r and Q_v are adjusted by varying the rotational constants and vibrational frequencies of a species. Entropy of activation values are usually reported at 600 K, so T = 600. Negative values of $\Delta S^{\ddagger}$

imply that the TS is more ordered than its parent ion and therefore is referred to as being "tight" [2]. A positive value of $\Delta S^{\ddagger}$ implies exactly the opposite, that the TS is less ordered and is thus called "loose". Tight and loose TS's tend to be characteristic of rearrangement reactions and simple bond cleavages, respectively.

2.2.2 The effect of internal energy on ion chemistry

The number of dissociation channels a molecular ion possesses does not depend solely on the size of the molecule but also on the internal energy content [4]. For example, if an ion has an internal energy of X then it can access dissociation channels A through C but not D and E, Figure 2.1. Fragmentation pathways D and E can only be accessible if the internal energy of the ion is at the minimum or above the required energy.

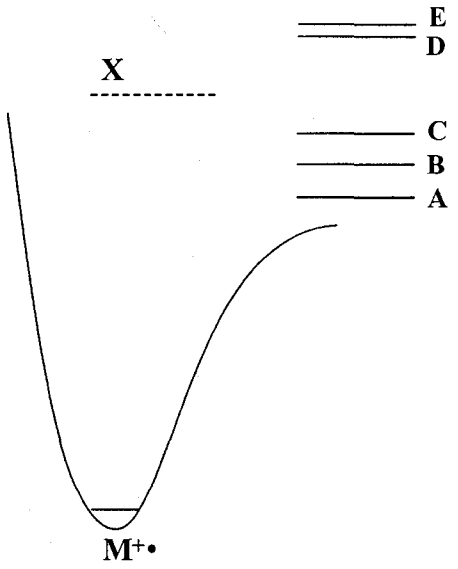

Figure 2.1. A typical PES surface diagram for a molecular ion with letters A to E representing the different dissociations channels it can undergo and their relative energies.

Furthermore, the percentage of ions dissociating through channels A, B and C does not occur randomly, but rather, is determined by the k(E) curves. Activation energy (E_0) and entropy of activation ($\Delta S^{\ddagger}$) are the two parameters that are varied (see Section 2.4.1) and consequently affect the rate constant k(E) as a function of internal energy [2]. Figure 2.2. clearly illustrates how a k(E) curve changes with $\Delta S^{\ddagger}$ and E_0, that is with each fragmentation channel (A, B and C). Moreover, the internal energy window being observed also affects the appearance of the k(E) curves. In internal energy window 1, channel C appears to have the highest rate constant while channel A has the lowest, Figure 2.2. In internal energy window 2, the reverse is depicted. Therefore, at low internal energies, channel C will be the dominant one, channel A the least dominant and channel B in between. The opposite applies for high internal energies, A > B > C.

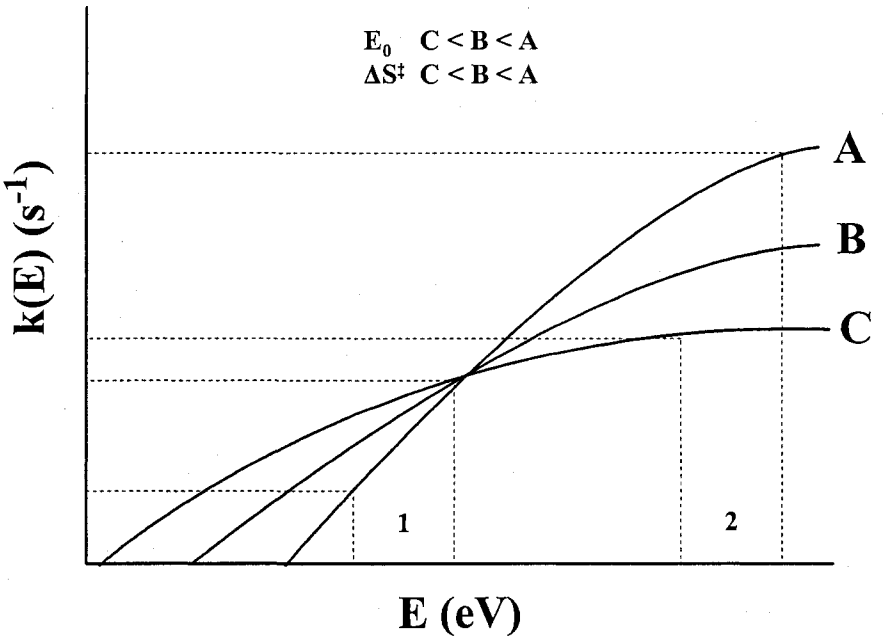

Figure 2.2. k(E) curves for three fragmentation channels (A, B, C), each having a different set of $\Delta S^{\ddagger}$ and E_o. In internal energy window 1, C > B > A and in internal energy window 2, A > B > C. Long and short experiment timescales correspond to internal energy window 1 and 2, respectively.

Apart from the internal energy content of the parent ion and the $\Delta S^{\ddagger}$ and E_o of each dissociating channel, the timescale of the experiment also governs the observed fragmentations. Short timescale experiments are dominated by fast reactions, high rate constants (internal energy window 2). While long timescale experiments are dominated by slow reactions, low rate constants (internal energy window 1).

2.3 Computational Chemistry

Theoretical calculations on structure, frequency and energy of various molecules open a whole new window on how chemistry is studied. It validates and may at times invalidate experimental evidence, gives insight on reactions, mechanisms, decomposition processes, etc. It is used in all areas of science: biochemistry, physical chemistry, drug discovery, particle physics, etc [5-7].

2.3.1 Ab initio Calculations

The Latin term *ab initio* refers to "from the beginning". This means that all calculations performed are based on first principles with no empirical parameters involved [8]. From this point of view, the computation starts with evaluating the electronic wave function (Ψ) of a molecule. This can be achieved by the well known Schrödinger equation, which is the basis of all computational chemistry theories,

$$\hat{H}\Psi = E\Psi \tag{2.5}$$

where $\hat{H}$ is the electronic Hamiltonian operator and E is the electronic energy. The Hamiltonian operator with the Born-Oppenheimer approximation (all nuclei are stationary with respect to the movement of electrons) is the following,

$$\hat{H} = -\sum_{i}^{electrons} \frac{\nabla_i^2}{2} - \sum_{i}^{nuclei} \sum_{j}^{electrons} \frac{Z_i}{r_{ij}} + \sum_{i<j}^{electrons} \frac{1}{r_{ij}} \tag{2.6}$$

where Z is the number of protons in a nucleus, r is the distance between two particles (e^--e^- / e^--nucleus) and ∇^2 is the Laplacian operator. The Laplacian operator is a 3D operator which takes the second derivative of a function,

$$\nabla_i^2 = \frac{\partial^2}{\partial x_i^2} + \frac{\partial^2}{\partial y_i^2} + \frac{\partial^2}{\partial z_i^2} \tag{2.7}$$

The first term in equation 2.3 evaluates the kinetic energy of the electrons, the second term evaluates the attraction between the electrons and nuclei and the third term is for the repulsion between electrons. The Hamiltonian operator for a many electron system can be very complex; consider a simple example of a two electron system, H_2 molecule (Figure 2.3),

$$\hat{H} = -\frac{\nabla_1^2}{2} - \frac{\nabla_2^2}{2} - \frac{1}{d} - \frac{1}{b} - \frac{1}{e} - \frac{1}{f} + \frac{1}{c} \tag{2.8}$$

where d, b, e, f and c are the distances between electrons and protons in Figure 2.3(b). As the number of electrons increases the complexity of the Hamiltonian operator and the wave function also increases. In particular, the inter electron repulsion (1/c) means there are no analytical solutions to the equation. This poses a problem for solving the exact wave function which contains all the properties of a system/molecule. To extract information from the wave function, the expectation value (<a>) of any property has to be calculated by the following equation

$$\langle a \rangle = \int \Psi^* \hat{A} \Psi d\tau \tag{2.9}$$

where $\hat{A}$ is the specific operator for the value a.

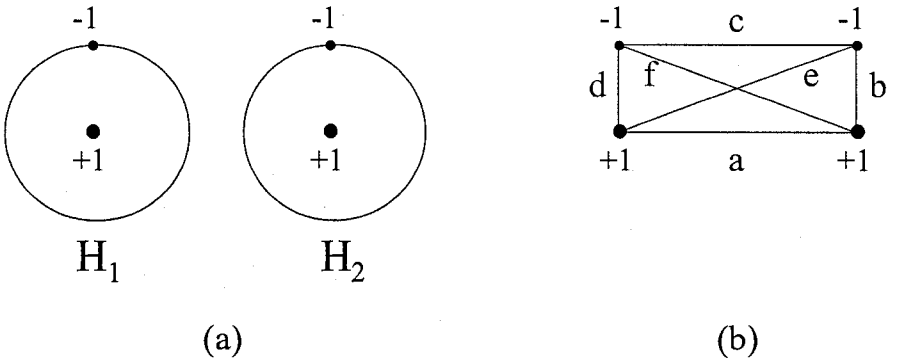

Figure 2.3. A diagram of two hydrogen atoms showing the relative positions of the protons/nuclei (+1) and electrons (-1) (a) and showing the distance between electrons, nuclei and electron-nucleus (b).

The complicacy of a many electron system can be solved by making approximations to the wave function. Although the solutions may not be exact, very accurate results depending on the level of theory being used can still be achieved. All *ab initio* methods today, namely, Hartree Fock (HF), Møller Plesset Perturbation (MPn, where n= 2, 3, 4, 5), Coupled Cluster (CC) and Configuration Interaction (CI) are based on approximations [8]. The level of theory characterized by the degree of accuracy for the above methods is

$$HF << MP2 < MP4 < CCSD \approx CI$$

HF is the lowest level of theory for *ab initio* methods and is rarely used on its own in today's computational chemistry. The true many electron wave function is simplified to many one electron wave functions that are often called molecular orbitals (M.O.) [9],

$$\Psi(1, 2, 3, 4...n) = \Psi_a(1)\overline{\Psi}_a(2)\Psi_b(3)\overline{\Psi}_b(4)....\overline{\Psi}_{n/2}(n) \qquad (2.10)$$

Each M.O. can be occupied by two electrons, one with spin α (e.g. Ψ_a) and the other with spin β (e.g. $\overline{\Psi}_a$). The method used to construct a one electron M.O. is a linear combination of atomic orbitals (L.C.A.O.),

$$\Psi = \sum_{i=1}^{k} c_i \chi_i \tag{2.11}$$

where χ is an atomic orbital and c is the coefficient of the i^{th} atomic orbital. The functions used to describe a one electron system will be further discussed in chapter 2, section 3.2. Once the one electron M.O.'s have been computed, the many electron wave function can be expressed in a single Slater determinant [10],

$$\Psi(1, 2, 3...n) = \frac{1}{\sqrt{n!}} \begin{vmatrix} \Psi_a(1) & \overline{\Psi}_a(1) & \cdots & \overline{\Psi}_{n/2}(1) \\ \Psi_a(2) & \overline{\Psi}_a(2) & \cdots & \overline{\Psi}_{n/2}(2) \\ \vdots & \vdots & \ddots & \vdots \\ \Psi_a(n) & \overline{\Psi}_a(n) & \cdots & \overline{\Psi}_{n/2}(n) \end{vmatrix} \tag{2.12}$$

Each row represents all the possible 1-electron wave function's for a specific electron (row 1-electron 1) and each column represents a particular 1-electron wave function with electrons 1 through n. The $1/\sqrt{n!}$ term is for normalization. When all the terms in the Slater determinant are multiplied and the many electron wave function is written as one equation, it satisfies two important rules in quantum mechanics. First, the electrons are indistinguishable and secondly, the Pauli Exclusion Principle [11], which says that when two identical fermions (electron is a fermion) are exchanged, the sign of the total wave function must change.

The primary approximation in HF is that each electron feels the repulsion of the rest of the electrons as an average [9]. In reality, the repulsion between two electrons is determined by their relative position at a given time (electron correlation). This is the main source of the low

level classification of this computational method. The error associated with electron correlation can in principle be calculated [9]:

$$E_{corr} = E - E_{HF} \tag{2.13}$$

where E_{corr} is the electron correlation energy, E is the true energy and E_{HF} is the energy calculated by the HF method. As a result, higher level methods that deal with correlation energy have been developed: Møller Plesset Perturbation theory, Coupled Cluster (CC), Configuration Interaction (CI) and DFT.

HF theory can be divided into two methods: restricted Hartree Fock (RHF) and unrestricted Hartree Fock (UHF) [8]. RHF is for closed shell systems where all electrons are paired up and the total spin is one. UHF method is for open shell systems where there is one or more unpaired electrons and the total spin is greater than one. The primary difference between the two methods is that in RHF the same functions are used for α and β spin electrons, while in UHF all α and β spin electrons are separated into two sets and are computed separately.

2.3.2 Basis sets

A basis set is a set of functions that describes the orbital shape (s, p, d, f) and the electron distribution around an atomic orbital and ultimately a molecule [8]. As mentioned in the previous section, a L.C.A.O. is used to define a particular M.O., Figure 2.4 for an example [10].

$$\Psi_i = \sum_{s=1}^{n} c_{si}\phi_s$$

Ψ_2 ——↑↓—— $\Psi_2 = c_{12}\phi_1 + c_{22}\phi_2$

Ψ_1 ——↑↓—— $\Psi_1 = c_{11}\phi_1 + c_{21}\phi_2$

Figure 2.4. An example of a L.C.A.O. for a molecule with two M.O.'s (Ψ_1 and Ψ_2). Φ is an atomic orbital, c_{si} is the coefficient of the ith M.O. and sth atomic orbital.

An atomic orbital or basis function containing one electron is accurately described by a Slater Type Orbital (STO) [12],

$$\phi = Nr^{n-1}e^{-\zeta r}Y_{lm}(\theta,\phi) \qquad (2.14)$$

where N is a normalization constant, r is the distance between an electron and a nucleus, θ and ϕ are spherical coordinates that further describe the position of an electron in an orbital, ζ is an exponent, and Y_{lm} describes the orbital shape (s, p, d). n, l, and m are the principal, angular momentum and magnetic quantum numbers, respectively. An STO is the exact solution of the Schrodinger equation for a Hydrogen atom (i.e. one electron in an orbital) [8]. However, a regular atomic orbital usually contains 2 electrons; using STO for such an orbital requires a lot of computer time [12]. Therefore, simpler functions, namely, Gaussian Type Orbitals (GTO) have been introduced. The mathematical differences between a GTO and an STO are that the exponential function, $e^{-\zeta r}$ is replaced with $e^{-\alpha r^2}$ (where α is the exponent), the pre-exponential factor r^{n-l} is dropped and Y_{lm} is simplified [12]. A linear combination of several GTO's (1, 2, 3) is made to fit an STO, Figure 2.5. This is the source for the basis set names of STO-1G, STO-2G and STO-3G, where 1G, 2G, and 3G is the number of Gaussian functions used [13]. It is clear from Figure 2.5 that the source of error in a GTO function is the behaviour of an electron near

the nucleus. This is improved as the number of GTO's is increased. It is important to mention that when a linear combination of GTO functions are used, they are contracted by a coefficient [12]. Here is an example,

$$\phi^{CGF} = 0.45\phi^{GTO} + 0.55\phi^{GTO} \tag{2.15}$$

Such functions are called, contracted Gaussian function (CGF).

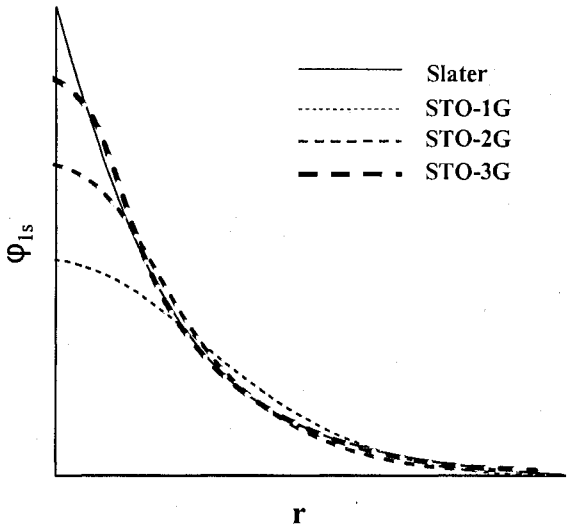

Figure 2.5. A comparison of the STO-1G, STO-2G, and STO-3G with a Slater function.

STO–nG where n= 2–6 are the simplest basis sets available but are rarely used in research. Instead they form the foundation for the Pople basis sets which were developed in the 1971 [14] and are widely used in today's computations. These basis sets are an extension of the STO–nG set which poorly account for change in orbital size (e.g H and C) in a molecular environment and anisotropy in the valence shell. Pople basis sets are designated by an n–ijG label, where n is the number of GTO functions used for a core orbital, i and j are the number of GTO functions used for a valence orbital, while G simply stands for Gaussian [15]. A valence shell has two sets of GTO functions, hence the two notations (i & j). This is referred to a split valence shell. For e.g. the 6–31G basis set has 6 GTO's for the formation of contracted

Gaussian function (CGF) for a core orbital, while the valence shell is split into two: core valence orbitals have 3 GTO's while the outer valence orbitals have 1 GTO for a contracted Gaussian function CGF. A valence shell can also be split into three, this would be designated by three numbers before the G (e.g. 6-311G). The numbers before the G are for s and p type orbitals.

Polarization functions are p, d, and f functions that are added to enhance the flexibility of the electron distribution [15-16]. This extra flexibility allows for correct predictions of molecular geometries, Figure 2.6 [10]. Polarization functions are denoted either with a single (*) or a double (**) star. A single star implies the addition of d orbitals to polarize the p orbitals. A second star is for H and He where p orbitals are added [17]. It is standard to add the stars after the G, e.g. 6-31G*, 6-31G**. An equivalent notation would be to designate the orbitals added in a bracket after the G, e.g. 6-311G(d,p). The right side of the bracket is for H and He and the left side is for all other atoms. Sometimes the basis set can get very complicated and f functions could be added as well, e.g. in 6-31G(3d2fg,2pd) three d functions, two f functions and one g function are added to heavy atoms and two p functions and one d function are added for the polarization of H and He.

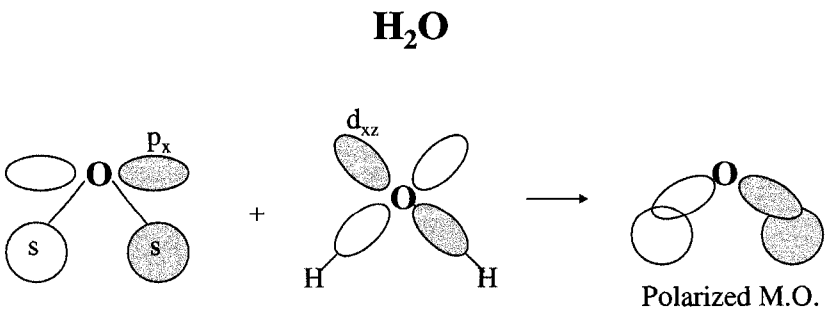

Figure 2.6. An addition of a d_{xz} orbital on an O polarizes the direction of the p_x orbital and thus enhances bonding with the two s orbtials on the H's. Green and whites lobes signify opposites signs.

Diffuse functions are implemented to improve the behaviour of an electron far away from the nucleus [10]. In this region, it allows for a more delocalized electron density. This is well illustrated on a Slater function, where the tail is more continuous. This is particularly favorable for anions and intermolecular interactions but is still used for simple organic molecules containing heteroatoms (e.g. N, O, Cl that have lone pairs). Diffuse functions are denoted by a + or ++ sign [17]. One + sign indicates an addition of one s and one p diffuse functions on heavy atoms only. While two + signs indicate s and p diffuse functions on all atoms. The plus signs are added before the G, e.g. 6-31+G and 6-31++G.

In general the bigger the basis set the better the results. To determine the best balance between computational cost and accuracy (optimum basis set) for a particular system, an assessment should be done; this allows monitoring to what degree a certain parameter changes as the size of the basis set increases. As soon as a plateau region is reached (convergence), that is, no significant change in a parameter, such as reaction energy or bond length, the basis set should be selected.

2.3.3 Density Functional Theory (DFT)

Unlike *ab initio* methods that attempt to solve the many electron wave function, DFT is based on calculating the total electron density of a molecule [18]. The true wave function is a function of four variables: 3 spatial coordinates (x, y and z) and 1 spin component. Multiplying this by the total number of electrons (n), the total dependency is on 4n variables. On the contrary, the electron density is a function of a total of 3 variables: the spatial coordinates (x, y

and z) which are independent of the total number of electrons. This significantly simplifies the computational procedure which saves time but still yields accurate results (comparable to MP2) [8]. For this reason, DFT methods have become very popular.

Electron density (ρ) is calculated by finding the probability of an electron with coordinates (x, y, z) in a volume of $dx\ dy\ dz$ [19]. Hohenberg and Kohn showed that if the ground state electron density is known, all other properties can be determined. One important property is the ground state energy (E_o) of a molecule,

$$\rho(r) \longrightarrow E_o \tag{2.16}$$

where r represents the spatial coordinates (x, y, z). There exists an energy functional which can determine the molecular energy from the electron density. The term functional means a function of a function which converts a function into a number [10]. For comparison, $f(x) = x^3$ is a function that converts a variable into a number. Here is an example of a functional:

$$F = \int_0^2 f(x)dx \tag{2.17}$$

So,

$$E_o = E[\rho(r)]$$

where $E[\ ]$ is the energy functional F and $\rho(r)$ is a function. The problem with this theorem is that the energy functional is not defined and no information exists on how to construct one.

Modern Density Functional Theory that is utilized in today's computational chemistry was introduced in 1965 by Kohn and Sham [20]. They proposed that the energy functional is linearly dependant on four terms [18]:

$$E[\rho(r)] = T_o + V_{nuc} + V_{ee} + E_{xc} \tag{2.18}$$

where,

T_o is the kinetic energy of a non interacting reference system,

V_{nuc} is the nuclear-electron P.E. functional,

V_{ee} is the electron-electron repulsion energy functional and

E_{xc} is the exchange-correlation functional.

V_{nuc} and V_{ee} are classical coulombic expressions of the P.E. A non-interacting reference system refers to a fictitious system with electrons that do no interact with each other and where the electron density is equal to the one in the real system: $\rho(r) = \rho_o$. This approximation creates a small deviation in the kinetic energy of the electrons [19],

$$\Delta T = T_{true} - T_o \tag{2.19}$$

which is later accounted in E_{xc}. Since the electrons do not interact with each other, the total kinetic energy is simply the sum of the individual kinetic energies. This is easily calculated by using equation (2.6) and constructing one electron M.O.'s. The expression for T_o then becomes,

$$T_o = \sum_{i=1}^{n} \int \Psi_i^{KS} \left(-\frac{1}{2} \nabla^2 \right) \Psi_i^{KS} \tag{2.20}$$

All first three terms can be calculated exactly; this leaves the fourth term, E_{xc} which is an unknown functional. The exchange correlation functional does not contribute a large part to the total molecular energy, therefore the approximations made to E_{xc} are not as drastic and thus DFT

can be regarded as a nearly exact theory [21]. The equations developed for E_{xc} are complex and can be found elsewhere [19]. Instead the qualitative aspect of this term is briefly summarized:

E_{xc} accounts for:

- Quantum mechanical electron-electron repulsion energy which in itself includes the exchange and correlation energy, hence the name exchange-correlation functional.
- Discrepancy in the kinetic energy of the electrons, ΔT (equation 2.19)

Current density functional computational methods involve variations of the exchange-correlation functional. Each functional is named after its developers and sometimes includes the year as well. For B3LYP [19],

- B is an abbreviation for the exchange functional developed by Becke in 1988.
- LYP is an abbreviation for the correlation functional introduced by Lee, Yang and Parr in 1988. It contains one empirical parameter and is based on the correlation energy of the He atom.
- B3 is a hybrid exchange functional developed by Becke in 1993. This functional is a mix of DFT and HF exchange functional, hence the name hybrid. The number 3 refers to 3 (a, b, and c) empirical coefficients that control the amount of the DFT (a) and HF (b) exchange functional as well as the correlation functional (c), in this case LYP.

The difference between B3LYP and B3PW91 is the correlation functional. PW91 is a correlation functional with no empirical parameters developed by Perdew and Wang in 1991 [19]. BHandHLYP (Becke–half and half–Lee–Yang–Parr) is a hybrid of HF exchange

functional (50%) and DFT exchange-correlation functional (50%) which was also introduced by Becke in 1993 [22].

2.3.4 Gaussian-3 (G3) theory

G3 theory is a combination of several *ab initio* methods and basis sets that accurately predicts molecular energies and heats of formations [23]. It was first introduce by Pople et al. in 1989 who formulated Gaussian-1 theory [24]. Further developments lead to G2, G3 and G4 theory with increasingly higher accuracy [23,25-26]. G3 is of particular interest to physical and theoretical chemists who seek to understand relative stabilities and energetics of molecules and ions.

G3 theory is composed of the following seven steps [23]:

1. Equilibrium structure is obtained by geometry optimization at the HF level with 6-31G(d) basis set. RHF is used for singlet states and UHF for higher states.
2. Harmonic frequencies of the equilibrium structure obtained in step (1) are calculated at HF level with 6-31G(d) basis set. This also computes zero point energy. A scaling factor of 0.8929 is used for the frequencies.
3. The equilibrium geometry obtained in step (1) is further optimized at the MP2(full) level of theory with 6-31G(d) basis set. This is the final geometry, which is used for all subsequent single point calculations.

4. Multiple single point (SP) energy calculations (total 8) are executed at the MP4 and MP2 level of theory with 6-31G(d), 6-31+G(d) and 6-31G(2df,p) basis sets. An additional 2 SP calculations are carried out: QCISD(T)/6-31G(d) and MP2(full)/G3large. The following corrections are calculated from the above 8 SP energies:

   a) A correction for diffuse functions,

   $\Delta E(+) = E$[MP4/6-31+G(d)] - E[MP4/6-31G(d)]

   b) A correction for polarization functions,

   $\Delta E(2df,p) = E$[MP4/6-31G(2df,p)] - E[MP4/6-31G(d)]

   c) A correction for electron correlation,

   $\Delta E(QCI) = E$[QCISD(T)/6-31G(d)] - E[MP4/6-31G(d)]

   d) A correction for larger basis set,

   $\Delta E(G3large) = E$[MP2(full)/G3large] - E[MP2/6-31G(2df,p)]
   - E[MP2/6-31+G(d)] + E[MP2/6-31G(d)]

5. The above four corrections are added to the energy calculated at MP4/6-31G(d)

   $E(combined) = E$[MP4/6-31G(d)] + $\Delta E(+)$ + $\Delta E(2df,p)$ + $\Delta E(QCI)$ + $\Delta E(G3large)$
   + $\Delta E(SO)$

   $\Delta E(SO)$ is the spin-orbit correction applied to atomic species only, for a full explanation see Ref [23].

6. A "higher level correction" (HLC) is calculated for molecules and subsequently added to the above energy (5) by the following equations,

   $E(HLC) = -An_\beta - B(n_\alpha - n_\beta)$ where n_α =# α valence electrons, n_β =# β valence electrons, A and B are empirical parameters of 6.386 and 2.977 mhartrees, respectively.

   $E_e(G3) = E(combined) + E(HLC)$

7. The zero point energy calculated in step two is added to the above total energy (6),

   $E_o(G3) = E_e(G3) + E(ZPE)$

   $E_o(G3)$ is the G3 energy at 0K. ZPE is scaled by a factor of 0.9135.

It is evident from the above representation of G3 theory that it was designed to take into account electron correlation and the incompleteness of a basis set.

2.3.5 Green's Function

Green's function was designed to take into account perturbations of a system by the removal of an electron from a specific M.O [27]. In this thesis, it was used to calculate the vertical ionization energies ($I.E._v$) of molecular orbitals (M.O.) of acetone azine and azo-tert-butane.

2.3.6 Frequency Calculations and Geometry Optimizations

A geometry optimization attempts to find a stationary point which is defined as one where the first order derivative of the energy with respect to one spatial coordinate is zero [15]. A molecule can have many stationary points; the one with the lowest energy in the potential energy surface (PES) is called a *global* minimum, all others are *local* minima, Figure 2.7(a). A transition state is also a stationary point, i.e. first derivative is zero. To confirm the nature of the stationary point a frequency calculation is necessary. A frequency calculation computes the second derivative of the energy with respect to spatial coordinates and determines the curvature

of the PES [8]. If the second derivative is greater than zero (i.e. positive) in all directions of the PES then the stationary point is a true minimum, an equilibrium structure [15]. If the second derivative is positive in all directions except one, then it's a first order saddle point, a transition state, Figure 2.7(b). This results in one negative frequency which is called an imaginary frequency. The imaginary frequency corresponds to a vibrational mode which leads the reactant to its products.

A frequency calculation also computes the vibrational zero point energy (ZPE) by the following equation,

$$E_{ZPE} = \sum_{i=1}^{N} \left(\frac{h\upsilon_i}{2} \right) \tag{2.21}$$

where h is Planck's constant, υ_i is the frequency of the i^{th} vibrational mode and N is the total number of frequencies [7]. ZPE accounts for the vibrational motion of a molecule even at zero K which is added to the electronic energy computed from the geometry optimization. This correction is essential when relative stabilities of molecular ions and decomposition products are considered.

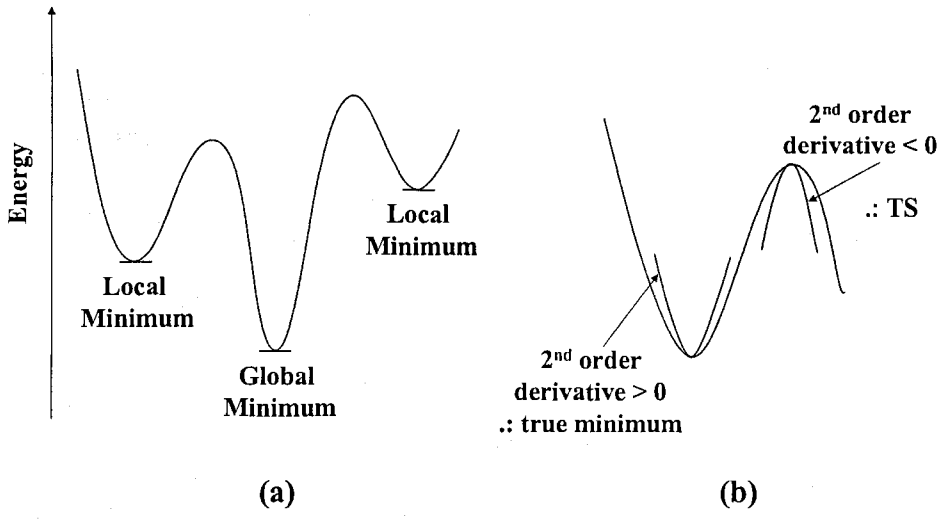

Figure 2.7. Two potential energy surface diagrams: (a) shows the difference between a local and a global minimum and (b) shows the identification of a true minimum and a TS.

Frequencies and ZPE values are often scaled by factors that account for deviation from experimental results [28]. Each scale factor can be < or > than 1 and varies with the level of theory. See next section for scale factors used in the computational work of this thesis.

2.4 Procedures

2.4.1 Fitting method

The procedure involves fitting theoretical breakdown curves to experimental ones obtained from TPEPICO spectroscopy (discussed in chapter 3, section 5.1). The following summarizes the generation of a theoretical breakdown curve:

I. The rate constants are calculated by equation 2.3. The reaction degeneracy, σ, for ATB and AA was taken as 1. The sum and density of states were calculated by the direct count method [29]. The ion's vibrational frequencies used in the direct count method were

calculated at the B3LYP/6-31+G(d) level of theory (see chapter 2, section 4.2). The transition state's vibrational frequencies were the ion's vibrational frequencies with one vibrational mode corresponding to the bond cleavage removed. The range of internal energies used was determined in the following manner:

$E_{min} = E_{min}(exp) - 0.115$ eV

$E_{max} = E_{max}(exp)$ + range of population distribution

II. For a multiple dissociation channel system (e.g. 3), at each internal energy the three rate constants are combined to calculate the total rate constant. The total rate constant governs the dissociation of the parent ion, while the relative rate constant of each dissociating channel governs the associated fragmentation.

For ATB: m/z 142 dissociates by three channels, m/z 57, m/z 85 and m/z 56.

Rate constants for m/z 142, m/z 57, m/z 85 and m/z 56 are k_{tot}, k_1, k_2 and k_3, respectively.

Where, $k_{tot} = k_1 + k_2 + k_3$

The intensity of each ion at each internal energy is:

k_{tot} for m/z 142

k_1/k_{tot} for m/z 57

k_2/k_{tot} for m/z 85

k_3/k_{tot} for m/z 56

For AA: m/z 112 has one dissociation channel, m/z 97.

Rate constants for m/z 112 and m/z 97 are k_{tot} and k_1, respectively.

Therefore, $k_{tot}=k_1$

III. The theoretical data is convoluted with the following experimental factors: the parent ion thermal energy (rotational and vibrational motion in RT), the electron analyzer transmission efficiency and monochromator resolution.

III.I The parent ion thermal energy is calculated as a population distribution as a function of internal energy of the neutral molecule. The neutral molecule is used since the ionization in TPEPICO is a vertical process, i.e. the structure does not change significantly. The population distribution (P(E)) is calculated by the following equation:

$$P(E) = \frac{\rho(E)e^{-E/kT}}{Q_{vib}\,Q_{rot}}$$

Where, ρ(E) is the density of states, E is the internal energy, k is the boltzman's constant ($1.38*10^{-23}$ JK^{-1}), T is the temperature (298 K) and Q is the partition function. The density of states is calculated by the direct count method [29]. The equations for the partition functions are the following:

$$Q_{vib} = \sum_{v=1}^{N} \frac{1}{1-e^{-hvc/kT}} \qquad Q_{rot} = \frac{1}{\sigma}\left(\frac{kT}{hc}\right)^{3/2}\left(\frac{\pi}{ABC}\right)^{1/2}$$

where A, B and C are rotational constants and ν are the vibrational frequencies of the neutral molecules calculated by B3LYP/ 6-31+G(d) (see chapter 2, section 4.2).

III.II The electron analyzer transmission efficiency takes into account the detection of non-threshold electrons (see section 3.4 for threshold electrons). It was measured experimentally by the photoionization of Krypton under the conditions used in the TPEPICO measurements as a threshold electron spectrum (Intensity vs. electron kinetic energy)

III.III The monochromator bandpass accounts for the resolution of the monochromator which is 2 meV (FWHM) [30].

IV. The final step is to account for the residence time (1.116, 3.116, 5.116 and 7.116 μsec). Steps I to IV are carried out for each residence time (see chapter 3, section 5.1).

V. Steps I to V describe the generation of one breakdown curve. The fitting process requires many breakdown curves to be calculated to obtain the best fit to the experimental data. For each dissociation channel, the two parameters that can be adjusted to obtain the fit are E_0 and $\Delta S^{\ddagger}$ (step I). $\Delta S^{\ddagger}$ is adjusted by scaling the 5 lowest TS vibrational frequencies.

2.4.2 Computational Procedures

Calculations were carried out using the Gaussian 98 or 03 suite of programs [31-32]. The *ab initio* calculations performed (see Table 2.1 for a summary) for ATB and AA are geometry optimizations, frequency and energy calculations at three density functional levels of theory: B3LYP, B3PW91 and BHandHLYP. Single point G3 computations were also performed to determine more accurate values for the energy of the ions and neutrals studied. A slight variation of the G3 theory described in chapter 2, section 4.4 was implemented in this study. Steps 1 & 2 were performed at the B3LYP, B3PW91 and BHandHLYP level of theory with 6-31+G(d) basis set. The scale factor used for the harmonic frequencies and ZPE is summarized in Table 2.2 [28]. M.O. ionization energies and coefficients of azo-tert-butane and acetone azine were calculated using the restricted outer valence green's function (ROVGF) and B3LYP, respectively. Anne-Marie Boulanger, a former Ph.D. graduate student performed a basis set assessment on ionized 1,1-dimethylhydrazine and its dissociation products [33]. According to her results, 6-31+G(d) gave the best balance between computational cost and accuracy and hence was the choice of basis set for all ab initio calculations performed in this thesis work.

Table 2.1. A summary of all the computations performed.

Theory	Type of Calculation	Keywords Used
G3	Single point energy	———
B3LYP	Geometry optimization, frequency and M.O. coefficients	opt, freq, pop=full, geom=check[a]
B3PW91	Geometry optimization, frequency	opt, freq, geom=check[a]
BHandHLYP	Geometry optimization, frequency	opt, freq, geom=check[a]
ROVGF	M.O. ionization energies	geom=check[a]

[a] geom=check → the geometry is read from a checkpoint file

Table 2.2. List of scale factors used for ZPE and frequencies at 3 DFT's.

Level of Theory	ZPE	Frequencies
B3LYP	0.9806	0.9614
B3PW91	0.9774	—
BHandHLYP	0.9806[a]	—

[a] No scale factor published for BHandHLYP, .: used the same one as for B3LYP

References

[1] T. Baer, W.L. Hase, *Unimolecular Reactions Dynamics – Theory and Experiments*, 1996, Oxford: Oxford University Press.

[2] T. Baer, P.M. Mayer, *J. Am. Soc. Mass Spectrom.* 1997, 8, 103-115.

[3] W. Forst, *Theory of Unimolecular Reactions*, 1973, New York: Academic Press.

[4] T. Baer, *The Encyclopedia of Mass Spectrometry*, M.L. Gross, R. Caprioli, P.B. Armentrout, Editors. Vol 1. 2003, Amesterdam: Elsevier. p. 388-389.

[5] Y. Xu, D. Xu, J. Liang, *Computational methods for protein structure prediction and modeling*, 2007, New York: Springer Publishing.

[6] R. M. Stroud, J.F. Moore, *Computational and Structural Approaches to Drug Discovery: Ligand Protein Interactions*, 2008, Cambridge: RSC Publishing.

[7] H. Dass, *Current Science* 2005, 88, 394-396.

[8] D. Young, *Computational Chemistry – A Practical Guide for Applying Techniques to Real World Problems*, 2001, New York: John Wiley & Sons.

[9] C.J. Cramer, *Essentials of Computational Chemistry – Theories and Models*, 2004, Chichester: John Wiley & Sons.

[10] E. Lewars, *Computational Chemistry – Introduction to the Theory and Applications of Molecular and Quantum Mechanics*, 2003, Boston: Kluwer Academic Publishers.

[11] P. Atkins, J. de Paula, *Physical chemistry*, 2002, New York: W.H. Freeman and Company.

[12] Computational Chemistry List,
Website: http://www.ccl.net/cca/documents/basis-sets/basis.html

[13] W.J. Hehre, R.F. Stewart, J.A. Pople, *J. Chem. Phys.* 1969, 51, 2657-2664.

[14] R. Ditchfield, W.J. Hehre, J.A. Pople, *J. Chem. Phys.* 1971, 54, 724-728.

[15] F. Jensen, *Introduction to Computational Chemistry*, 2007, Chichester; John Wiley & Sons.

[16] C.M. Quinn, *Computational Quantum Chemistry – An Interactive Guide to Basis Set Theory*, 2002, San Diego; Academic press.

[17] M.J. Frisch, J.A. Pople, J.S. Binkley, *J. Chem. Phys.* 1984, 80, 3265-3269.

[18] K. Burke, J.P. Perdew, M. Levy, *Modern Density Funcitonal Theory – A Tool for Chemistry*, J.M. Seminario, P. Politzer, Editors. 1995, Amsterdam: Elsevier Science.

[19] W. Koch, M.C. Holthausen, *A Chemist's Guide to Density Functional Theory*, 2000, Weinheim: John Wiley & Sons.

[20] W. Kohn, L.J. Sham, *Phys. Rev. A* 1965, 137, 1697-1705.

[21] S. Kummel, L. Kronik, *Rev. Mod. Phys.* 2008, 80, 3-60.

[22] M. Miura, Y. Aoki, B. Champagne, *J. Chem. Phys.* 2007, 127, 1-16.

[23] L.A. Curtiss, K. Raghavachari, P.C. Redfern, V. Rassolov, J.A. Pople, *J. Chem. Phys.* 1998, 109, 7764-7776.

[24] J.A. Pople, H.G. M. Head-Gordon, D.J. Fox, K. Raghavachari, L.A. Curtiss, *J. Chem. Phys.* 1989, 90, 5622-5629.

[25] L.A. Curtiss, K. Raghavachari, G.W. Trucks, J.A. Pople, *J. Chem. Phys.* 1991, 94, 7221-7230.

[26] L.A. Curtiss, P.C. Redfern, K. Raghavachari, *J. Chem. Phys.* 2007, 126, 1-12.

[27] M. Springborg, *Methods of Electronic Structure Calculations – From Molecules to Solids*, 2000, Chichester: John Wiley & Sons.

[28] J.P. Merrick, D. Moran, L. Radom, *J. Phys. Chem. A* 2007, 111, 11683-11700.

[29] T. Beyer, D.R. Swinehart, *ACM Commun.* 1973, 16, 379.

[30] SRS Daresbury Laboratory homepage

Website: http://www.srs.ac.uk/srs/stations/station3.2.htm

[31] M.J. Frisch, G.W. Trucks, H.B. Schlegel, G.E. Scuseria, M.A. Robb, J.R. Cheeseman, V.G. Zakrzewski, J.A. Montgomery, R.E. Stratmann, J.C. Burant, S. Dapprich, J.M. Millam, A.D. Daniels, K.N. Kudin, M.C. Strain, O. Farkas, J. Tomasi, V. Barone, M. Cossi, R. Cammi, B. Mennucci, C. Pomelli, C. Adamo, S. Clifford, J. Ochterski, G.A. Petersson, P.Y. Ayala, Q. Cui, K. Morokuma, D.K. Malick, A.D. Rabuck, K. Raghavachari, J.B. Foresman, J. Cioslowski, J.V. Ortiz, B.B. Stefanov, G. Liu, A. Liashenko, P. Piskorz, I. Komaromi, R. Gomperts, R.L. Martin, D.J. Fox, T. Keith, M.A. Al-Laham, C.Y. Peng, A. Nanayakkara, C. Gonzalez, M. Challacombe, P.M.W. Gill, B. Johnson, W. Chen, M.W. Wong, J.L. Andres, C. Gonzalez, M. Head-Gordon, E.S. Replogle, J.A. Pople, in "*GAUSSIAN 98 Rev. A.7*", Gaussian Inc.: Pittsburgh PA, 1998.

[32] M.J. Frisch, G.W. Trucks, H.B. Schlegel, G.E. Scuseria, M.A. Robb, J.R. Cheeseman, J.A. Montgomery, T. Vreven, K.N. Kudin, J.C. Burant, J.M. Millam, S.S. Iyengar, J. Tomasi, V. Barone, B. Mennuci, M. Cossi, G. Scalmani, N. Rega, G.A. Petersson, H. Nakatsuji, M. Hada, M. Ehara, K. Toyota, R. Fukuda, J. Hasegawa, M. Ishida, T. Nakajima, Y. Honda, O. Kitao, H. Nakai, M. Klene, X. Li, J.E. Knox, H.P. Hratchian, J.B. Cross, V. Bakken, C. Adamo, J. Jaramillo, R. Gomperts, R.E. Stratmann, O. Yazyev, A.J. Austin, R. Cammi, C. Pomelli, J.W. Ochterski, P.Y. Ayala, K. Morokuma, G.A. Voth, P. Salvador, J.J. Dannenberg, V.G. Zakrzewski, S. Dapprich, A.D. Daniels, M.C. Strain, O. Farkas, D.K. Malick, A.D. Rabuck, K. Raghavachari, J.B. Foresman, J.V. Ortiz, Q. Cui, A.G. Baboul, S. Clifford, J. Cioslowski, B.B. Stefanov, G. Liu, A. Liashenko, P. Piskorz, I. Komaromi, R.L. Martin, D.J. Fox, T. Keith, M.A. Al-Laham, C.Y. Peng, A. Nanayakkara, M.

Challacombe, P.M.W. Gill, B. Johnson, W. Chen, M.W. Wong, C. Gonzalez, J.A. Pople, in "*GAUSSIAN 03 Rev. C.02*.", Gaussian Inc.: Wallingford CT, 2004.

[33] A.M. Boulanger, E.E. Rennie, D.M.P. Holland, D.A. Shaw, P.M. Mayer, *J. Phys. Chem. A* 2007, 111, 5388-5398.

Chapter 3

Experimental Concepts and Techniques

3.1 Introduction to Mass Spectrometry

A mass spectrometer generally consists of three main parts: an ion source, mass analyzer and a detector, Figure 3.1. The ion source is responsible for generating the molecular ions and sometimes the fragment ions. The mass analyzer has the capability of selecting a particular ion according to its mass-to-charge (m/z) ratio and fragmenting it. The detector detects the molecular and fragment ions and then sends a signal to a computer which generates a mass spectrum.

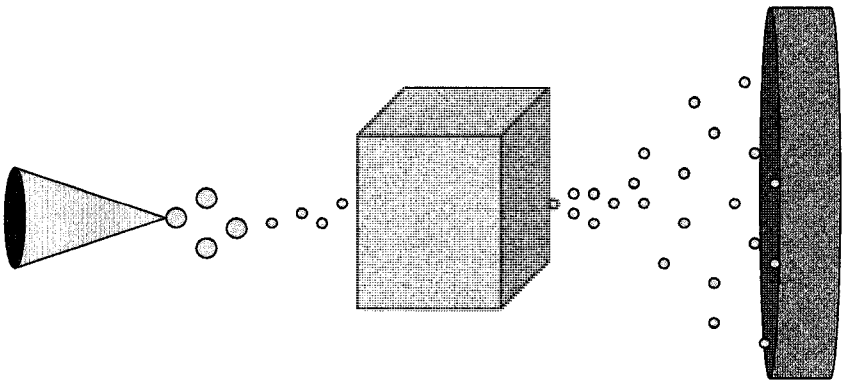

Figure 3.1. A schematic diagram depicting the three main parts of a mass spectrometer: ion source, mass analyzer and detector.

The advancement of mass spectrometers has lead to a versatile selection of ion sources: electron ionization (EI), photoionization (PI), chemical ionization (CI), fast atom bombardment

(FAB), electrospray ionization (ESI), matrix assisted laser desorption ionization (MALDI) and inductively coupled plasma (ICP) [1-7]. Reactions 3.1 through 3.9 describe how the ionization takes place. In EI, a neutral molecule collides with a high energy electron beam, usually of 70 eV which is sufficient to ionize a molecule and form a radical cation. In PI, a neutral molecule absorbs a photon of energy equal to or greater than its ionization potential which generates an ion – electron pair. The ionization via CI takes place through a charge transfer, namely, electron, proton or hydride/anion transfer. The above three ionization methods are suitable for small molecules with high vapour pressures. On the other hand, FAB, ESI and MALDI have been designed for large molecules, such as proteins and polymers. The soft ionization in those three techniques generates ions by protonation, deprotonation or simply the extraction of an electron which are then transferred to the gas phase by a bombardment of high velocity Xe/Ar atoms, the application of high voltage and UV light for FAB, ESI and MALDI, respectively. ICP is a unique technique that fragments all molecules to their ionic elemental constituents in the presence of plasma (6,000 – 10,000 K).

EI: $M + e^- \rightarrow M^{+\bullet} + 2e^-$ (3.1)

PI: $M + h\upsilon \rightarrow M^{+\bullet} + e^-$ (3.2)

CI: $M + R^{+\bullet} \rightarrow M^{+\bullet} + R$ (3.3)

$M + RH^+ \rightarrow MH^+ + R$ (3.4)

$M + RH^- \rightarrow MH^- + R$ (3.5)

FAB: $M + \text{matrix} + Xe/Ar \rightarrow MH^+$ (3.6)

ESI: $M + \text{solvent} + \text{electric potential} \rightarrow MH^+$ (3.7)

MALDI: $M + \text{matrix} + UV \rightarrow M^{+\bullet} + MH^+$ (3.8)

ICP: $M + \text{plasma/high temp.} \rightarrow \text{ionic atomic fragments}$ (3.9)

Similar to the wide selection of ion sources, mass analyzers have also been extensively developed, these are: magnetic sector, electrostatic sector, triple-quadrupole, quadrupole ion trap and time-of-flight (TOF) [8]. Ions emerging from the ion source are selected according to the m/z by applying an appropriate magnetic field strength and electric potential difference in a magnetic and electrostatic sector, respectively. Quadrupole refers to four metal rods that are arranged in a square shape which upon a voltage application has the capability of selecting or trapping a specific ion according to its m/z. In TOF, each ion has a specific translational kinetic energy which is reflected in the time it takes to travel from the ion source to the detector. Hence, ions are analyzed according to their flight time. TOF is well known for its high resolution and is used in the analysis of high MW ions, such as proteins and polymers.

Two conventional detectors used in mass spectrometry are electron multipliers and photomultipliers [9]. An electron multiplier consists of several dynodes with a metal surface (e.g. Cu/Be), from which electrons are emitted upon collisions with high energy electrons and ions, Figure 3.2. As the positive ion beam enters the detector, it is attracted to a cathodic dynode that emits secondary electrons. The secondary electrons then travel to the next dynode and the e^- gain is multiplied. An increasingly positive potential directs the electrons from dynode to dynode as they are multiplied until they reach the terminal anode. A photomultiplier consists of a photocathode, dynodes and an anode. The principal of operation of a photomultiplier is similar to that of an electron multiplier except in the first stage; as a photon strikes the photocathode, a photoelectric effect takes place and an electron is emitted. The first dynode is set to a positive potential of 90 V and as a result the emitted electrons produced from the photocathode are attracted to it. Secondary electrons are generated at each dynode and this process is repeated

nine times until all the electrons reach the anode. A photomultiplier can achieve a current gain of 10^7 for each incident photon while an electron multiplier 10^7 for the total gain.

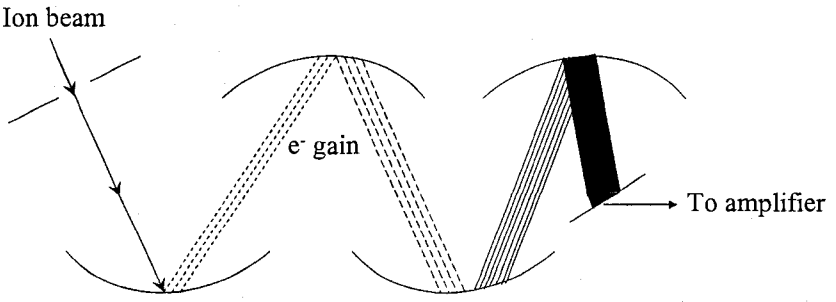

Figure 3.2. A schematic diagram of a discrete dynode electron multiplier.

The two instruments employed in the investigation of azo-tert-butane and acetone azine are the VG ZAB mass spectrometer and TPEPICO spectrometer. The following four sections describe the instrumentation and the types of experiments performed.

3.2 Modified VG ZAB Mass Spectrometer

The components of the VG ZAB mass spectrometer are an EI ion source, magnetic & electrostatic analyzers and two photomultiplier detectors, Figure 3.3. The instrument can operate in double or triple focusing modes. In a double focusing geometry, the ion beam is focused first after the magnetic sector and then after the electrostatic sector (BE geometry). In a triple focusing geometry, the ion beam is focused in three places: magnetic sector, ESA1 and ESA2 (BEE geometry).

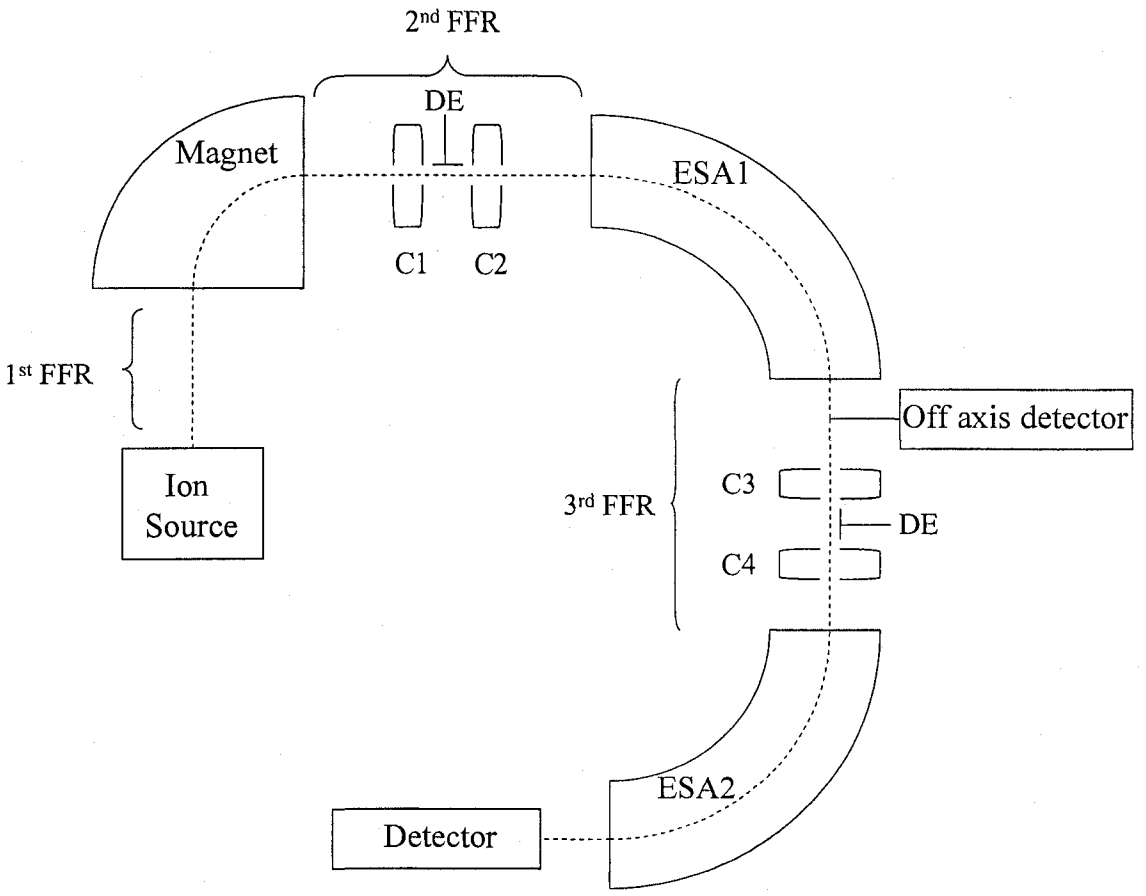

Figure 3.3. A schematic diagram of VG ZAB mass spectrometer. FFR represents field free region, C1 – cell 1, C2 – cell 2, DE - deflector electrode and ESA - electrostatic analyzer.

3.2.1 Ion Source

Figure 3.4 illustrates the components of a typical EI ion source. The electrons which are responsible for the ionization taking place are produced by heating up the filament to high temperatures. The region between the filament and entrance to the ion source block accelerates the electrons to 70 eV. It has been proven previously that at this energy, the ionization efficiency reaches a maximum plateau region and thus 70 eV became a standard for the accelerating voltage of electrons in EI ion source [10]. The accelerated electrons are concentrated into a

beam by being attracted to the trap electrode. A sample vapour containing the neural molecules is introduced to the ion source in a perpendicular direction to the e^- beam. Upon ionization, the newly formed radical cations are directed towards the mass analyzer by a repeller electrode. All ions leaving the ion source are accelerated to 8 kV in the accelerating region; therefore all ions regardless of their mass have the same translational kinetic energy (K.E.). The combination of the high energy electrons and the initial thermal distribution of the neutral molecules gives rise to a broad range of ion internal energies produced in the ion source.

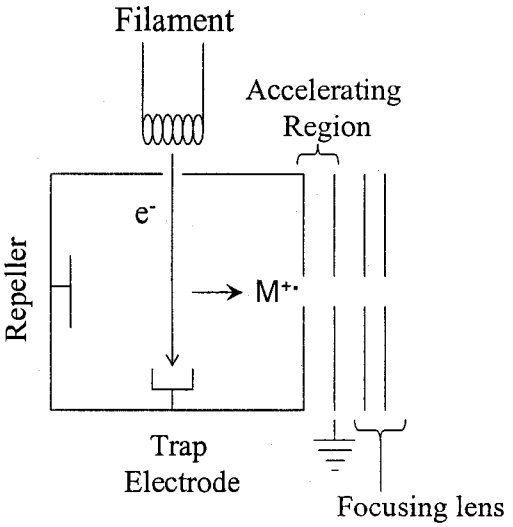

Figure 3.4. A diagram representing an electron ionization ion source.

3.2.2 Magnetic Analyzer

The magnetic analyzer consists of two parallel electromagnets with an iron core in between, Figure 3.5 [11]. The electromagnets produce a magnetic field by passing a current through a metal coil [12]. Modification of the electric current flowing through the coil affects the magnetic field produced and thus can be varied easily.

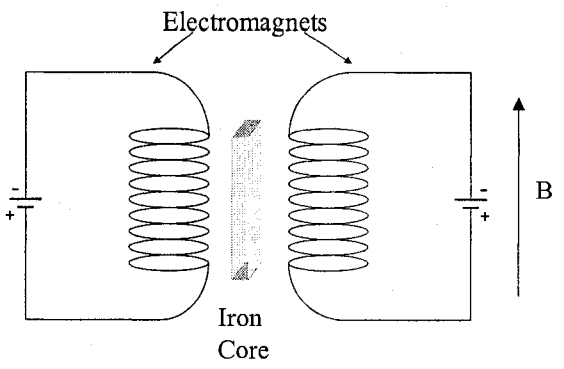

Figure 3.5. A diagram of a magnet in a magnetic analyzer.

A magnetic field allows separating ions traveling in the flight tube according to their momentum, which is governed by the following equation [13]:

$$mv = rBze \tag{3.10}$$

where m and v are the ion's mass and velocity, r is the radius of the curvature of the ion's path, B is the magnetic field, z is the charge of the ion and e is the magnitude of an electron's charge. As discussed in the previous section, all ions leaving the ion source have the same translational kinetic energy. This K.E. can be related to the accelerating voltage (V_{acc}) by the following equation,

$$zeV_{acc} = 1/2mv^2 \tag{3.11}$$

An ion's velocity can thus be determined by the above equation and can be written as,

$$v = \left(\frac{2zeV_{acc}}{m} \right)^{1/2} \tag{3.12}$$

Substituting equation 3.12 into 3.10 establishes the following relationship,

$$m/z = \frac{B^2 r^2 e}{2V_{acc}} \tag{3.13}$$

The radius of the curvature of an ion's path (r) is constant but may vary from instrument to instrument, e is a constant value , V_{acc} can be selected by the operator but is held at a fixed value of 8 kV for all the experiments performed. Thus, an ion with a specific m/z can be selected by varying the magnetic field (B), which is the only parameter altered.

3.2.3 Field Free Region (FFR)

There are three field free regions (FFR) in the VG ZAB mass spectrometer that serve as reaction zones (Figure 3.3). When an ion travels in a FFR, it is not subject to a magnetic or an electric field and it may undergo dissociations either metastably or collisionally induced [11]. Section 3.3.1 and 3.3.2 discusses the nature of these fragmentation reactions.

The second FFR has been modified by an addition of a second collision cell (C2) and a deflector electrode (DE) [14]. The third FFR and consequently ESA2 and the second detector is part of a modification of the VG ZAB which was added to the mass spectrometer [15]. C3, C4 and ESA2 are analogous to C1, C2 and ESA1, respectively, Figure 3.3. These modifications of the instrument enable new experiments to be performed, which are discussed in section 3.3.

3.2.4 Electrostatic Analyzer (ESA)

An electrostatic sector is composed of two curved metal plates to which a potential difference is applied and as a result an electric field is generated [11]. The ions passing through

the sector have a certain translational K.E. which is related to the intensity of the electric field by the following [16],

$$E_K = \frac{zeER}{2} \tag{3.14}$$

where E_K and z is the ion's K.E. and charge, e is the charge of an electron, E is the electric field's intensity and R is the radius of the curvature. By varying the intensity of the electric field (E), ions of specific translational K.E. are selected. Therefore, ESA is really an energy analyzer rather than a mass analyzer. The relationship between an ion's m/z and equation 3.14 will be discussed in chapter 3, section 3.1.

3.2.5 Detector

The detector in the VG ZAB mass spectrometer contains three components: a conversion dynode, a scintillator and a photomultiplier tube, Figure 3.6. As the ion beam emerges from the ESA, it interacts with the conversion dynode which is set at a negative potential (-20 kV) for the detection of positive ions. The resulting collision produces secondary electrons which are then directed towards a CaF_2 scintillator. The electromagnetic radiation produced by the secondary electrons is absorbed by the scintillator and in turn photons with lower energy are emitted [17]. The photons enter the photomultiplier and consequently the signal is amplified. The principal of operation of a photomultiplier is described in the second last paragraph of section 3.1.

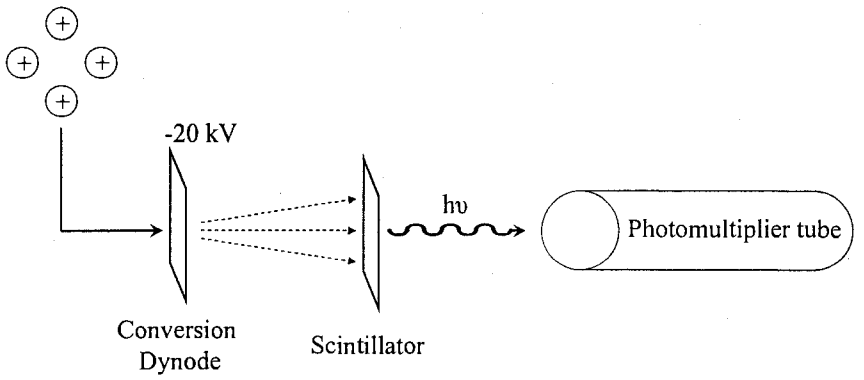

Figure 3.6. A diagram of the VG ZAB detector showing the three main parts: conversion dynode, scintillator and a photomultiplier.

3.3 Experiments performed on VG ZAB mass spectrometer

3.3.1 Mass Analyzed Ion Kinetic Energy Spectrometry (MIKES)

A MIKES experiment incorporates the use of the ESA for the analysis of MI dissociation and CID. In these two types of dissociation, a molecular ion is selected in the magnetic analyzer and then dissociates in the 2nd FFR either metastably (MI dissociation) or through a collision with a target gas (CID). Metastable dissociation refers to a unimolecular decomposition of an ion that has sufficient internal energy acquired in the ion source (i.e. without activation) [18]. An ion $AB^{+\bullet}$ dissociating in the FFR has a translational K.E. that is partitioned between its two fragments: A^+ and $B^\bullet$ [19]. The velocity of the fragment A^+ is the same as of the molecular ion $AB^{+\bullet}$ and thus has a lower K.E. than of the precursor ion. Rearrangement of the K.E. expressions for A^+ and $AB^{+\bullet}$ leads to,

$$v^2 = \frac{2E_{K(A^+)}}{m_{A^+}} \qquad v^2 = \frac{2E_{K(AB^{+\bullet})}}{m_{AB^{+\bullet}}} \tag{3.15}$$

Equating the two expressions above and using the direct proportionality of E_k to E in equation 3.14 allows determining the mass of the fragment ion,

$$m_{A^+} = \frac{E_{A^+}}{E_{AB+\bullet}} m_{AB^{+\bullet}} \tag{3.16}$$

The molecular fragment $AB^{+\bullet}$ passes through the ESA at 8 kV, since it was accelerated by 8 kV in the region following the ion source (see section 3.2.1). Thus, a MIKES scan involves transmitting fragment ions at potentials starting from 8 kV to zero. The resulting spectrum is ion intensity vs. ESA potential which is then converted to ion intensity vs. m/z.

The timescale of experiments for MI is 8-15 μs which means that slower reactions are observed, hence lower internal energy window [20]. The long timescale allows for ions to rearrange prior to dissociation, therefore isomerization in addition to simple bond cleavages must be considered when deducing ion structures. Rearrangements often lead to isomers which are thermodynamically favoured, i.e. more stable structures that have lower heats of formation than the molecular ion.

3.3.2 Collision Induced Dissociation (CID)

Collision induced dissociation in a double and triple focusing mass spectrometer is an effective tool in interpreting ion structure [20]. CID is a high energy process which implies that simple bond cleavages dominate over rearrangements. For this reason, the spectra obtained gives insight to ion connectivity. Ions undergoing CID are ones that do no have sufficient excess

energy to dissociate as in MI dissociation. Hence, it is less likely for ions to rearrange prior to dissociation.

Collision induced dissociation are categorized as a high internal energy processes due to collisional activation. Once an ion is activated, the subsequent rate constants of the fragmentations are high. The dissociation efficiency for fragmentation reactions with rate constants of 10^5 s^{-1} and higher is 100% [20].

The unique quality of a CID is that upon collisions there is no momentum transfer, i.e. the ion trajectory is not disturbed from a collisional event but is rather excited [20]. During the excitation process, some of the ion's original translational K.E. is transferred to internal energy. Following the excitation is the dissociation. The fragment ions produced are then analyzed by the ESA as described in the previous section.

CID experiments can be performed either in 2^{nd} or 3^{rd} FFR. Using the 2^{nd} FFR; an ion (parent or daughter) produced in the ion source is selected in the magnetic sector and fragmented in C1. Using the 3^{rd} FFR; an ion (usually parent ion) is selected in the magnetic sector, dissociates metastably in the 2^{nd} FFR and its corresponding daughter ion is selected in ESA1 and fragmented in C3.

3.3.3 Collision Induced Dissociative Ionization (CIDI)

Collision induced dissociative ionization (CIDI) experiments were also performed for the elucidation of a neutral fragment's structure. The experiment involves deflecting charged fragments from the ion beam by a deflector in the 2nd FFR and exciting the neutral fragment in the C2 [14]. The deflector electrode (DE) which is set to a negative potential (-500 to -1000 V) deflects all positive fragment ions produced in C1 and allows for the neutral counterparts to pass to C2. In C2, the neutral fragments undergo ionization and their dissociations products are analyzed in ESA1. Figure 3.7 clearly illustrates this process.

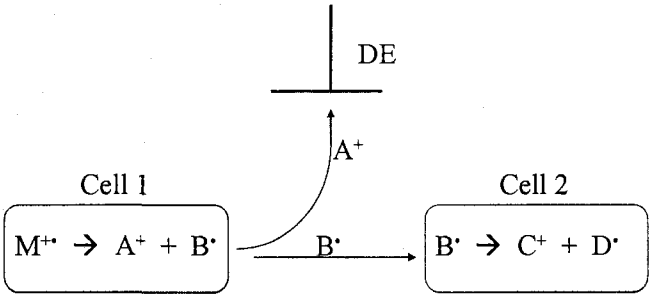

Figure 3.7. Schematic diagram illustrating the collisional processes occurring in the 2nd FFR.

3.4 TPEPICO Spectroscopy

This section describes the design of the TPEPICO (threshold photoelectron photoion coincidence) spectrometer developed by Holland et al. [21]. The TPEPICO spectrometer is comprised of a synchrotron radiation source, time-of-flight (TOF) ion tube, electron & hemispherical analyzer and two detectors (one for ions and another for the electrons), Figure 3.8. The interaction region, situated between the TOF ion tube and electron analyzer is where the gas

phase ion chemistry takes place. In the interaction region, a neutral molecule absorbs a photon with a well defined energy, creating an ion-electron pair. The kinetic energies of the electrons produced are equal to or greater than zero. The unique feature of the TPEPICO instrument is that only electrons with initially zero kinetic energy (threshold electrons) are detected. The electron lens (Figure 3.8) is designed such that upon application of an electric field across the interaction region, the zero kinetic energy electrons are extracted in a linear fashion, while those that have kinetic energies above zero collide with the walls of the tube during their flight. The threshold electrons travel through the hemispherical analyzer and arrive at the detector. As soon as an electron is detected, a voltage is applied across the interaction region to remove the ion; hence the ion is detected in coincidence with the electron.

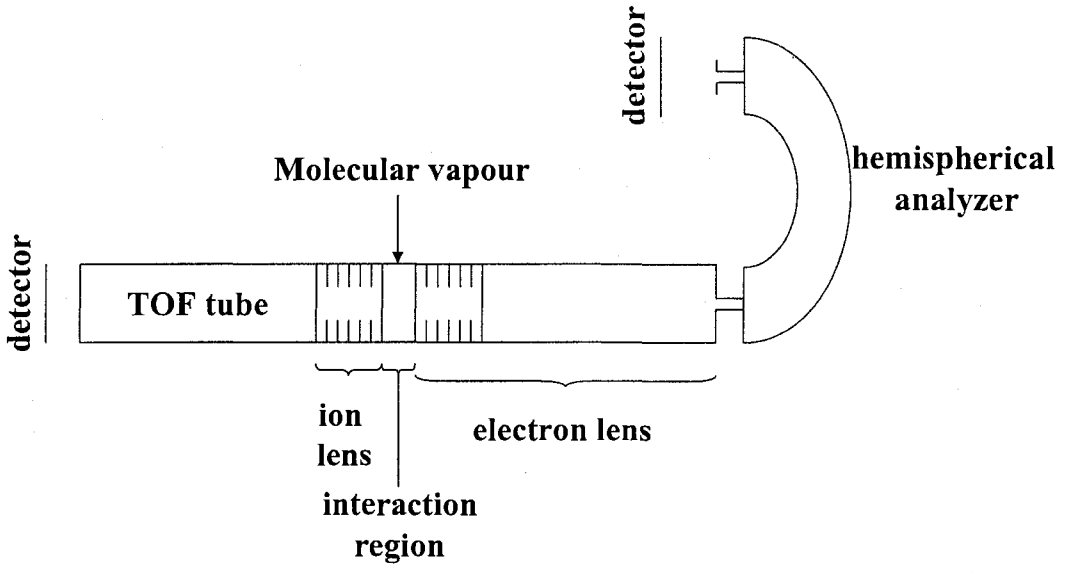

Figure 3.8. A diagram representing a TPEPICO mass spectrometer with the main parts: time-of-flight (TOF) ion tube, electron and hemispherical analyzer .

Fragmentation of the parent ion may occur in the interaction region if sufficient internal energy is acquired. The daughter ion is detected in the same way as the parent ion, i.e. in

coincidence with the threshold electron. The time of flight is defined as the time between the extraction and detection of the parent ion or associated daughter ion.

The Daresbury synchrotron radiation source produces electromagnetic waves (photons) with a continuous distribution [22]. The principle of operation is the acceleration of charged particles (electrons) to relativistic speed in a circular motion. The centripetal acceleration of the electrons causes them to emit radiation. In TPEPICO, the energy of the photon that ionizes the molecule in interest is well defined. Therefore, the continuous distribution of synchrotron radiation must be monochromatized, see Ref. [23] for a detailed description of the monochromator.

3.5 Experiments performed on TPEPICO spectrometer

TPEPICO experiments were carried out in the Daresbury laboratory in United Kingdom by Anne-Marie Boulanger, a former Ph.D. graduate student. She collected breakdown curves and photoelectron spectra for ATB and AA. The analysis of this data is presented in chapters 4 and 5.

3.5.1 Breakdown Curves

Breakdown curves represent the dissociation of the parent ion and formation of the daughter ions as a function of photon energy. The photon energy can later be converted to the internal energy of the ion by the following relationship [24],

$$h\upsilon = I.E. + E_{\text{int}} + E_e \tag{3.17}$$

where *I.E.* is the ionization energy of the neutral molecule, E_{int} is the ion's internal energy and E_e is the kinetic energy of the electron after ionization. Since in TPEPICO, the electrons detected are the ones that have initially zero kinetic energies, the equation above with a rearrangement reduces to,

$$E_{\text{int}} = h\upsilon - I.E. \tag{3.18}$$

The photon energy is well defined by the synchrotron radiation source and the I.E. is calculated using the high accuracy G3 theory [28]. Thus, the internal energy of the molecular ion is easily determined and the resulting spectra are plotted as intensity vs. internal energy. By converting the photon energy to internal energy, RRKM theory can be used to fit the experimental breakdown curves [25].

The residence (or delay) time is defined as the time between the formation of the electron-ion pair and the extraction of the ion from the interaction region [26]. The minimum time required for the coincidence detection is 1.116 μsec. The purpose of the four residence times is to observe the kinetic nature of the fragmentation pathways. If a progressive (i.e. increasing) shift is observed for breakdown curves as the delay time increases then this is an implication that the fragmentation reaction is slow, Figure 3.9(A). If there is no observed shift then this indicates that the fragmentation reaction is fast, Figure 3.9(B). The slow kinetic behaviour can be explained by the following: the longer the time an ion spends in the interaction region the greater the probability that the energy will be distributed in the ion such that a particular vibrational mode will result in decomposition [21]. In a fast system, the rate constant is so high that even if the molecule has more time to distribute its energy it does not affect the

dissociation and hence the breakdown curves are superimposable on each other and there is no kinetic shift. Another useful feature of the residence times is in the fitting process. Breakdown curves at four residence times requires four fits to be generated that satisfy 1 set of two parameters (E_a and $\Delta S^{\ddagger}$) for that one particular system.

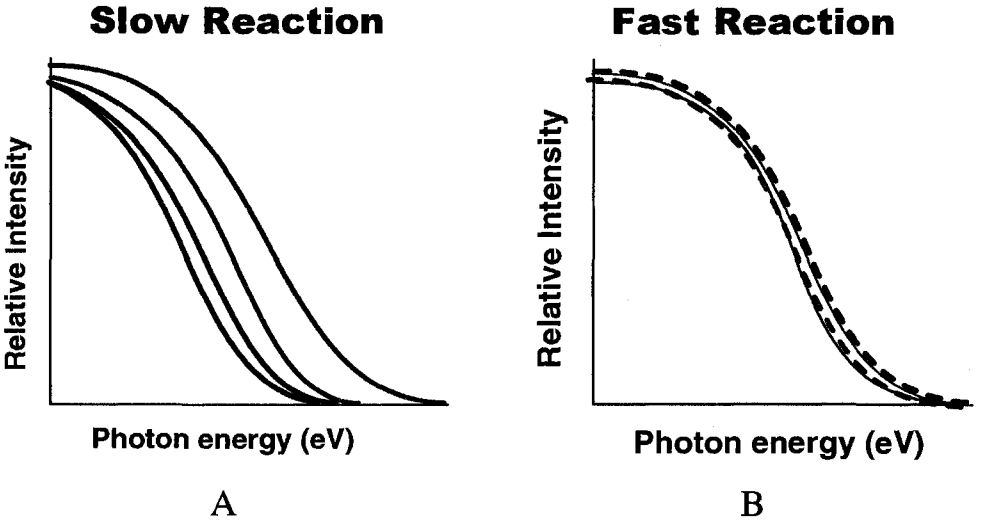

Figure 3.9. Typical breakdown curves showing the kinetic nature of (A) a slow reaction (observed shift) and (B) a fast reaction (no shift). Light blue – 1.116 usec, pink -3.116 usec, green – 5.116 usec and dark blue – 7.116 usec.

3.5.2 Photoelectron Spectrospcopy

Photoelectron spectroscopy is a method used to probe the electronic structure of molecules [27]. The basis of the method is the photoelectric effect which states that electrons will be emitted upon absorption of a photon [12]. Photons with increasingly higher energy are absorbed by electrons in core M.O.'s. The intensity of the electrons emitted is recorded as a function of photon energy. Since in TPEPICO, electrons with zero K.E. are detected, the resulting spectrum reveals ionization energies of M.O.'s.

3.6 Procedures

3.6.1 VG ZAB

The following two tables summarize the types of experiments carried out on the VG ZAB mass spectrometer and the conditions incorporated.

Table 3.1. Tandem mass spectrometry experiments performed on ATB and AA

Type of Experiment	Molecule Analyzed	Fragment and its Source
MI dissociation	ATB	m/z 142
CID	ATB	m/z 142 m/z 85, metastably generated
CIDI	ATB	m/z 57 + 85 amu
MI	AA	m/z 112
CID	AA	m/z 112
CID	AA	m/z 97, metastably generated
KER[a]	AA	m/z 112 and m/z 97 metastably generated

[a] kinetic energy release discussed in chapter 5

Table 3.2. VG ZAB conditions employed

V_{acc} for electrons in the ion source	70 V
V_{acc} for ions	8 kV
C1 target gas	He[a]
C2 target gas	O_2[b]
C3 target gas	He[a]

[a] For CID experiments, He gas was used for cell 1 and cell 3

b For CIDI experiments, He gas was used for cell 1 and O_2 gas for cell 2.

3.6.2 TPEPICO

The data for the breakdown curves are generated by obtaining a mass spectrum at each photon energy with an interval of 0.05 eV. The intensity of each peak is then recorded as a function of photon energy. The data is further normalized such that the sum of the intensities of all peaks at each photon energy is equal to 1. For ATB, the data for the breakdown curves were recorded at photon energies from 7.45 to 10.20 eV for 1.116 μsec residence time and 7.45 to 8.30 eV for 3.116, 5.116 and 7.116 μsec residence times. The dissociation at higher photon energies was not examined due to an impurity in the sample that ionizes at higher energies. For AA, the data for the breakdown curves was collected at photon energies from 9.10 to 25.00 eV for 1.116 μsec residence time and 9.10 to 10.05 eV for 3.116, 5.116 and 7.116 μsec residence times.

The data for the photoelectron specta of azo-tert-butane and acetone azine were collected at photon energies in the range of 7.20 to 10.50 eV and 7.60 to 32.15 eV, respectively.

The electron transmission function was measured by the photoionization of Krypton under the conditions used in the TPEPICO measurements as a threshold electron spectrum [21].

3.6.3 Materials

Acetone azine (98%) and azo-tert-butane (97%) were purchased from Sigma-Aldrich and were used without further purification for the VG ZAB experiments. For the TPEPICO experiments, each sample was subject to three freeze-pump-thaw cycles to remove air [28].

References

[1] F.H. Field, J.L. Franklin, *Electron Impact Phenomena – and the properties of gaseous ions*, 1957, New York: Academic Press.

[2] J. Berkowitz, *Photoabsorption Photoionization and Photoelectron Spectroscopy*, 1979, New York: Academic Press.

[3] A.G. Harrison, *Chemical Ionization Mass Spectrometry*, 1983, Boca Raton: CRC Press.

[4] M. Barber, R.S. Bordoli, G.J. Elliot, R.D. Sedgwick, A.N. Tyler, *Anal. Chem.* 1982, 54, 645A-657A.

[5] S.J. Gaskell, Electrospray: principles and practice, *J. Mass Spectrom.* 1997, 32, 677-688.

[6] M. Karas, F. Hillenkamp, *Anal. Chem.* 1988, 60, 2299-2301.

[7] H.E. Taylor, *Inductively Coupled Plasma Mass Spectrometry – Practices and Techniques*, 2001, San Diego: Academic Press.

[8] K.L. Busch, G.L. Glish, S.A. McLuckey, *Mass Spectrometry/Mass Spectrometry – Techniques and Applications of Tandem Mass Spectrometry*, 1988, New York: VCH Publishers.

[9] D.A. Skoog, F.J. Holler, T.A. Nieman, *Principles of Instrumental Analysis*, 1998, Philadelphia: Saunders College Publishing.

[10] R. Davis, M. Frearson, *Mass Spectrometry – Analytical Chemistry by Open Learning*, 1987, London: John Wiley & Sons.

[11] P.M. Mayer, *The Encyclopedia of Chemical Physics and Physical Chemistry*, J.H. Moore, N.D. Spencer, Editors. Vol 2. 2001, Bristol and Philadelphia: Institute of Physics Publishing. p. 1151-1152.

[12] D. Halliday, R. Resnick, J. Walker, *Fundamentals of Physics*, 2003, Hoboken, NJ: John Wiley & Sons.

[13] R.G. Cooks, J.H. Beynon, R.M. Caprioli, G.R. Lester, *Metastable Ions*, 1973, Amsterdam: Elsevier Scientific Publishing.

[14] J.L. Holmes, A.A. Mommers, J.K. Terlouw, C.E.C.A. Hop, *Int. J. Mass Spectrom. Ion Processes* 1986, 68, 249-264.

[15] J.L. Holmes, P.M. Mayer, *J. Phys. Chem.* 1995, 99, 1366-1370.

[16] K.R. Jennings, *Ionic Processes in the Gas Phase*, A. Ferreira, Editor. Vol 118. 1984, Holland: D. Reidel Publishing.

[17] R.S. Khandpur, *Handbook of Analytical Instruments*, 2007, New York: McGraw-Hill Companies.

[18] T. Baer, *Gas Phase Ion Chemistry*, M.T. Bowers, Editors. Vol 1. 1979, New York: Academic Press.

[19] E. de Hoffmann, V. Stroobant, *Mass Spectrometry – Principles and Applications*, 2007, Chichester: John Wiley & Sons.

[20] J.L. Holmes, A. Christiane, P.M. Mayer, *Assigning Structures to Ions in Mass Spectrometry*, 2007, Boca Raton: CRC Press.

[21] D.M.P. Holland, D.A. Shaw, I. Sumner, M.A. Hayes, R.A. Mackie, B. Wannberg, L.G. Shpinkova, E.E. Rennie, L. Cooper, C.A.F. Johnson, J.E. Parker, *Nucl. Instr. Meth. Phys. Res. B* 2001, 179, 436-454.

[22] V. Schmidt, *Electron Spectrometry of Atoms using Synchrotron Radiation*, 1997, Cambridge: Cambridge University Press.

[23] D.M.P. Holland, J.B. West, A.A. Macdowell, I.H. Munro, A.G. Beckett, *Nucl. Instrum. Methods Phys. Res., Sect. B* 1989, 44, 233-241.

[24] R. Stockbauer, *Int. J. Mass Spectrom. Ion Phys.*, 1977, 25, 89-101.

[25] O. Dutuit, *Fundamentals of Gas Phase Ion Chemistry*, K.R. Jennings, Editor. Vol C 347. 1991, Dordrecht: Kluwer Academic Publishers. p. 21-54.

[26] E.E. Rennie, L. Cooper, C.A.F. Johnson, J.E. Parker, R.A. Mackie, L.G. Shpinkova, D.M.P. Holland, D.A. Shaw, M.A. Hayes, *Chem. Phys.* 2001, 263, 149-165.

[27] J.H.D. Eland, *Photoelectron Spectroscopy*, 1984, London: Butterworth & Co Publishers.

[28] A.M. Boulanger, E.E. Rennie, D.M.P. Holland, D.A. Shaw, P.M. Mayer, *J. Phys. Chem. A* 2007, 111, 5388-5398.

Chapter 4

Results and Discussion for Azo-tert-butane

Ionized azo-tert-butane (m/z 142) has three fragmentation pathways: formation of the t-butyl cation (1), the t-butyl + N_2 cation (2) and an isobutene cation (3), Scheme 4.1. This is observed both in TPEPICO (threshold photoelectron photoion coincidence) spectroscopy and tandem mass spectrometry.

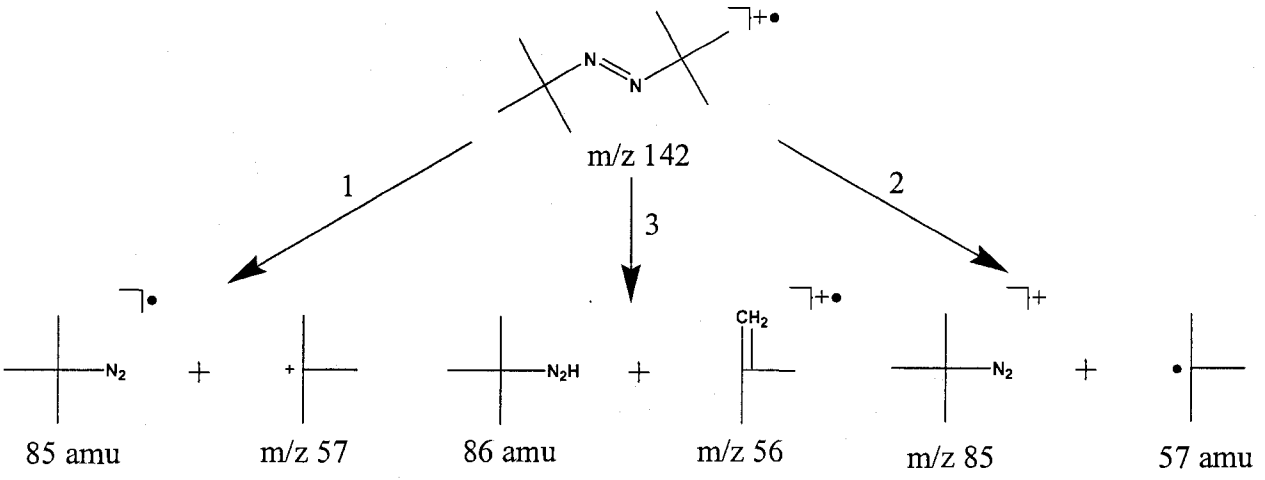

Scheme 4.1. The three fragmentation pathways of Azo-tert-butane (m/z 142), showing general unoptimized structures.

In tandem mass spectrometry, the dominant fragmentation pathways when m/z 142 dissociates metastably are reactions 2 & 3, Figure 4.1. CID of m/z 142 generates mainly m/z 57 (reaction 1). This phenomenon suggests that reaction 1 is a high energy channel relative to

reactions 2 & 3 (see chapter 3, sections 3.1 & 3.2). A high or low energy channel refers to a molecular ion that has a high or low internal energy, respectively (see chapter 2, section 2.2).

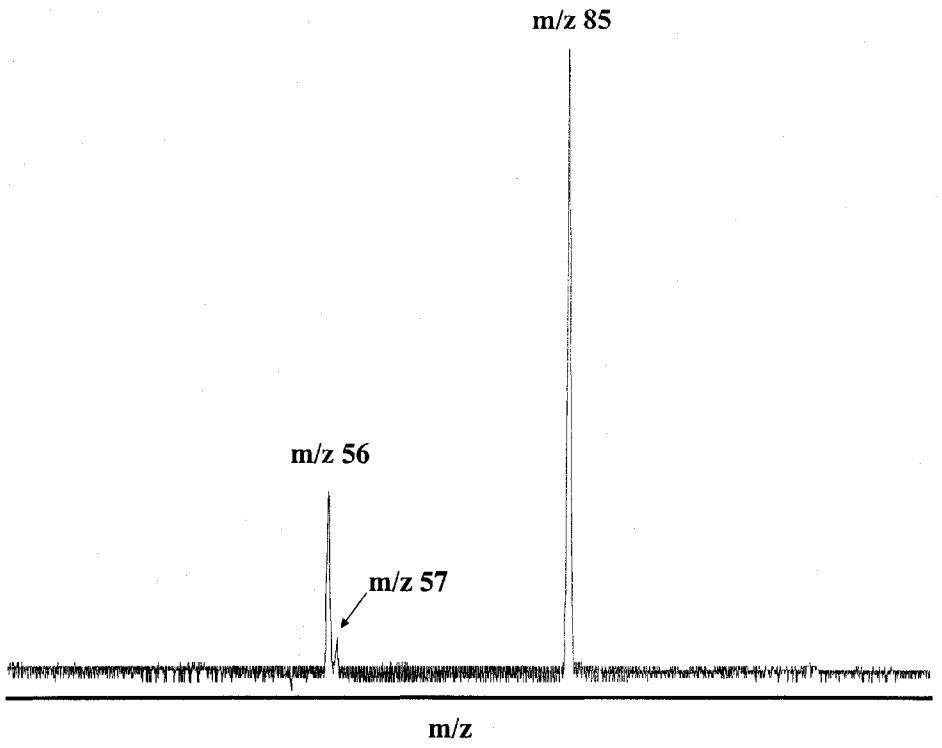

Figure 4.1. Mass spectrum of m/z 142 showing MI peaks, m/z 85 and m/z 56.

In TPEPICO spectroscopy, the dominant dissociation channel is formation of m/z 57 (reaction 1), while formation of m/z 85 and m/z 56 are less important, Figure 4.2. This agrees well with the tandem mass spectrometry results. The time (t) window of observation in TPEPICO is $t \leq 1.116$ to $t \leq 7.116$ μsec, while that in MI dissociation is $8 \leq t \leq 15$ μsec (see chapter 2, section 2.2). This means that higher internal energy ions can contribute to the TPEPICO spectra, resulting in m/z 57 being the dominant channel. Comparing the breakdown curves at the four delay times (1.116, 3.116, 5.116 and 7.116 μsec) indicates that the fragmentation reactions are fast (see chapter 3, section 5.1), Figure 4.3.

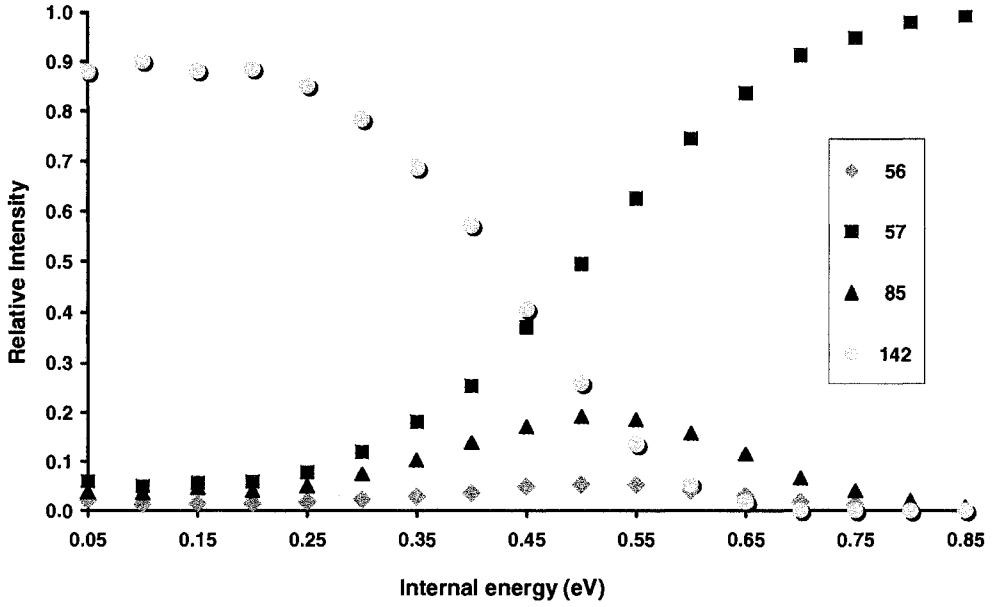

Figure 4.2. TPEPICO breakdown curve of ionized azo-tert-butane (m/z 142) at 1.116 μsec delay time, showing the three dissociation channels: m/z 57, m/z 85 and m/z 56.

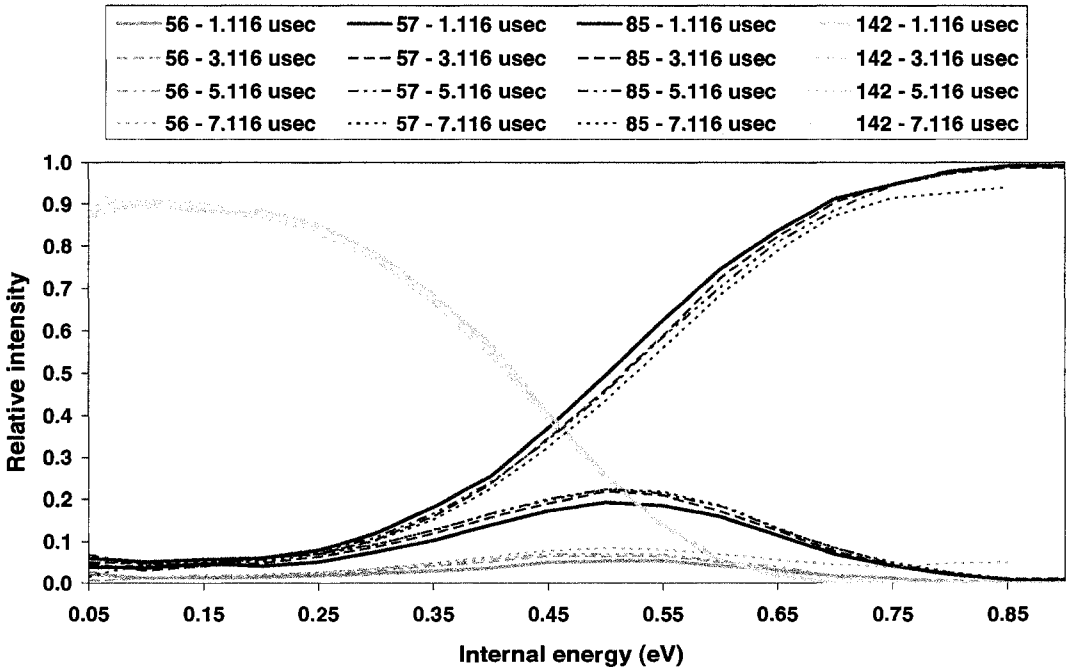

Figure 4.3. TPEPICO breakdown curve of ionized azo-tert-butane (m/z 142) at four delay times (1.116, 3.116, 5.116 and 7.116 μsec).

Six theoretical fits were obtained for the experimental breakdown curves of ionized azo-tert-butane at the four delay times (1.116, 3.116, 5.116 and 7.116 μsec). The best fit is shown in

Figure 4.4. Table 4.1 summarizes the activation energies (E_0) and entropies ($\Delta S^{\ddagger}$) obtained from the six fits. The free rotor model takes into account internal rotations, such as methyl torsions that are counted as vibrational modes in the harmonic oscillator model and treats them as free rotors, thereby making the molecule unhindered [1]. According to the harmonic oscillator model, the entropies of activation ($\Delta S^{\ddagger}$) for formation of fragment ions m/z 57, m/z 85 and m/z 56 are 17 ± 1, -49 ± 4 and -90 J K^{-1} mol^{-1}, respectively, Table 4.2. As discussed in chapter 2, section 2.1, positive and negative values of $\Delta S^{\ddagger}$ tend to imply that reactions occur by simple bond cleavages and rearrangements, respectively. The vibrational frequencies of ionized azo-tert-butane calculated at the B3LYP/6-31+G(d) level of theory and the scaled vibrational frequencies of the transition statse corresponding to the three dissociation channels that were used in the best fit are listed in Table 4.3.

Table 4.1. Summary of the activation energies (E_0) and entropies ($\Delta S^{\ddagger}$) obtained from RRKM fits and the free rotor model

	E_0 (eV)			$\Delta S^{\ddagger}$ (harmonic oscillator)[a]			$\Delta S^{\ddagger}$ (free rotor)[a]		
Fit	m/z 57	m/z 85	m/z 56	m/z 57	m/z 85	m/z 56	m/z 57	m/z 85	m/z 56
1	0.540	0.430	0.410	18	-47	-90	14	-45	-82
2	0.540	0.430	0.410	18	-49	-90	14	-43	-82
3	0.540	0.430	0.410	18	-47	-90	14	-45	-82
4	0.540	0.430	0.410	17	-53	-90	14	-47	-82
5	0.530	0.425	0.410	16	-51	-90	13	-45	-82
6	0.530	0.425	0.410	16	-47	-90	13	-41	-82

[a] values are in J K^{-1} mol^{-1} at 600K

Table 4.2. Average values for activation energies (E_0) and entropies ($\Delta S^{\ddagger}$) obtained from RRKM fits and the free rotor model for fragment ions m/z 57, m/z 85 and m/z 56

m/z	E_0 (eV)	$\Delta S^{\ddagger}$ (harmonic oscillator)[a]	$\Delta S^{\ddagger}$ (free rotor)[a]
57	0.537 ± 0.007	17 ± 1	14 ± 1
85	0.428 ± 0.003	-49 ± 4	-44 ± 3
56	0.410	-90	-82

[a] values are in J K^{-1} mol^{-1} at 600K

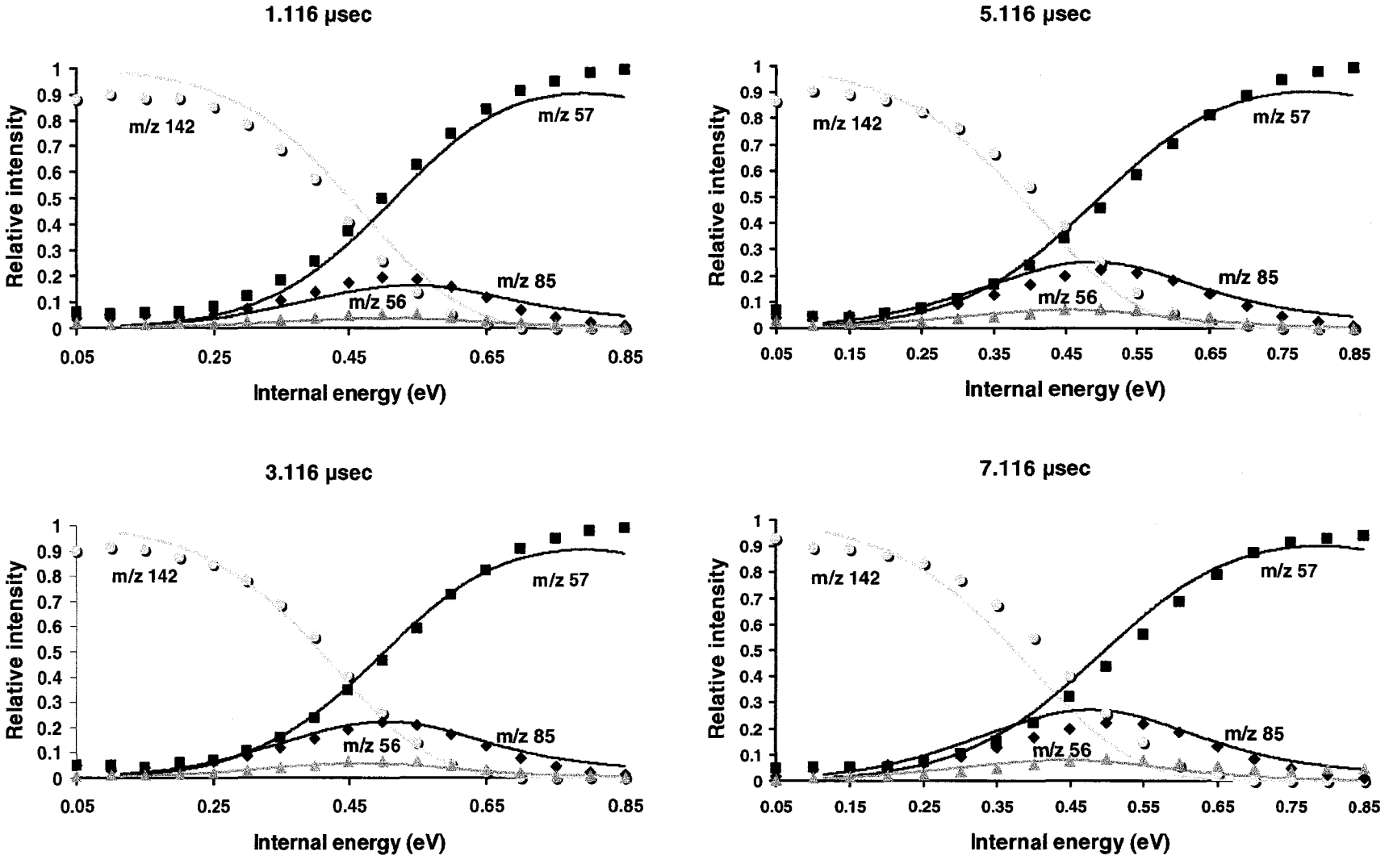

Figure 4.4. Best theoretical fit (solid line) to the experimental breakdown curves of m/z 142, m/z 57, m/z 85 and m/z 56 at four delay times (1.116, 3.116, 5.116 and 7.116 µsec).

Table 4.3. Vibrational frequencies and rotational constants used in the best fit of ionized ATB and transition states corresponding to formation of m/z 57, m/z 85 and m/z 56

Ionized azo-tert-butane		Transition state 1[c]		Transition state 2[c]		Transition state 3[c]	
ν (cm^{-1})[a]	A, B & C (GHz)[b]	ν (cm^{-1})[a]	A, B & C (GHz)[b]	ν (cm^{-1})[a]	A, B & C (GHz)[b]	ν (cm^{-1})[a]	A, B & C (GHz)[b]
9.5309	2,1	5.9092	2,1	28.5928	2,1	96.2624	2,1
75.0460		46.5285		225.1381		757.9648	
76.9680		47.7201		230.9039		777.3763	
87.9381		54.5216		263.8143		888.1749	
202.5192		125.5619		607.5576		2045.4439	
203.9491		203.9491		203.9491		203.9491	
207.9933		207.9933		207.9933		207.9933	
246.3933		246.3933		246.3933		246.3933	
260.8385		260.8385		260.8385		260.8385	
261.1342		261.1342		261.1342		261.1342	
263.8051		263.8051		263.8051		263.8051	
269.0647		269.0647		269.0647		269.0647	
325.5612		325.5612		325.5612		325.5612	
329.0200		329.0200		329.0200		329.0200	
329.7363		329.7363		329.7363		329.7363	
369.7668		369.7668		369.7668		369.7668	
413.6148		413.6148		413.6148		413.6148	
437.8595		437.8595		437.8595		437.8595	
440.8331		440.8331		440.8331		440.8331	
469.1209		469.1209		469.1209		469.1209	
479.4716		479.4716		479.4716		479.4716	
594.8611		594.8611		594.8611		594.8611	
652.2514		652.2514		652.2514		652.2514	
743.2344		743.2344		743.2344		743.2344	
748.1677		748.1677		748.1677		748.1677	
897.0338		897.0338		897.0338		897.0338	
897.2830		897.2830		897.2830		897.2830	
903.9113		903.9113		903.9113		903.9113	
904.1415		904.1415		904.1415		904.1415	
952.0262		952.0262		952.0262		952.0262	
952.2446		952.2446		952.2446		952.2446	
1004.8170		1004.8170		1004.8170		1004.8170	
1009.5685		1009.5685		1009.5685		1009.5685	
1015.1501		1015.1501		1015.1501		1015.1501	
1023.0751		1023.0751		1023.0751		1023.0751	
1121.0939		1121.0939		1121.0939		1121.0939	
1131.1538		1202.0037		1202.0037		1202.0037	
1202.0037		1208.1148		1208.1148		1208.1148	
1208.1148		1217.1785		1217.1785		1217.1785	
1217.1785		1227.4268		1227.4268		1227.4268	
1227.4268		1366.8275		1366.8275		1366.8275	
1366.8275		1367.7350		1367.7350		1367.7350	
1367.7350		1371.9155		1371.9155		1371.9155	
1371.9155		1373.0888		1373.0888		1373.0888	
1373.0888		1398.3875		1398.3875		1398.3875	
1398.3875		1400.4995		1400.4995		1400.4995	
1400.4995		1432.4357		1432.4357		1432.4357	
1432.4357		1432.9475		1432.9475		1432.9475	
1432.9475		1443.4135		1443.4135		1443.4135	
1443.4135		1443.7212		1443.7212		1443.7212	
1443.7212		1447.9241		1447.9241		1447.9241	
1447.9241		1448.3792		1448.3792		1448.3792	
1448.3792		1456.0561		1456.0561		1456.0561	

Table 4.3. (Continued)

Ionized azo-tert-butane		Transition state 1[c]		Transition state 2[c]		Transition state 3[c]	
ν (cm^{-1})[a]	A, B & C (GHz)[b]	ν (cm^{-1})[a]	A, B & C (GHz)[b]	ν (cm^{-1})[a]	A, B & C (GHz)[b]	ν (cm^{-1})[a]	A, B & C (GHz)[b]
1456.0561		1456.4126		1456.4126		1456.4126	
1456.4126		1460.4164		1460.4164		1460.4164	
1460.4164		1461.3536		1461.3536		1461.3536	
1461.3536		1478.2440		1478.2440		1478.2440	
1478.2440		1478.6842		1478.6842		1478.6842	
1478.6842		1869.3885		1869.3885		1869.3885	
1869.3885		2947.4379		2947.4379		2947.4379	
2947.4379		2947.5009		2947.5009		2947.5009	
2947.5009		2948.6119		2948.6119		2948.6119	
2948.6119		2948.6963		2948.6963		2948.6963	
2948.6963		2953.1905		2953.1905		2953.1905	
2953.1905		2953.4504		2953.4504		2953.4504	
2953.4504		3018.8990		3018.8990		3018.8990	
3018.8990		3019.0749		3019.0749		3019.0749	
3019.0749		3020.2575		3020.2575		3020.2575	
3020.2575		3020.4337		3020.4337		3020.4337	
3020.4337		3024.8177		3024.8177		3024.8177	
3024.8177		3024.9475		3024.9475		3024.9475	
3024.9475		3026.1114		3026.1114		3026.1114	
3026.1114		3026.3178		3026.3178		3026.3178	
3026.3178		3027.8191		3027.8191		3027.8191	
3027.8191		3027.8677		3027.8677		3027.8677	
3027.8677		3030.6625		3030.6625		3030.6625	
3030.6625		3030.7809		3030.7809		3030.7809	
3030.7809							

[a] vibrational frequencies

[b] 1 is the rounded average of the two lowest rotational constants (0.71347 and 0.71018 GHz)

[c] transition states 1, 2 and 3 correspond to formation of m/z 57, m/z 85 and m/z 56, respectively

The experimental study is coupled to theoretical calculations which allow us to better understand gas phase ion chemistry. The theoretical study involves geometry optimizations and energy calculations of each species observed in the mass spectrometer performed at the G3 and three density functional levels of theory, namely, B3LYP, B3PW91 and BHandHLYP to establish the most suitable level of theory. The assessment is performed via two ways: first by comparing geometric parameters of the neutral and ionized azo-tert-butane (ATB) and second by comparing the relative energies of each dissociation channel, Tables 4.4, 4.5 and 4.6. Table 4.4 demonstrates that there is no significant difference in the geometric parameter values (e.g. R_{NN} = 1.236, 1.234, 1.220 Å for B3LYP, B3PW91 and BHandHLYP, respectively) between the

theories and thus all are equally suitable. The appropriate situation for discarding a particular level of theory would be when several parameters are different then at the other levels of theory.

Table 4.4. Optimized geometric parameters[a] of neutral and ionized azo-tert-butane

Level of theory	R_{NN}	R_{CN}	R_{CC}	<NNC	<NCC1	<NCC2	<CCC	<CNNC
			Neutral Azo-tert-butane					
B3LYP	1.236	1.497	1.532	115.3	114.5	105.1	110.0	180.0
B3PW91	1.234	1.489	1.527	115.1	114.5	105.1	109.9	180.0
BHandBHLYP	1.220	1.479	1.522	115.7	114.4	105.3	110.0	180.0
			Ionized Azo-tert-butane					
B3LYP	1.174	1.543	1.531	130.3	108.7	104.5	112.1	179.8
B3PW91	1.173	1.520	1.527	130.5	109.0	104.7	111.8	179.9
BHandBHLYP	1.156	1.532	1.520	130.9	108.5	104.6	112.2	180.0

[a] bond lengths (R) are in Å and angles (<) in degrees

According to Table 4.5, which lists the relative energies at B3LYP, B3PW91 and BHandHLYP levels of theory, B3PW91 appears to be inconsistent with the other two theories, for each dissociation channel. For example, formation of m/z 57, the B3PW91 relative energy is 44 kJ mol^{-1}, while the B3LYP and BHandHLYP relative energies are 25 and 23 kJ mol^{-1}, respectively. However, the G3 calculations show that all three levels of theory (B3LYP, B3PW91 and BHandHLYP) are compatible and any one can be chosen, Table 4.6. B3LYP was selected since it's a commonly used computational method. Hence, all theoretical fits and comparisons between experiment and theory are carried out with the geometries and frequencies obtained from B3LYP and energies from G3 (B3LYP).

Table 4.5. Comparison of the relative energies of the fragment ions and neutrals of ionized azo-tert-butane at three different levels of theory (B3LYP, B3PW91, BHandHLYP)

	$((CH_3)_3CN)_2^{+\bullet}$		$(CH_3)_3C^+ + N_2C(CH_3)_3^\bullet$		$(CH_3)_3C^\bullet + N_2C(CH_3)_3^+$		$(CH_3)_2CCH_2^{+\bullet} + HN_2C(CH_3)_3$	
Level of Theory	Absolute[a]	Relative[b]	Absolute	Relative	Absolute	Relative	Absolute	Relative
B3LYP	-424.66478	0	-424.65507	25	-424.65694	21	-424.58090	220
B3PW91	-424.50685	0	-424.48997	44	-424.49140	41	-424.41856	232
BHandBHLYP	-424.37106	0	-424.36220	23	-424.36452	17	-424.28672	221

[a] absolute energy values are in hartrees

[b] relative energy values are in kJ mol^{-1}

Table 4.6. Comparison of the relative energies of the fragment ions and neutrals of ionized azo-tert-butane at the G3 level of theory

	$((CH_3)_3CN)_2^{+\bullet}$		$(CH_3)_3C^+ + N_2C(CH_3)_3^\bullet$		$(CH_3)_3C^\bullet + N_2C(CH_3)_3^+$		$(CH_3)_2CCH_2^{+\bullet} + HN_2C(CH_3)_3$	
Level of Theory[c]	Absolute[a]	Relative[b]	Absolute	Relative	Absolute	Relative	Absolute	Relative
G3 (B3LYP)	-424.48099	0	-424.45721	62	-424.46126	52	-424.38239	259
G3 (B3PW91)	-424.48064	0	-424.45763	60	-424.46141	51	-424.38266	257
G3 (BHandBHLYP)	-424.47248	0	-424.44943	61	-424.45345	50	-424.37330	260

[a] absolute energy values are in hartrees

[b] relative energy values are in kJ mol^{-1}

[c] G3 calculation using the optimized geometries obtained at the B3LYP, B3PW91 and BHandHLYP level of theory

For each species, there were several structures that were considered for the geometry optimizations. The structures with the lowest energy were chosen for the energy assessment of the three density functional theories. The optimized structures of neutral and ionized azo-tert-butane and its corresponding fragments are presented in Figure 4.5. The initial structures for optimization of neutral and ionized azo-tert-butane were taken from NIST and Aldrich [2-3]. The structures of fragment ion m/z 57 and neutral fragment 57 amu are straight forward; both structures optimized to a planar configuration. Fragment ion m/z 56 optimized to an isobutene like structure. Its constituent neutral fragment (86 amu) is one with a H-shift from a methyl to the nearest nitrogen. Fragment ion m/z 85 optimized to a complex like structure comprising of t-butyl and N_2. Several initial structures of intact fragment ion m/z 85 formed by a simple bond cleavage were optimized, yet all attempts lead to the complex like structure. Similar results were observed for neutral fragment 85 amu, where the intact structure optimized to a complex like structure. However, since this "complex" is neutral, there are only weak forces holding the t-butyl and N_2 parts together. Whereas in the charged complex, the positive charge on t-butyl may be interacting with the N_2 lone pairs. The structure for neutral fragment 85 amu shown in Figure 4.5 is in fact a transition state with one imaginary frequency. The energy for this transition state is the one used in the energy assessment tables (4.5 and 4.6).

To determine what actually takes place in the mass spectrometer, the energy of each complex were compared with the separated fragment energies, Table 4.7. From this table, it is clear that the energy difference between the neutral complex and its separated fragments is very small (1.16 kJ mol^{-1}), hence upon formation of the neutral complex it immediately breaks into

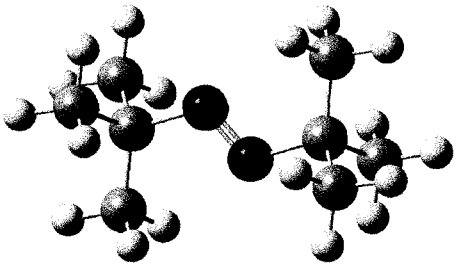

Neutral Azo-tert-butane

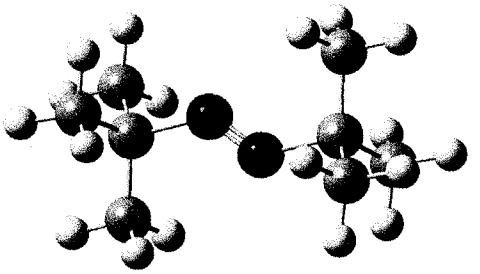

Ionized Azo-tert-butane

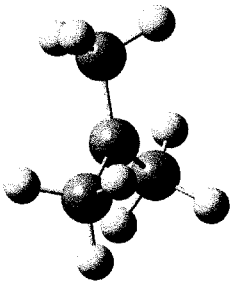

m/z 57

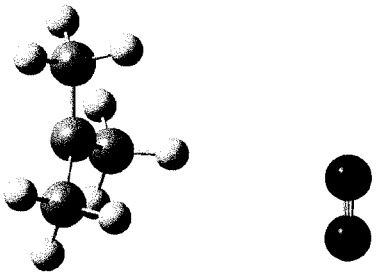

85 amu

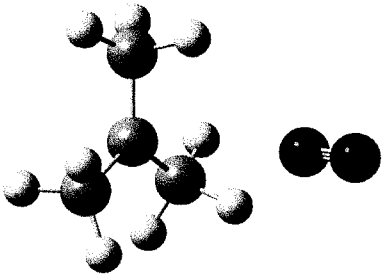

m/z 85

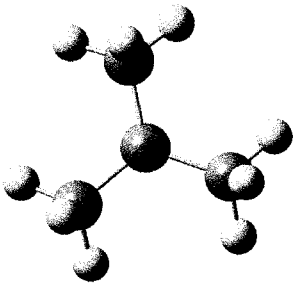

57 amu

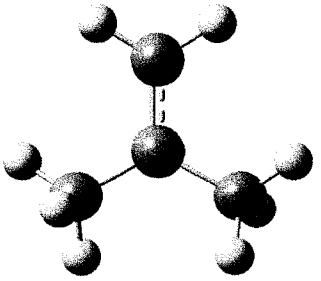

m/z 56

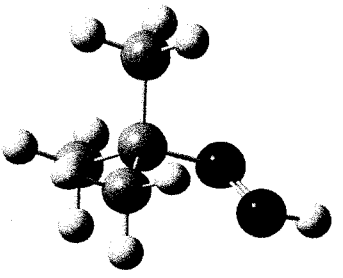

86 amu

Figure 4.5. Optimized structures of neutral and ionized azo-tert-butane and its corresponding fragments.

corresponding constituents. While the charged complex has a significant energy difference from its separated fragments (11.76 kJ mol^{-1}), hence it is more likely that it stays as an intact complex.

Table 4.7. Comparison of absolute[a] and relative[b] energies[c] of the charged and neutral complex (m/z 85 & 85 amu) with its corresponding separated fragments

Energy	$N_2C(CH_3)_3^+$	$(CH_3)_3C^+ + N_2$	$N_2C(CH_3)_3\bullet$	$(CH_3)_3C\bullet + N_2$
Absolute	-266.84995	-266.84547	-267.09781	-267.09737
Relative	0	11.76	0	1.16

[a] absolute energy values are in hartrees
[b] relative energy values are in kJ mol^{-1}
[c] G3(B3LYP) energies

The negative value for entropy of activation (-49 ± 4 J K^{-1} mol^{-1}) for t-butyl radical loss (m/z 85) suggests that a rearrangement as opposed to a simple bond cleavage takes place. There are two scenarios for formation of fragment ion m/z 85: isomerization or a simple bond cleavage, Figure 4.6. If a rearrangement occurs then the G3 value for the products should be lower then the activation energy, [4]. If a simple bond cleavage occurs then the G3 value for the products should be slightly higher then the activation energy. The comparison between the G3 relative energy (0.643 eV) and the activation energy (0.537 eV) point to case b, a simple bond cleavage reaction, Table 4.8. Alternatively, formation of fragment ions m/z 57 and m/z 85 occur by the same (C-N) bond cleavage and the only difference is the charge transfer, which moves either to the t-butyl or t-butyl + N_2 part. Therefore, we propose that, formation of fragment ion m/z 85 occurs by a simple bond cleavage with a transition state that is tighter than for formation of fragment ion m/z 57, which has a positive value for its entropy of activation (17 ± 1 J K^{-1} mol^{-1}), see chapter 2, section 2.1. The neutral counterpart of m/z 57 ($(CH_3)_3C\bullet + N_2$) is entropically more favoured than for m/z 85 ($(CH_3)_3C\bullet$), hence the reason for a more positive value for $\Delta S^{\ddagger}$.

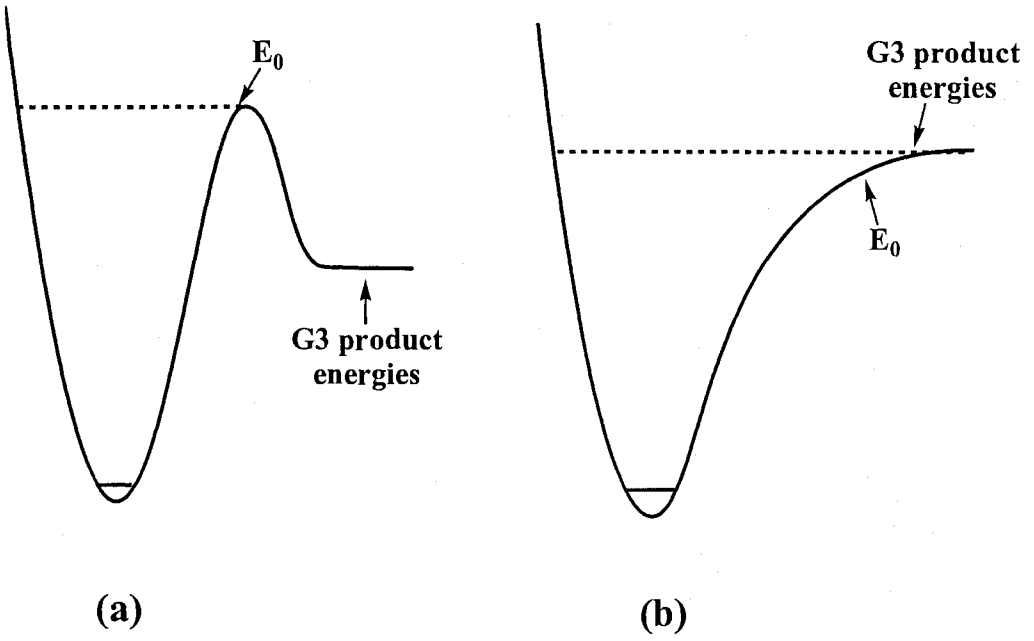

Figure 4.6. Typical potential energy surface diagrams for (a) rearrangement reaction and (b) simple bond cleavage. In case (a) E_0 > G3 product energies and case (b) E_0 < G3 product energies.

Table 4.8. Comparison of the G3 relative energies[a] of the dissociation products of ionzed ATB with the E_0 [b] obtained from RRKM theory

Theory	$(CH_3)_3C^+ + N_2C(CH_3)_3^{\bullet}$	$(CH_3)_3C^{\bullet} + N_2C(CH_3)_3^+$	$(CH_3)_2CCH_2^{+\bullet} + HN_2C(CH_3)_3$
G3 (B3LYP)	0.643	0.539	2.68
RRKM	0.537	0.428	0.41

[a] value taken from Table 4.6 and converted from kJ mol^{-1} to eV

[b] values are in eV

Formation of fragment ion m/z 57 is straight forward, it has a positive entropy of activation (17 ± 1 J K^{-1} mol^{-1}) and the G3 product energies (0.643 eV) are higher than the activation energy (0.537 eV), hence a simple bond cleavage reaction, Tables 4.2 & 4.8.

The entropy of activation ($\Delta S^{\ddagger}$) for formation of fragment ion m/z 56 is more negative by a significant amount than for formation of fragment ion m/z 57 ($17 > -90$ J K^{-1} mol^{-1}). The atom

connectivity of ionized ATB does not allow fragment ion m/z 56 to be formed through a single bond dissociation but rather through a H shift. Hence, we propose that this dissociation channel takes place by a rearrangement process. The G3 product energies (2.68 eV) are way above the activation energy (0.41 eV), Table 4.8, suggesting that product geometries used in the calculation do not correspond to the actual products being formed. Fragment ion m/z 56 has a molecular formula of $C_4H_8^+$ and several isomeric forms [5-6]. While its neutral counterpart 86 amu also has several isomeric forms, such as a H shift to a C or the second nitrogen, Figure 4.5. To determine the actual structures being formed, an extensive computational study has to be taken. Since this is a small dissociation channel (Figure 4.3), its significance is minimal and thus no further studies were conducted.

Tandem mass spectrometry experiments, namely CID and CIDI, were used to characterize the structures of ionized and neutral fragments m/z 85 and 85 amu, respectively. The CID mass spectrum of fragment ion m/z 85 generated metastably reveals that the dominant peak is m/z 57, Figure 4.7. Hence, the structure of fragment ion m/z 85 is not a rearranged one but rather contains an N_2 and t-butyl moiety; this agrees well with the TPEPCIO, RRKM and computational results. The main purpose of the CIDI experiment was to see whether neutral fragment 85 can be observed intact. However, only its fragments were observed (Figure 4.8), which leads to the thought that it has a very low stability and dissociates immediately. This agrees well with the computational result that shows that the neutral complex (85 amu) is not very stable, Table 4.7. Most importantly, m/z 57 was observed. However, other fragments such as, m/z 41 and m/z 39 were also observed. The latter two fragments could be daughter ions of m/z 57.

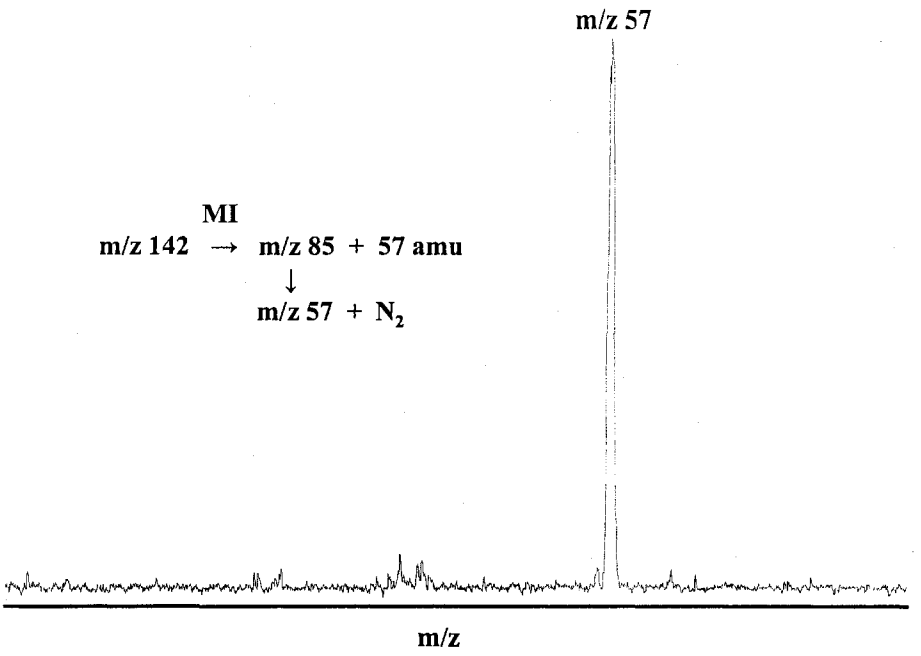

Figure 4.7. CID spectrum of fragment ion m/z 85 generated from the metastable dissociation of the parent ion (m/z 142).

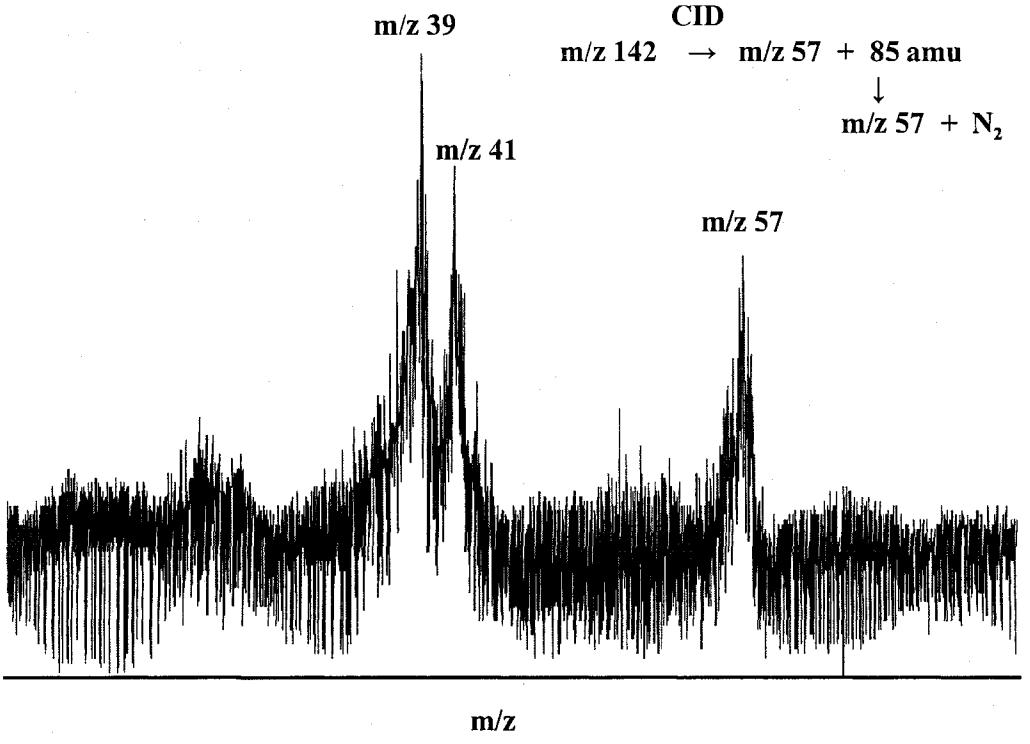

Figure 4.8. CIDI spectrum of neutral fragment 85 amu generated through CID of m/z 142.

Threshold Photoelectron Spectrum

The threshold photoelectron spectrum (PES) was recorded up to 10.50 eV of photon energy due to an impurity that ionizes beyond this energy. For this reason, the threshold photoelectron spectrum (PES) reveals a single band at 8.10 eV that corresponds to the vertical ionization of azo-tert-butane (ATB), Figure 4.9. According to the ROVGF/6-31+G(d) calculation, the highest occupied molecular orbital (HOMO) has an energy of 7.978 eV and corresponds to molecular orbital (M.O.) # 40.

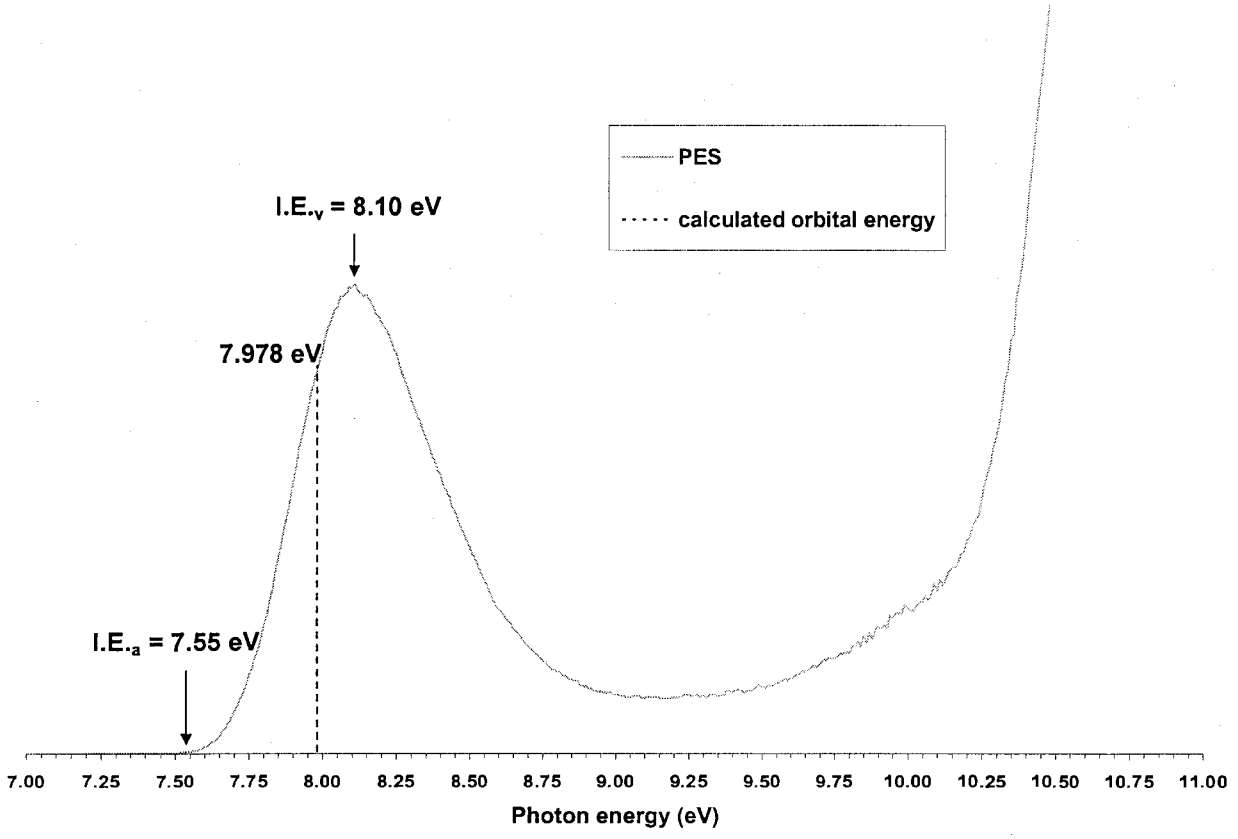

Figure 4.9. Threshold photoelectron spectrum (PES) of ATB - showing the experimental adiabatic and vertical ionization energies ($I.E._a$ and $I.E._v$) and the ROVGF calculated orbital energy.

The population analysis performed at the B3LYP/6-31+G(d) level of theory, shows that M.O. # 40 has a Π like character centered on the nitrogens, where the lone pairs presumably reside, Figure 4.10. Hence the vertical ionization of ATB takes place by a removal of an electron from one of the nitrogen's lone pair.

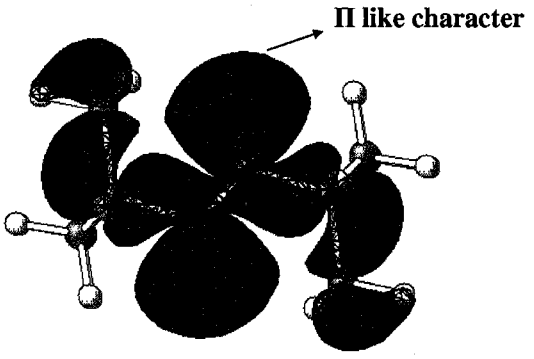

M.O. # 40

Figure 4.10. 3D representation of molecular orbital (M.O.) # 40 of azo-tert-butane.

Table 4.9 summarizes the vertical and adiabatic ionization energies ($I.E._v$ and $I.E._a$) of azo-tert-butane obtained experimentally from the threshold photoelectron spectrum (Figure 4.10) and theoretically from ROVGF/6-31+G(d) and G3 calculations. The experimental and the theoretical values are in good agreement.

Table 4.9. Comparison of the vertical and adiabatic I.E.'s obtained experimentally and theoretically

$I.E._v$[a]		$I.E._a$[a]	
PES[b]	ROVGF[c]	PES[b]	G3
8.1 ± 0.05	7.978	7.55 ± 0.05	7.40

[a] values are in eV [b] photoelectron spectrum [c] basis set used – 6-31+G(d)

References

[1] A.L.L. East, L. Radom, *J. Chem. Phys.* 1997, 106, 6655-6674.

[2] Sigma-Aldrich

Website: http://www.sigmaaldrich.com/catalog/search/ProductDetail/ALDRICH/452106

[3] NIST Chemistry WebBook

Website: http://webbook.nist.gov/cgi/cbook.cgi?ID=C927833&Units=SI

[4] J.L. Holmes, A. Christiane, P.M. Mayer, *Assigning Structures to Ions in Mass Spectrometry*, 2007, Boca Raton: CRC Press.

[5] E. Soh, P.M. Mayer, T. Baer, *Int. J. Mass Spectrom. Ion Processes* 1997, 160, 63-71.

[6] NIST Chemistry WebBook

Website: http://webbook.nist.gov/cgi/cbook.cgi?Formula=C4H8&NoIon=on&Units=SI

Chapter 5

Results and Discussion for Acetone Azine

Acetone azine (AA) has several fragmentation pathways which vary with the instrument being used and the type of experiment being performed. In TPEPICO, there are 21 dissociation channels that appear at different photon energies and of varying intensity, Figure 5.1. The appearance energy values for the 21 fragment ions are listed in Table 5.1. The section of the breakdown curve in Figure 5.1 that is of most significance is between 9 and 10.5 eV and is referred to as the first cross over region. In this region the parent ion, m/z 112 crosses over with the first fragment ions: m/z 97 (methyl radical loss), m/z 71 (allyl radical loss) and m/z 58. The first cross over region is of most importance due to two reasons: it represents the dissociation channels of the parent ion m/z 112 rather than secondary fragmentations and RRKM theory can be used to fit the experimental data. As described in chapter 2, section 4.1, the fitting process using RRKM theory requires the thermal energy of the ion to be calculated. This type of calculation for a fragment ion is not straight forward and hence fitting breakdown curves beyond the cross over region is not feasible at this point.

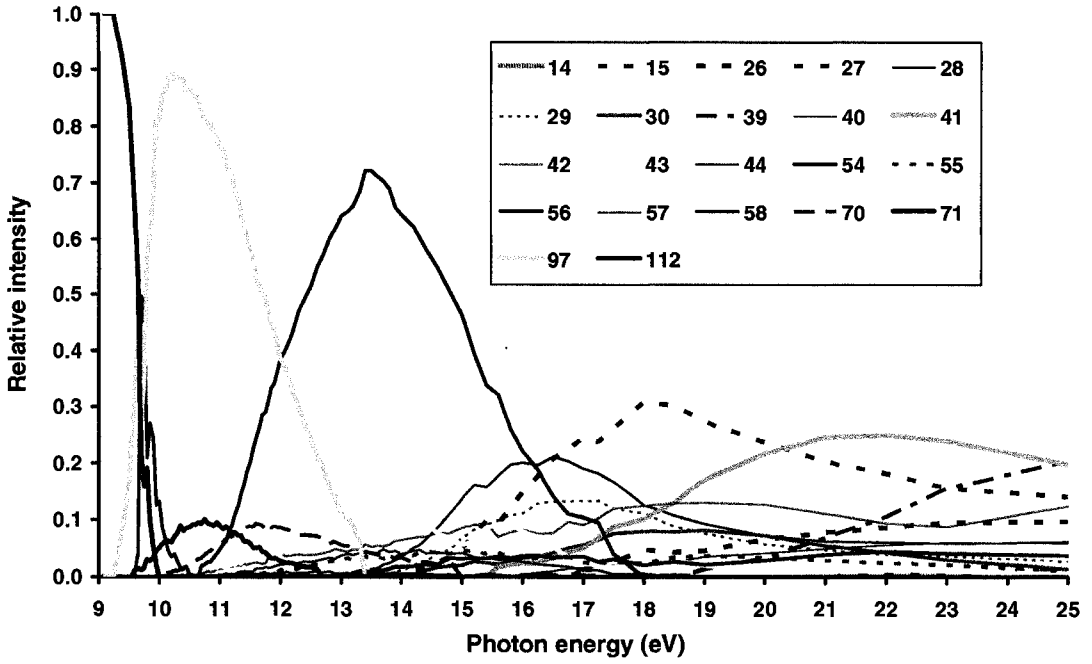

Figure 5.1. TPEPICO breakdown curve of ionized AA (m/z 112) showing all the dissociation channels (legend indicates m/z values) from 9 to 25 eV at 1.116 μsec delay time. The shaded area is the first cross over region between 9 and 10.25 eV.

Table 5.1. Appearance energy (AE) and disappearance energy (DE) values[a] of fragments from TPEPICO breakdown curve[b].

Fragment (m/z)	AE (eV) - 1.116 usec	DE (eV) - 1.116 usec
14	21.00	
15	13.80	
26	22.00	
27	17.00	
28	13.50	
29	13.90	
30	14.40	
39	19.00	
40	16.00	
41	15.60	
42	10.40	
43	10.40	
44	10.60	
54	13.20	
55	11.35	
56	10.70	18.00
57	10.80	18.50
58	9.60	10.55
70	10.25	15.00
71	9.60	12.70
97	9.30	13.30
112		9.95

[a] values (± 0.05 eV) are expressed in photon energies [b] breakdown curve shown in Figure 5.1

Figure 5.2 represents the cross over region at four delay times (1.116, 3.116, 5.116 and 7.116 μsec). The ion with m/z 58 is not a fragment ion but rather an impurity; there are two indicators suggesting this. First, the shape of the curve is "oscillating" which is unusual and consequently disrupts the shape of the other curves (m/z 112 and m/z 97). A regular shape is smooth and gradual without oscillations (see m/z 97 & m/z 56 in Figure 5.1). Second, the position of the curve remains unchanged with increasing delay time (Figure 5.3), suggesting that the source of this peak is not the parent ion m/z 112 but rather an impurity in the sample; this is discussed in further detail in the next paragraph.

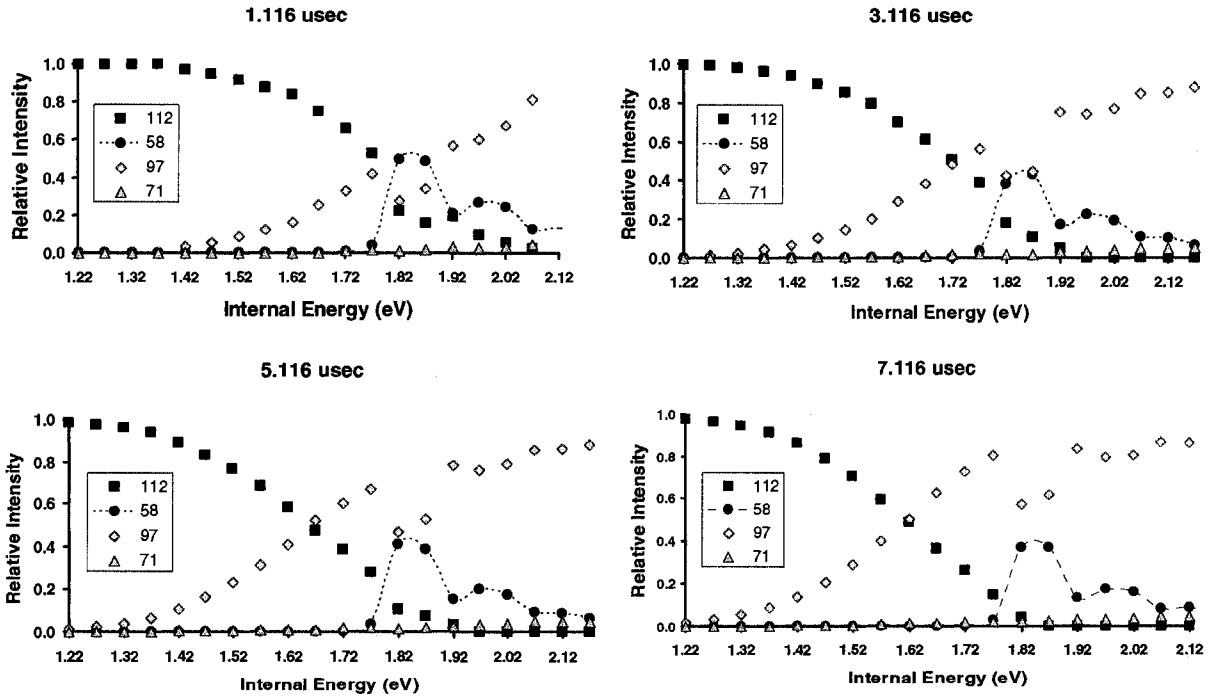

Figure 5.2. TPEPICO breakdown curve of acetone azine at the first cross over region at 4 delay times (1.116, 3.116, 5.116, 7.116 μsec). Parent ion – m/z 112, methyl radical loss – m/z 97, allyl radical loss – m/z 71 and impurity – m/z 58.

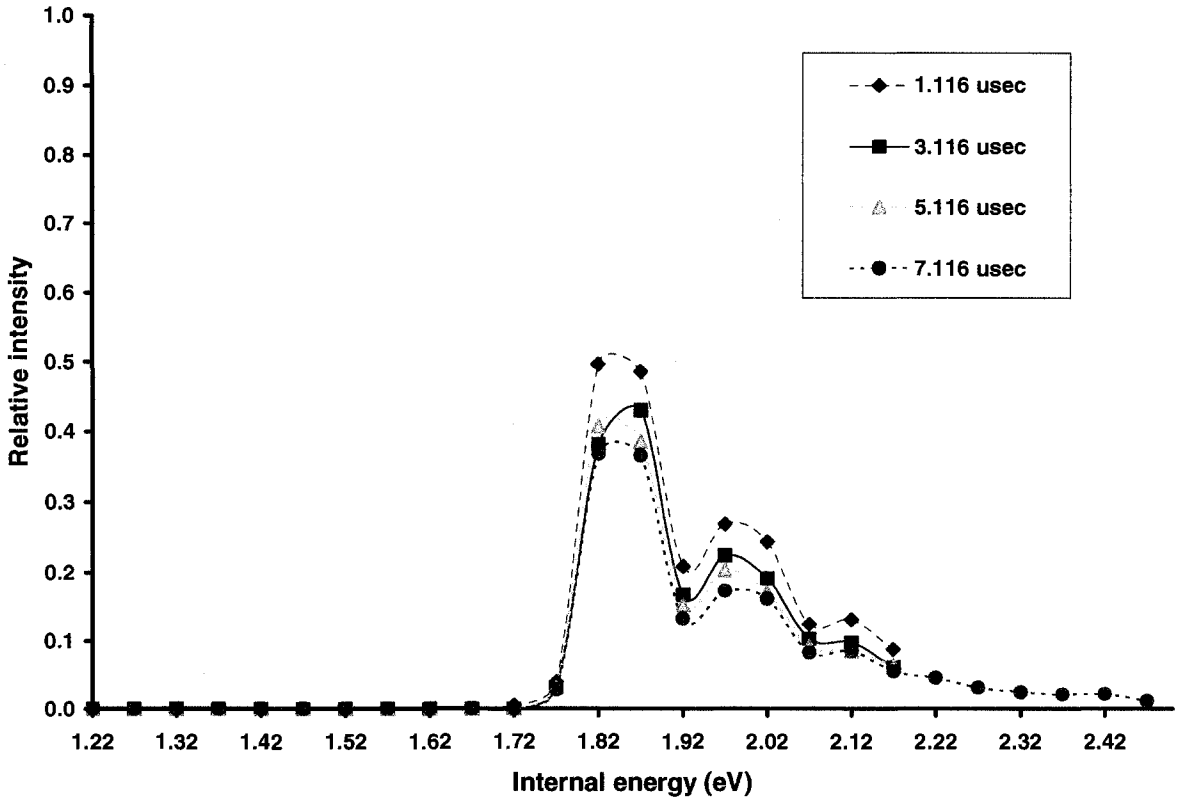

Figure 5.3. TPEPICO breakdown curves of ion m/z 58 at four delay times (1.116, 3.116, 5.116 and 7.116 μsec).

The kinetics observed in TPEPICO for AA is that of slow fragmentation reactions. In a slow system, the increasing delay time allows for more energy distribution throughout the molecule and therefore it can dissociate at a lower energy (see Chapter 3, section 5.1, page 53). This is evident in a shift of the curves to the left, which is the case for acetone azine, Figure 5.4. For example, m/z 112 at 1.116 μsec and 3.116 μsec has an intensity of 0.5 at 1.79 eV and at 1.72 eV, respectively. Another feature of the kinetic shift in slow reactions is that with increasing delay time, the spacing between the curves shortens, Figure 5.5. The impurity in the breakdown curve m/z 58, causes problems when RRKM theory is used to fit the experimental data. The electrons that are produced from m/z 58 interfere with the electrons that are detected from m/z

112 and m/z 97. Therefore, the curves for m/z 112 and m/z 97 in the region where m/z 58 appears are not the true curves and are shifted from their real positions. As mentioned previously, the spacing between the curves normally shortens as the delay time increases, but in AA this is not observed (the spacing between 1.116 - 3.116, 3.116 - 5.116 and 5.116 – 7.116 is 0.07 eV, 0.07 eV and 0.04 eV, respectively), compare Figure 5.4 and 5.5. To avoid this problem, only the breakdown curve at 7.116 μsec is used for the theoretical fit. At this delay time, m/z 58 does not coincide with m/z 112 and m/ 97 and is well separated, unlike the three other delay times (1.116, 3.116 and 5.116 μsec), Figure 5.2. The impurity does not affect the curves up to 1.77 eV and thus the fits are generated up to this internal energy. Fragment ion m/z 71 has a very low intensity up to 1.77 eV of internal energy and thus is not fitted.

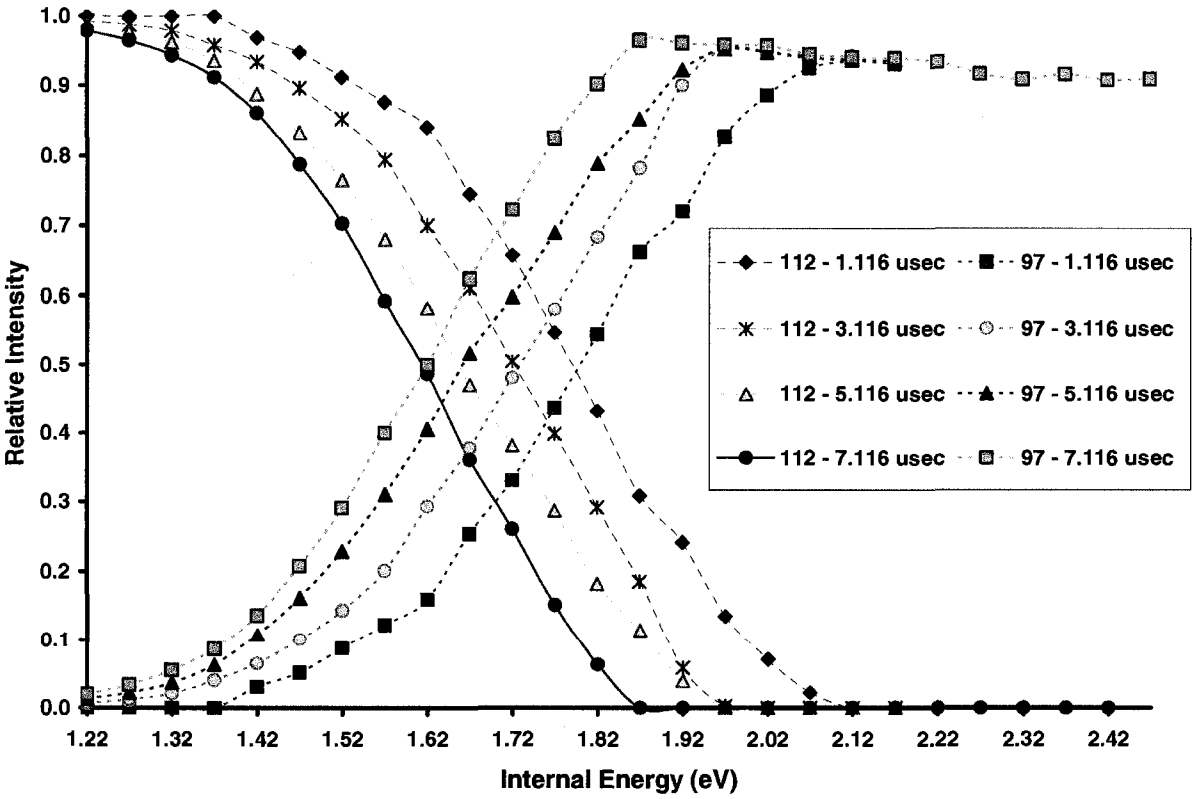

Figure 5.4. TPEPICO breakdown curves for m/z 112 (parent ion) and m/z 97 (methyl radical loss) at four delay times (1.116, 3.116, 5.116 and 7.116 μsec) showing the kinetic shift.

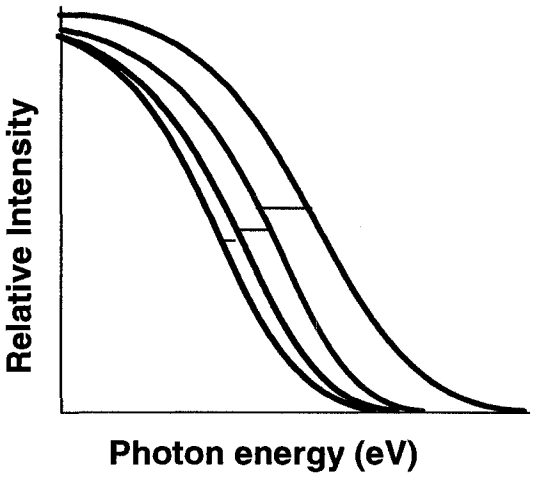

Figure 5.5. Typical breakdown curve for a slow fragmentation reaction showing the kinetic shift and the reduction in the spacing between the curves as the delay time increases. Light blue – 1.116 μsec, pink -3.116 μsec, green – 5.116 μsec and dark blue – 7.116 μsec.

Table 5.2 summarizes the activation energy (E_0) and entropy ($\Delta S^{\ddagger}$) extracted from the three theoretical fits that were successfully generated for the 7.116 μsec delay time and the entropy of activation ($\Delta S^{\ddagger}$) calculated using the free rotor model. All three fits produced are in excellent agreement with the experimental breakdown curve for the methyl radical loss (m/z 97) of ionized acetone azine (m/z 112). Figure 5.6 shows one of the fits produced. The average activation energy (E_0) and entropy ($\Delta S^{\ddagger}$) is 1.045 ± 0.015 eV and -21 ± 3 J K^{-1} mol^{-1} at 600K. The vibrational frequencies of ionized acetone azine calculated at the B3LYP/6-31+G(d) level of theory and the scaled vibrational frequencies of the transition state corresponding to the methyl loss used for the three fits are listed in Table 5.3.

Table 5.2. Summary of the activation energies (E_0) and entropies ($\Delta S^{\ddagger}$) obtained from RRKM fits and the free rotor model

Fit	E_0 (eV)	$\Delta S^{\ddagger}$ (RRKM)[a]	$\Delta S^{\ddagger}$ (free rotor)[a]
1	1.060	-19	-6.2
2	1.045	-21	-7.0
3	1.030	-24	-7.0
Average	1.045 ± 0.015	-21 ± 3	-6.7 ± 0.5

[a] values are in J K^{-1} mol^{-1} at 600K

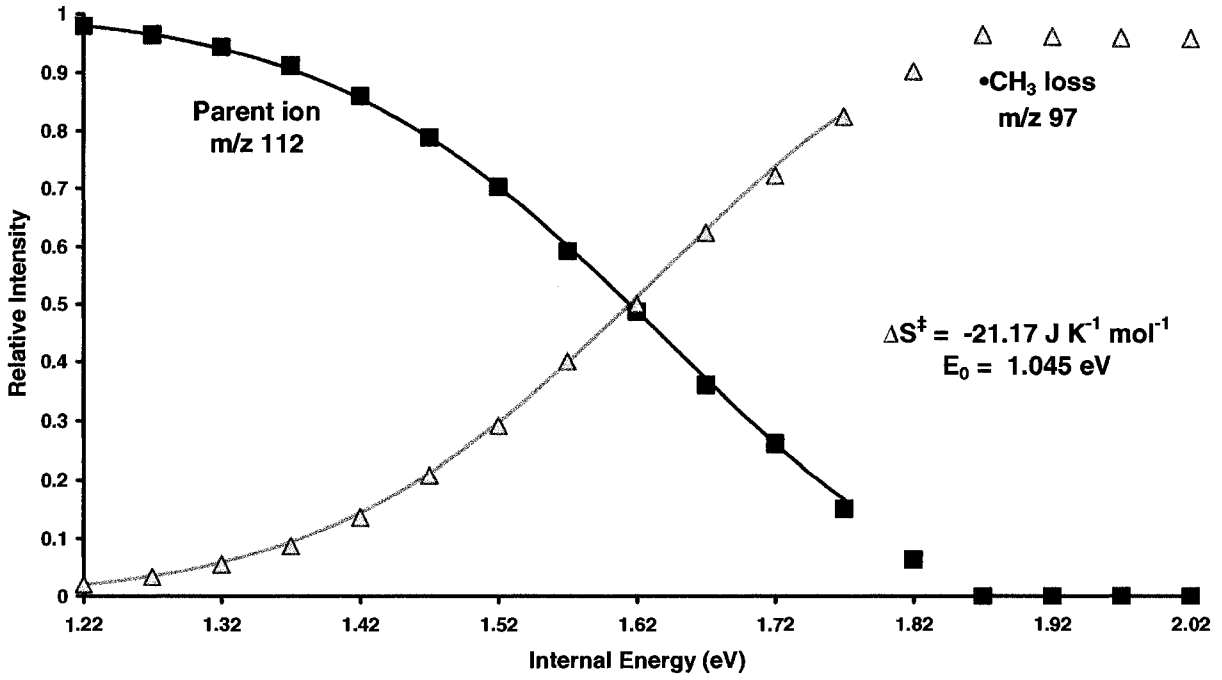

Figure 5.6. Theoretical fit (solid line) to the experimental breakdown curves of m/z 97 (▲) and m/z 112 (■).

Table 5.3. Vibrational frequencies and rotational constants of ionized acetone azine and transition states corresponding to the three theoretical fits

Ionized acetone azine		Transition state 1[c]		Transition state 2[c]		Transition state 3[c]	
ν (cm^{-1})[a]	A, B & C (GHz)[b]	ν (cm^{-1})[a]	A, B & C (GHz)[b]	ν (cm^{-1})[a]	A, B & C (GHz)[b]	ν (cm^{-1})[a]	A, B & C (GHz)[b]
28.3118	4,1	42.4677	4,1	45.2989	4,1	48.1300	4,1
32.9089		49.3634		52.6543		55.9452	
78.7371		118.1057		125.9794		133.8531	
102.3827		153.5740		163.8123		174.0505	
102.9731		154.4596		164.7569		175.0542	
132.4791		132.4791		132.4791		132.4791	
159.3143		159.3143		159.3143		159.3143	
253.7528		253.7528		253.7528		253.7528	
311.3927		311.3927		311.3927		311.3927	
312.3048		312.3048		312.3048		312.3048	
371.3622		371.3622		371.3622		371.3622	
461.7310		461.7310		461.7310		461.7310	
465.3672		465.3672		465.3672		465.3672	
520.3666		520.3666		520.3666		520.3666	
539.4930		539.4930		539.4930		539.4930	
789.7070		789.7070		789.7070		789.7070	
813.0342		813.0342		813.0342		813.0342	
901.3126		901.3126		901.3126		901.3126	
918.5532		918.5532		918.5532		918.5532	
920.4978		920.4978		920.4978		920.4978	
921.1383		921.1383		921.1383		921.1383	
992.1821		992.1821		992.1821		992.1821	
1060.2271		1060.2271		1060.2271		1060.2271	
1061.0203		1061.0203		1061.0203		1061.0203	
1061.4808		1061.4808		1061.4808		1061.4808	
1190.9871		1190.9871		1190.9871		1190.9871	
1215.9489		1215.9489		1215.9489		1215.9489	
1237.8862		1352.6100		1352.6100		1352.6100	
1352.6100		1357.3218		1357.3218		1357.3218	
1357.3218		1365.9645		1365.9645		1365.9645	
1365.9645		1369.7431		1369.7431		1369.7431	
1369.7431		1415.6105		1415.6105		1415.6105	
1415.6105		1417.3781		1417.3781		1417.3781	
1417.3781		1423.1277		1423.1277		1423.1277	
1423.1277		1423.6180		1423.6180		1423.6180	
1423.6180		1431.1676		1431.1676		1431.1676	
1431.1676		1437.7458		1437.7458		1437.7458	
1437.7458		1440.2474		1440.2474		1440.2474	
1440.2474		1444.5608		1444.5608		1444.5608	
1444.5608		1604.0997		1604.0997		1604.0997	
1604.0997		1644.6429		1644.6429		1644.6429	
1644.6429		2937.3367		2937.3367		2937.3367	
2937.3367		2937.5414		2937.5414		2937.5414	
2937.5414		2943.8856		2943.8856		2943.8856	
2943.8856		2943.9782		2943.9782		2943.9782	
2943.9782		2992.1162		2992.1162		2992.1162	
2992.1162		2992.1470		2992.1470		2992.1470	
2992.1470		2998.4642		2998.4642		2998.4642	
2998.4642		2998.5114		2998.5114		2998.5114	
2998.5114		3052.6700		3052.6700		3052.6700	
3052.6700		3052.7725		3052.7725		3052.7725	
3052.7725		3056.4367		3056.4367		3056.4367	
3056.4367		3056.9472		3056.9472		3056.9472	
3056.9472							

[a] vibrational frequencies [b] 1 is the average of the two lowest rotational constants (1.08336 and 0.90481 GHz)
[c] transition states 1, 2 and 3 correspond to fits 1, 2 and 3 respectively

Geometry optimizations and energy calculations for m/z 112, m/z 97 and methyl radical were performed at three density functional levels of theory (B3LYP, B3PW91 and BHandHLYP) using the same basis set (6-31+G(d)) to determine the most suitable theory for this particular system. The first assessment was performed by comparing the geometries of neutral and ionized acetone azine at the three density functional levels of theory, Table 5.4. All three theories resulted in similar geometric parameters.

Table 5.4. Optimized geometric parameters[a] of neutral and ionized acetone azine

Level of theory	R_{NN}	R_{CN}	R_{CC}	<NNC	<NCC1	<NCC2	<CCC	<CNNC
Neutral Acetone azine								
B3LYP	1.394	1.288	1.505	115.5	117.3	125.2	117.6	149.4
B3PW91	1.381	1.287	1.500	115.7	117.4	124.7	117.9	144.5
BHandBHLYP	1.386	1.273	1.497	115.0	117.3	125.9	116.8	165.5
Ionized Acetone azine								
B3LYP	1.305	1.286	1.499	129.7	117.5	122.8	119.7	180.0
B3PW91	1.297	1.285	1.493	129.9	117.5	122.7	119.8	180.0
BHandBHLYP	1.297	1.272	1.491	129.8	117.6	122.9	119.5	180.0

[a] bond lengths (R) are in Å and angles (<) in degrees

The second assessment was performed by comparing the relative energies of the dissociation products (methyl radical loss) at the G3 and three density functional levels of theory. According to Table 5.5, which lists the relative energies at B3LYP, B3PW91 and BHandHLYP levels of theory, B3PW91 (199 kJ mol^{-1}) appears to be inconsistent with the other two theories

(189 & 188 kJ mol^{-1}). However, the G3 calculations on these geometries show that this inconsistency is lifted from the B3PW91 (175 kJ mol^{-1}) and it is BHandHLYP (149 kJ mol^{-1}) geometries that lead to the incompatible data, Table 5.6. Therefore, since G3 calculations are higher in accuracy than DFT's, the energy assessment is done according to G3 results, Table 5.6. At this stage, either B3LYP or B3PW91 can be chosen, but since B3LYP is the most commonly used DFT method, it has been selected for the following computational studies. Hence, all theoretical fits and comparisons between experiment and theory are carried out with the geometries and frequencies obtained from B3LYP and energies from G3 (B3LYP).

Table 5.5. Comparison of the relative energies of the fragment ion and neutral of ionized acetone azine at three different levels of theory (B3LYP, B3PW91, BHandHLYP)

	$((CH_3)_2CN)_2^{+\bullet}$		$(CH_3)_2CNNC(CH_3)^+ + CH3^\bullet$	
Level of Theory	Absolute[a]	Relative[b]	Absolute[a]	Relative[b]
B3LYP	-344.9059075	0	-344.8339476	189
B3PW91	-344.7742603	0	-344.6984784	199
BHandBHLYP	-344.6691755	0	-344.5976491	188

[a] absolute energy values are in hartrees

[b] relative energy values are in kJ mol^{-1}

Table 5.6. Comparison of the relative energies of the fragment ion and neutral of ionized acetone azine at the G3 level of theory

	$((CH_3)_2CN)_2^{+\bullet}$		$(CH_3)_2CNNC(CH_3)^+ + CH3^\bullet$	
Level of Theory[c]	Absolute[a]	Relative[b]	Absolute[a]	Relative[b]
G3 (B3LYP)	-344.7353346	0	-344.6702060	171
G3 (B3PW91)	-344.7356465	0	-344.6690074	175
G3 (BHandBHLYP)	-344.7293603	0	-344.6725657	149

[a] absolute energy values are in hartrees

[b] relative energy values are in kJ mol^{-1}

[c] G3 calculation using the optimized geometries obtained at the B3LYP, B3PW91 and BHandHLYP level of theory

The structure of acetone azine is shown in Figure 5.7 [1-2]. Kobuchev et al. conducted a theoretical analysis at the MP2/6-31G* level of theory on the structure of neutral acetone azine and its isomers and have found that the minimum energy structure of neutral acetone azine has a noncoplanar gauche conformation (<CNNC = 120°) [3]. The initial structures used in the geometry optimizations of neutral acetone azine conducted in this thesis work at the B3LYP/6-31+G(d) level of theory have all led to the same conformation. The structure with the greatest thermodynamic stability has a point group symmetry of C_2 and a dihedral angle (<CNNC) of 150.4°, Figure 5.8(a). A similar approach was taken for ionized acetone azine, where several different initial structures with various point group symmetries and geometries were optimized. All led to the trans conformation; dihedral angle (<CNNC) is 180.0°, Figure 5.8(b). The initial structures considered for the methyl radical loss forming fragment ion m/z 97 were for simple bond cleavage reactions. The optimized structures for fragment m/z 97 and methyl radical are shown in Figure 5.9.

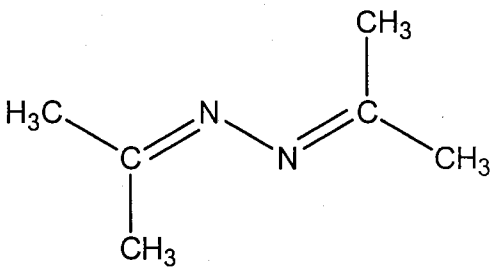

Figure 5.7. General unoptimized structure of acetone azine.

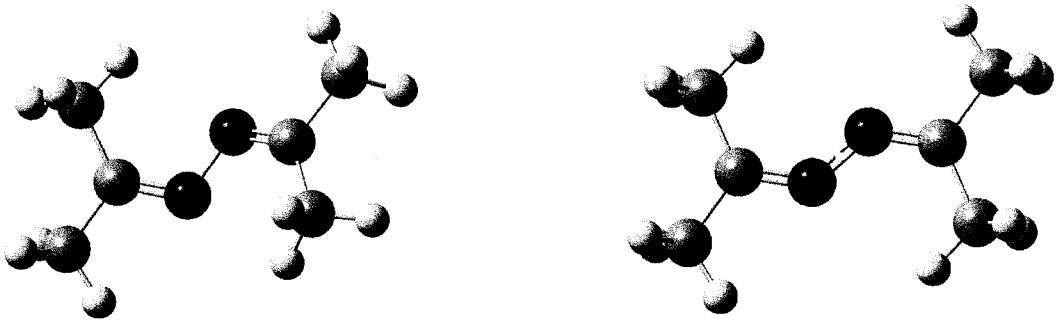

(a) (b)

Figure 5.8. Optimized structures of (a) neutral and (b) ionized acetone azine at the B3LYP/6-31+G(d) level of theory.

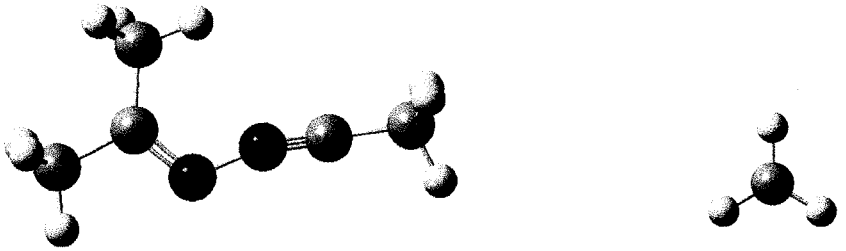

Figure 5.9. Optimized structures of fragment ion m/z 97 (left) and methyl radical (right).

The energies for the structures presented in Figure 5.8 & 5.9 are the ones used to calculate the G3 energies. Therefore, if a simple bond cleavage for the methyl radical loss takes place, then the energies of the dissociated fragments (m/z 97 and 15 amu) should be relatively higher than the transition state (TS) energy leading to those products, Figure 5.10 [4-5]. However, the G3 relative energies for fragment ion m/z 97 and methyl radical are well above the activation energy (E_0) obtained from the theoretical fits, Table 5.7. This indicates that the optimized geometry for fragment ion m/z 97 does not correspond to the structure that actually forms. So, the combination of the large difference between the G3 (1.77 eV) and E_0 (1.045 eV)

values and the negative value for the entropy of activation (-21 J K^{-1} mol^{-1}) suggests that the methyl radical loss does not occur by a simple bond cleavage but rather through a rearrangement process (see chapter 2, section 2.1). Thus the activation energy (E_0) is characteristic to the rearrangement that takes place prior to the methyl loss, Figure 5.11.

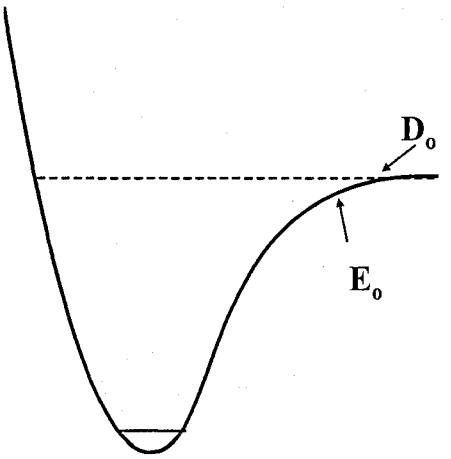

Figure 5.10 Typical potential energy surface diagram for a simple bond cleavage showing the dissociation energy (D_0) and approximate activation energy (E_0). The dissociation energy (D_0) is the fragments total energy and activation energy (E_0) is the transition state (TS) energy.

Table 5.7. Comparison of the G3 relative energy[a] of the products of methyl radical loss with the E_0 obtained from RRKM theory

$(CH_3)_2CNNC(CH_3)^+ + CH3^{\bullet}$	
G3 (B3LYP)	RRKM
1.77 eV	1.045 eV

[a] value taken from Table 5.6 and converted from kJ mol^{-1} to eV

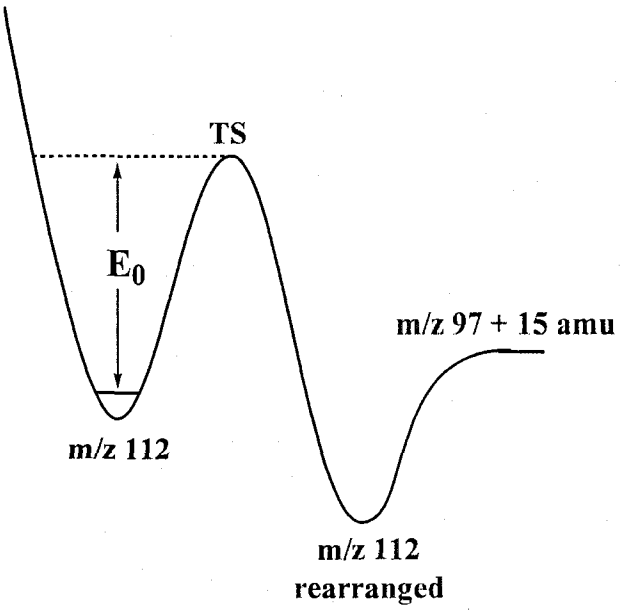

Figure 5.11. Potential energy surface diagram presenting the proposed process for the methyl radical loss of ionized acetone azine: rearrangement prior to methyl loss. TS – transition state.

To determine the isomerization that takes places, several structures for fragment ion m/z 97 were considered and their energies computed at the B3LYP/6-31+G(d) level of theory. The goal was to find an equilibrium structure characteristic of a rearrangement with an energy below the activation energy (1.045 eV). The isomerizations considered were H shifts from one of the methyls to a C or N, Figure 5.12. None of the rearrangements considered resulted in energies below the activation energy and in fact were all higher in energy than the equilibrium structure presented in Figure 5.9, i.e. for a simple bond cleavage. Table 5.8 lists the absolute and relative energies of fragment ion m/z 97 formed by simple bond cleavage and its isomers shown in Figure 5.12. It is well known that potential energy surfaces can be multidimensional and hence very complex, so attempting to find a local minimum can be very time consuming and in this case has failed [6].

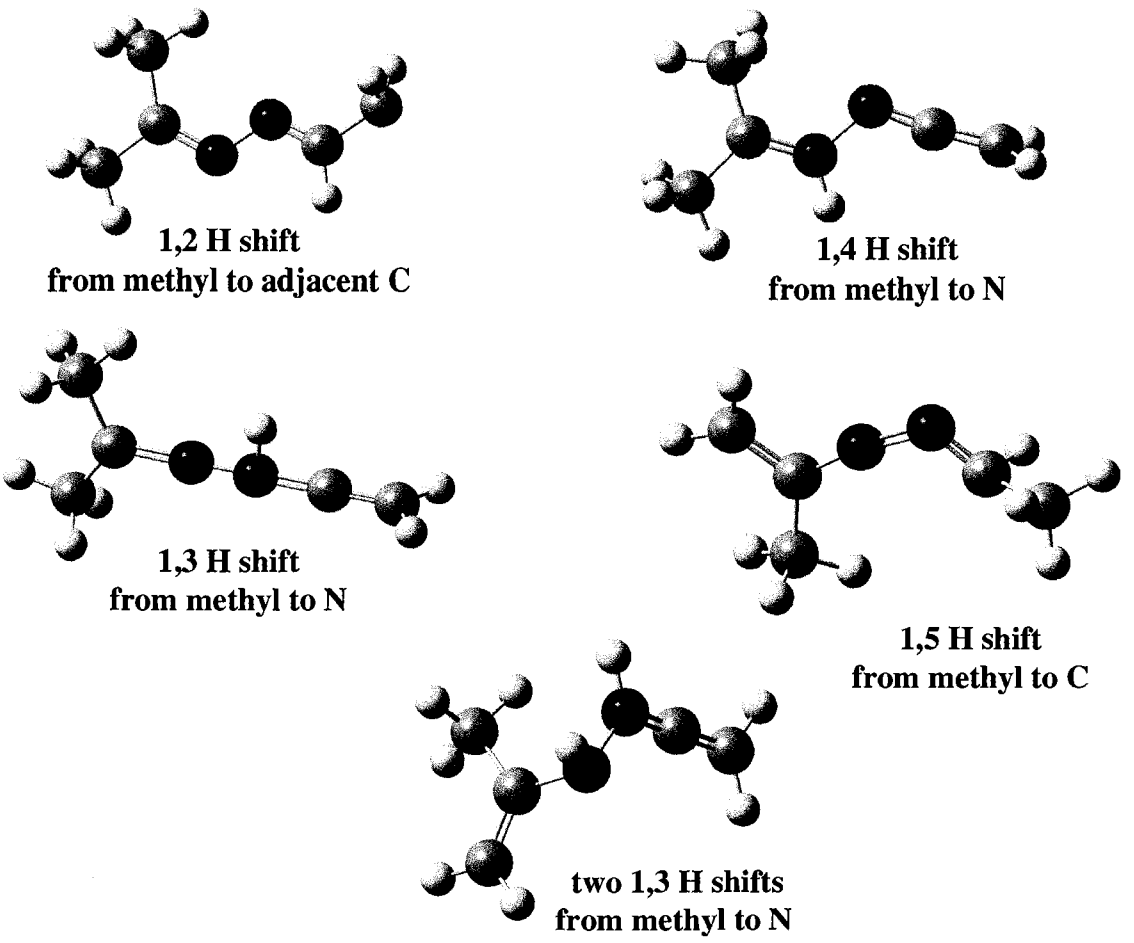

Figure 5.12. Unoptimized structures of rearranged fragment ions m/z 97 used for geometry optimizations.

Table 5.8. Comparison of the absolute[a] and relative[b] energies[c] of fragment ion m/z 97 formed by simple bond cleavage and its isomers[d]

Reaction type	Absolute	Relative
simple bond cleavage	-305.02060	0
1,2 H shift	-304.95608	169
1,3 H shift	-304.98455	95
1,4 H shift	-305.00995	28
1,5 H shift	-304.99574	65
two 1,3 H shifts	-304.96028	158

[a] absolute energy values are in hartrees

[b] relative energy values are in kJ mol^{-1}

[c] Energies computed at the B3LYP/6-31+G(d) level of theory

d Isomers shown in Figure 5.12

The metastable and collision induced dissociation (MI and CID) of ionized acetone azine (m/z 112) show that the methyl radical loss is the dominant channel, Figure 5.13. Tandem mass spectrometry can be used in two ways to determine the fragmentation reaction taking place: kinetic energy release (KER) and collision induced dissociation (CID) experiments [7]. The kinetic energy release is the transfer of excess internal energy of the ion into translational kinetic energy of the neutral and ionized products. The kinetic energy release for the methyl radical loss is 221 meV, which is characteristic of a rearrangement reaction (typical values: 100 meV – 1 V) [7]. As discussed in chapter 3, section 3.2, CID is a high energy reaction which leads to simple bond cleavages and in turn to structural information. The major daughter ions observed from the collision induced dissociation of metastably generated fragment ion m/z 97 are shown in Figure 5.14. To extract structural information from this spectrum, an analysis on the potential bond cleavages of fragment ion m/z 97 and its isomers was performed, Figure 5.15. Structure D (1,4 H shift) is the least likely one to be formed since two of its bond dissociations leads to 4 daughters ions that are not present in the CID spectrum, Figure 5.14 and 5.15. Structure B is the most plausible one to be formed, since all of its dissociations lead to observed peaks, but it lacks the possibility of forming daughter ion m/z 28 which appears as an intense peak in the CID spectrum. By looking at the most intense peaks in the CID spectrum (m/z 56, m/z 42, m/z 41 and m/z 28), structure E (1,5 H shift) has the highest potential of forming, Figure 5.14 and 5.15. This analysis is not conclusive since there are possibly other structures that have not be considered and the CID spectrum does not reveal unique features that are characteristic to one specific isomer.

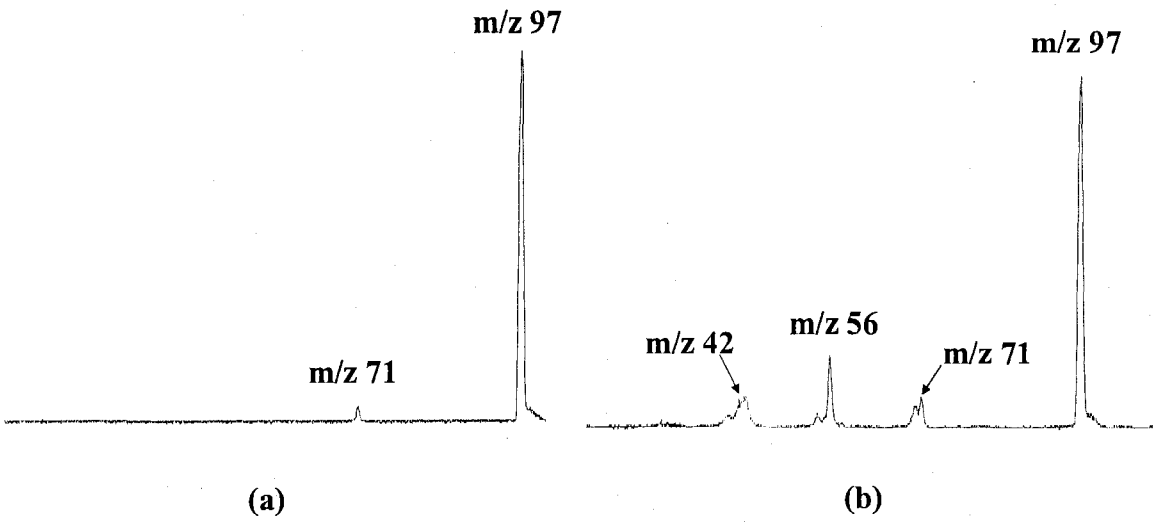

Figure 5.13. MI (a) and CID (b) mass spectra of ionized acetone azine (m/z 112).

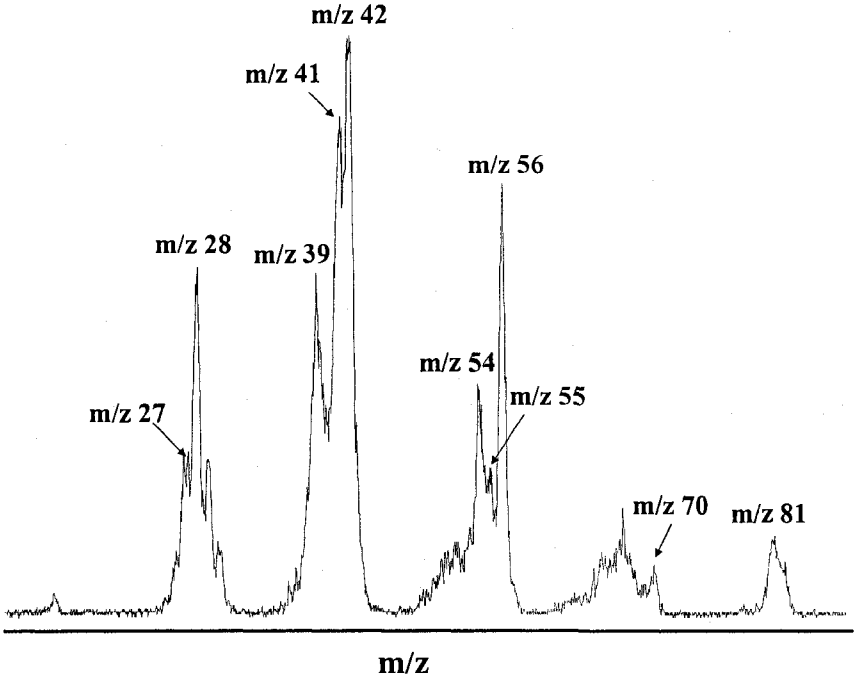

Figure 5.14. CID mass spectrum of metastably generated fragment ion m/z 97.

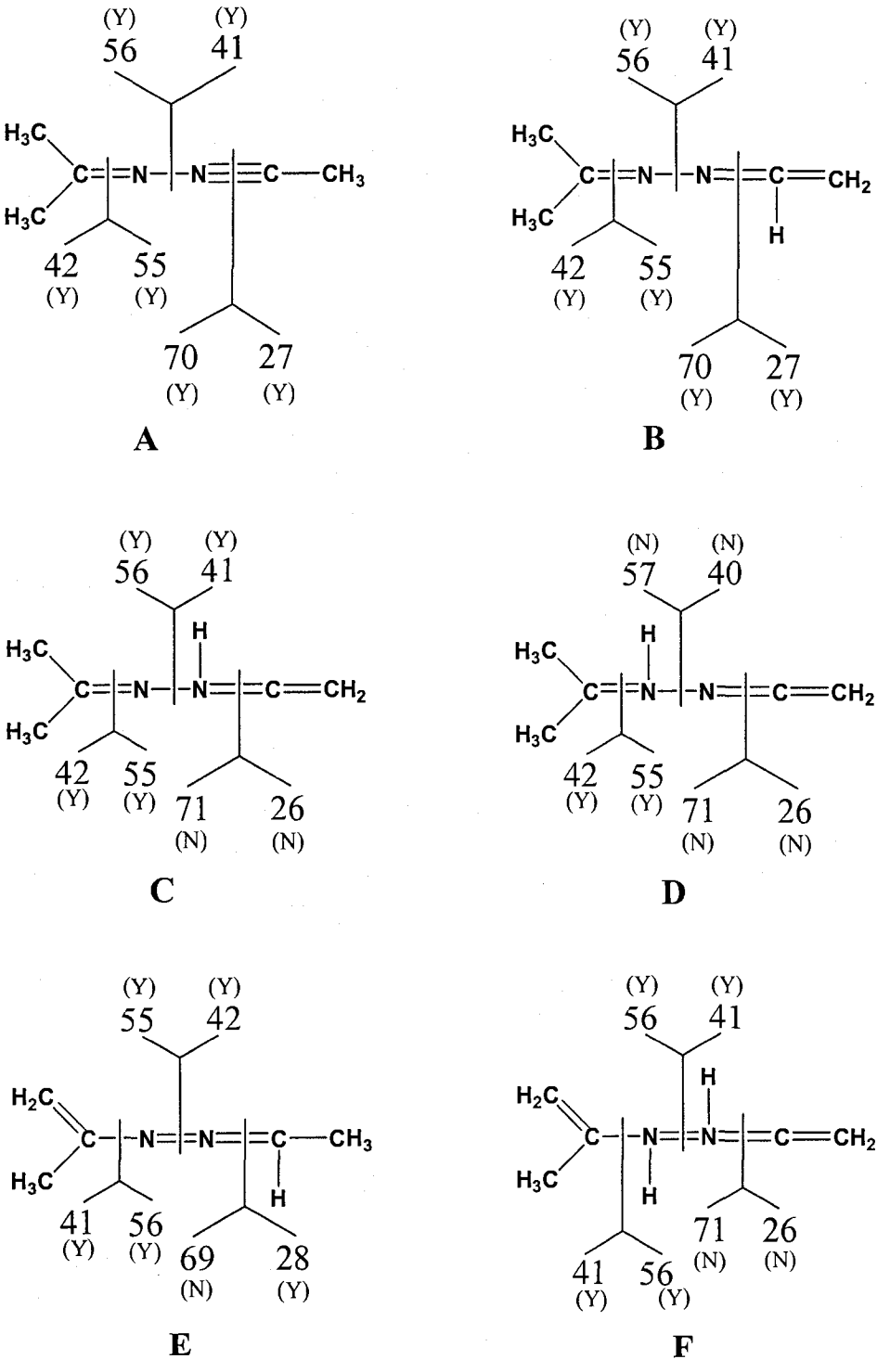

Figure 5.15. Unoptimized structures of fragment ion m/z 97 formed through simple bond cleavage (A), 1,2 H-shift (B), 1,3 H-shift (C), 1,4 H-shift (D), 1,5 H-shift (E) and two 1,3 H-shifts (F) showing the possible bond cleavages and consequently their potential daughter ions m/z. The notations (Y) and (N) correspond to yes and no, implying whether these m/z values are observed in the spectrum in Figure 5.13.

Threshold Photoelectron Spectrum

The threshold photoelectron spectrum of acetone azine reveals a well defined band at 8.4 eV and several other poorly resolved bands at higher photon energies, Figure 5.16. The impurity (m/z 58) starts to appear at 9.60 eV of photon energy (1.72 eV of internal energy, Figure 5.3). Therefore, the source of the obscured bands that appear after 9.60 eV is a combination of acetone azine and the impurity. Consequently, those bands were not assigned with molecular orbital (M.O.) ionization energies (I.E.) calculated by ROVGF.

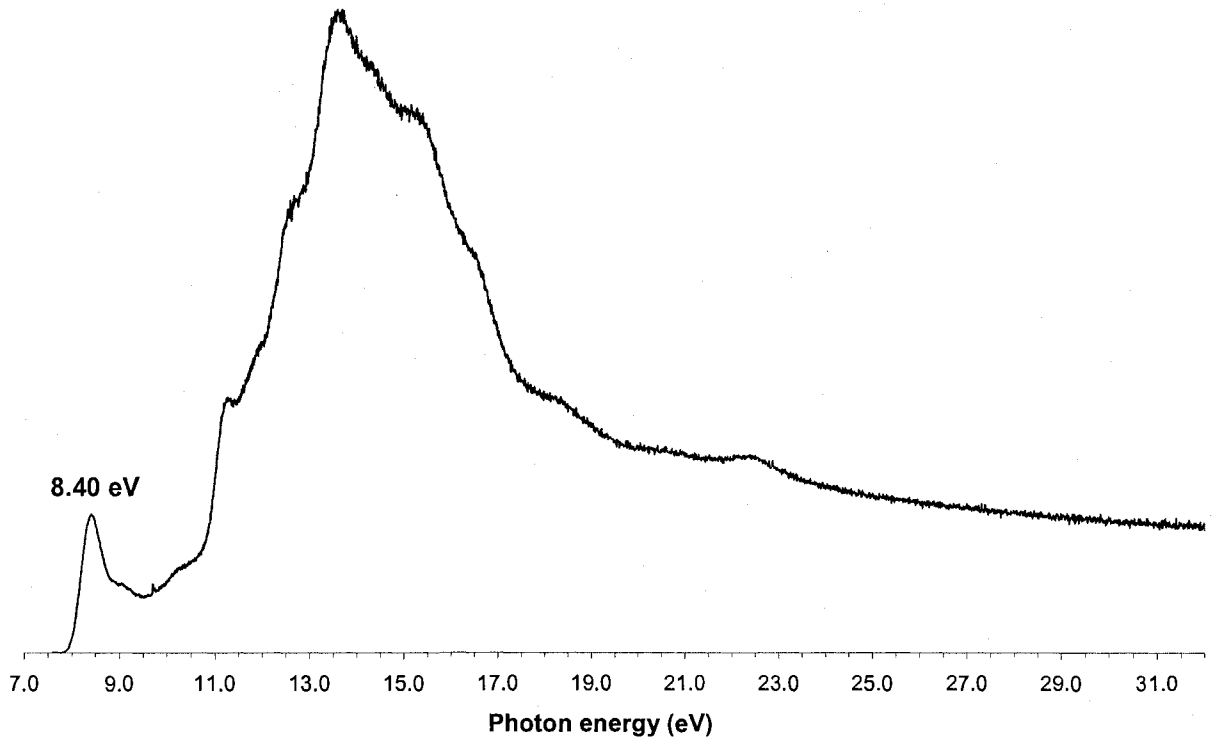

Figure 5.16. Threshold photoelectron spectrum of acetone azine, intensity vs. photon energy from 7.60 to 32.15 eV.

According to the ROVGF/6-31+G(d) calculation, the HOMO $I.E._v$ is 8.772 eV, corresponding to M.O. # 31. While M.O. # 30 has an I.E. of 8.283 eV. It is possible that the vertical ionization of those two M.O. leads to the appearance of the wide peak at 8.4 eV, Figure 5.17.

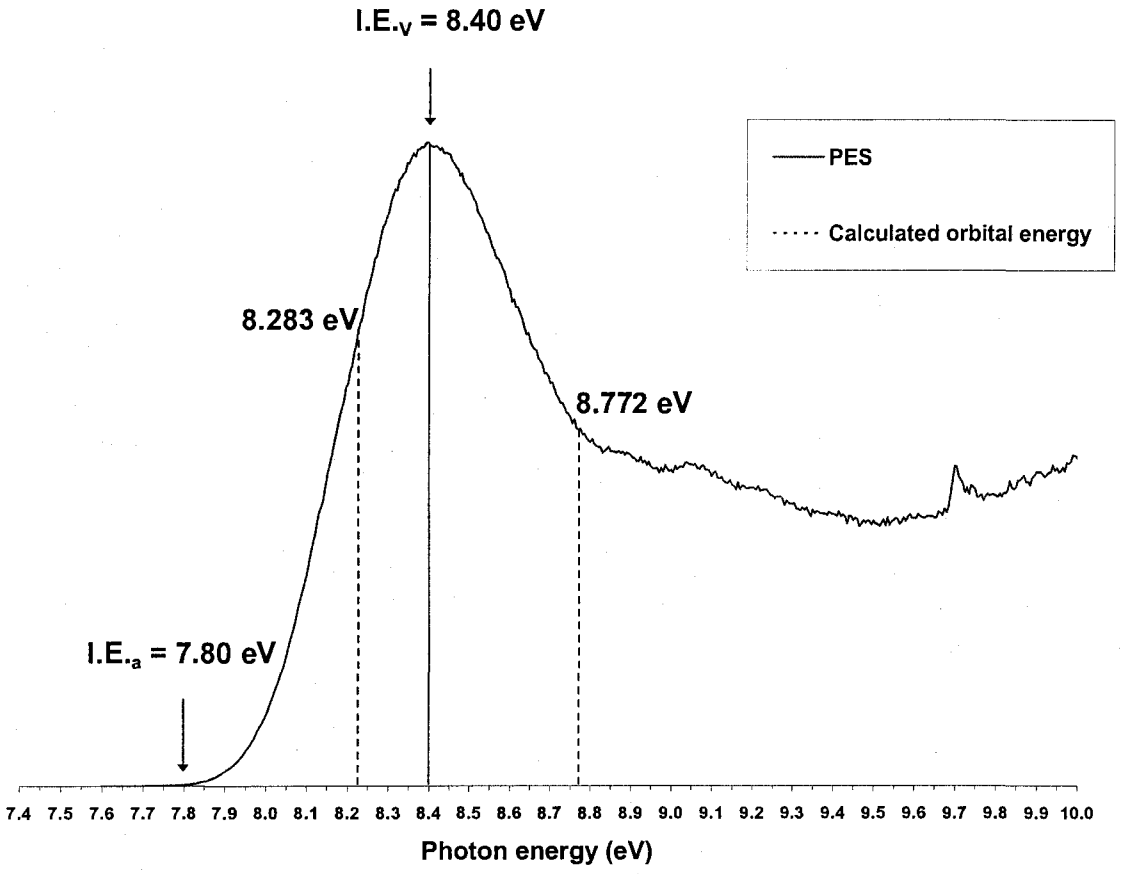

Figure 5.17. Threshold photoelectron spectrum (PES) of acetone azine - showing the experimental adiabatic and vertical ionization energies ($I.E._a$ and $I.E._v$) and the ROVGF calculated orbital energies.

Table 5.9 summarizes the vertical and adiabatic ionization energies ($I.E._v$ and $I.E._a$) of acetone azine obtained experimentally from the threshold photoelectron spectrum (shown in Figure 5.17) and theoretically from ROVGF/6-31+G(d) and G3 calculations. A good agreement

between theory and experiment is achieved. The G3 adiabatic ionization energy ($I.E._a$) is calculated as the difference between the neutral and ionized AA's energy; it was used to calculate the internal energy of the ionized AA in the TPEPICO spectra.

Table 5.9. Comparison of the vertical and adiabatic I.E.'s obtained experimentally and theoretically

$I.E._v$[a]		$I.E._a$[a]	
PES[b]	ROVGF[c]	PES[b]	G3
8.4 ± 0.05	8.283	7.8 ± 0.05	7.879

[a] values are in eV
[b] photoelectron spectrum
[c] basis set used – 6-31+G(d)

The population analysis performed at the B3LYP/6-31+G(d) level of theory allows us to see the character of each M.O. Molecular orbital # 31 has a Π like character centered on the nitrogens; presumably, the lone pairs reside there, Figure 5.18. Molecular orbital # 30 has a Π like bonding character between N and C on each side and an antibonding character between the two N-C orbital pairs, Figure 5.18. The ROVGF calculation has switched the order of M.O.'s 31 and 30. In this case, M.O.'s # 31 and 30 have an energy of 8.772 eV and 8.283 eV, respectively, thus leaving M.O. # 30 as the HOMO.

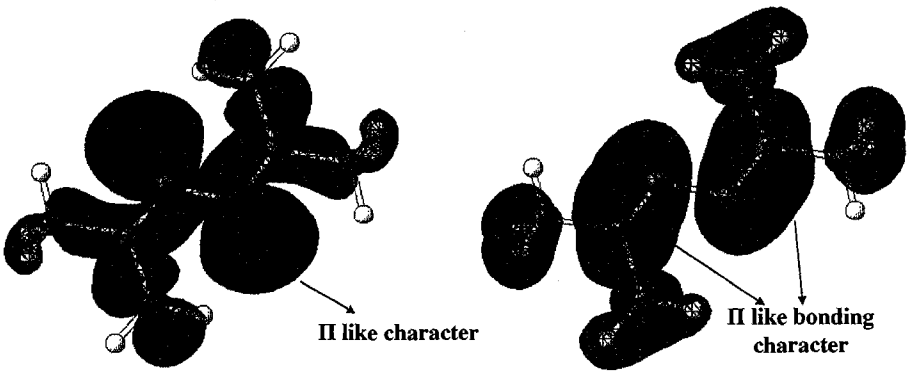

Figure 5.18. 3D representation of molecular orbitals 31 and 30 of acetone azine.

References

[1] Sigma-Aldrich

Website: http://www.sigmaaldrich.com/catalog/search/ProductDetail/ALDRICH/273155

[2] NIST Chemistry WebBook

Website: http://webbook.nist.gov/cgi/cbook.cgi?Name=acetone+azine&Units=SI

[3] V.B. Kobychev, N.M. Vitkovskaya, N.V. Pavlova, E. Yu. Schmidt, B.A. Trofimov, *J. Struct. Chem.* 2004, 45, 748-755.

[4] W. Forst, *Unimolecular Reactions*, 2003, Cambridge: Cambridge University Press.

[5] P. Atkins, J. de Paula, *Physical chemistry*, 2002, New York: W.H. Freeman and Company.

[6] I.N. Levine, *Quantum Chemistry*, 2000, New Jersey: Prentice Hall.

[7] J.L. Holmes, A. Christiane, P.M. Mayer, *Assigning Structures to Ions in Mass Spectrometry*, 2007, Boca Raton: CRC Press.

Chapter 6

Conclusions

Azo-tert-butane

The two competing dissociation channels of ionized azo-tert-butane, namely, m/z 57 and m/z 85 occur by a simple bond cleavage. The former dissociation channel dominates due to a higher entropy of activation (17 > -49 J K^{-1} mol^{-1}) which means that its transition state is looser and hence more entropically favoured. The activation energies for m/z 57 and m/z 85 dissociation channels are 0.537 ± 0.007 and 0.428 ± 0.003 eV, respectively. Fragment ion m/z 56 occurs by a rearrangement process with activation energy and entropy of 0.410 eV and -90 J K^{-1} mol^{-1}, respectively.

The experimental (PES) and theoretical (ROVGF) vertical ionization energy of azo-tert-butane are 8.10 and 7.978 eV, respectively. The experimental (PES) and theoretical (G3) adiabatic ionization energy of acetone azine is 7.55 and 7.40 eV. A good agreement between experiment and theory was observed.

Acetone Azine

The first cross over region has two dissociations but due the presence of the impurity only one of the dissociations was studied, and hence all information regarding the second one

was lost. The single dissociation studied of ionized acetone azine, methyl radical loss, occurs by a rearrangement with an activation energy and entropy of 1.045 ± 0.015 eV and -21 ± 3 J K^{-1} mol^{-1}. Agreement between TPEPICO experimental results and RRKM theory was excellent. Attempts to locate the equilibrium structure of m/z 97 formed through a rearrangement was unsuccessful.

The experimental (PES) and theoretical (ROVGF) vertical ionization energy of acetone azine are 8.4 and 8.283 eV, respectively. The experimental (PES) and theoretical (G3) adiabatic ionization energy of acetone azine is 7.80 and 7.879 eV. An excellent agreement between experiment and theory was achieved.

General Conclusions

To understand the type of reaction taking place: simple bond cleavage or rearrangement, the entropy of activation values of the dissociation channels of a particular system must be viewed relative to each other and not independently.

When there are two competing channels formed by the same bond cleavage, the one forming more products dominates, since it is entropically more favoured according to the 2^{nd} law of thermodynamics.

Conclusive statements can better be formed through a combination of several methods of study, in particular, experimental and theoretical methods. One method of study in not sufficient in understanding chemical and/or physical processes.

Appendix

Archive entries for B3LYP/6-31+G(d) optimized geometries

A. Azo-tert-butane

Neutral azo-tert-butane


```
1\1\GINC-MS7\Freq\RB3LYP\6-31+G(d)\C8H18N2\RABAEV\20-Dec-2007\0\\#N GE
 OM=ALLCHECK GUESS=TCHECK RB3LYP/6-31+G(D) FREQ\\ATB4\\0,1\N,-0.3012659
 055,0.5354395307,0.067691673\N,0.3012293962,-0.5353305934,-0.068222793
 1\C,-1.7713775175,0.4144692987,0.3260225343\C,1.7711863939,-0.41440433
 15,-0.3261674485\C,2.4439882504,-1.1991642484,0.8156915952\H,2.0441093
 295,-2.2172411287,0.8760885103\H,3.5254135853,-1.2590168318,0.64633308
 11\H,2.2753074103,-0.7062702104,1.7804769662\C,2.0027808878,-1.1346027
 041,-1.6677838724\H,1.5158902352,-0.5957646537,-2.4892377827\H,3.07577
 29777,-1.1925303756,-1.8847156708\H,1.5981633662,-2.1521604311,-1.6377
 551834\C,-2.4441719439,1.2011829336,-0.8142095295\H,-2.2747390711,0.71
 0521907,-1.7800036832\H,-3.5257269067,1.2600172726,-0.6452547306\H,-2.
 0449898235,2.2196750897,-0.87233288\C,-2.2914634577,-1.0258249687,0.37
 87386079\H,-1.8027314527,-1.5991560596,1.1730034609\H,-3.3710520037,-1
 .0168175549,0.5711462824\H,-2.1123252208,-1.5510456167,-0.5649482998\C
 ,-2.0021013995,1.1324162848,1.6689977129\H,-3.0750202686,1.190919745,1
 .8861691794\H,-1.5156606432,0.5915838754,2.4894019861\H,-1.5965146689,
 2.1496265707,1.6407003836\C,2.2910945832,1.025885569,-0.3809522403\H,2
 .1116495364,1.5523588233,0.5619530188\H,3.3706989723,1.0167796328,-0.5
 731895561\H,1.8023954321,1.598010385,-1.1761413997
```

Ionized azo-tert-butane


```
1\1\GINC-MS10\Freq\UB3LYP\6-31+G(d)\C8H18N2(1+,2)\RABAEV\11-Apr-2008\0
 \\#N GEOM=ALLCHECK GUESS=TCHECK UB3LYP/6-31+G(D) FREQ\\ATB10-ion\\1,2\
 N,0.3319946233,0.4838932427,-0.0031814284\N,-0.3319946233,-0.483893242
 7,-0.0031814284\C,-0.0747731727,1.972073368,-0.0011619947\C,0.07477317
 27,-1.972073368,-0.0011619947\C,-0.5199013673,-2.5309616838,1.29901271
 23\H,-1.6050368668,-2.3988340142,1.3365181744\H,-0.3062190566,-3.60430
 85736,1.3319002071\H,-0.068310046,-2.0686706233,2.1823019388\C,-0.6031
 355993,-2.5600219332,-1.2460082987\H,-1.6886595688,-2.4293146706,-1.21
 42373272\H,-0.2128359803,-2.1164363344,-2.1672618063\H,-0.3897055137,-
 3.6335595167,-1.2705143556\C,0.6031355993,2.5600219332,-1.2460082987\H
 ,1.6886595688,2.4293146706,-1.2142373272\H,0.2128359803,2.1164363344,-
 2.1672618063\H,0.3897055137,3.6335595167,-1.2705143556\C,-1.6022728478
 ,2.0635576277,-0.0501390164\H,-2.063647216,1.5918285269,0.8226873723\H
 ,-1.8748768383,3.1240439169,-0.0482890884\H,-2.0050695992,1.6104351962
 ,-0.961055531\C,0.5199013673,2.5309616838,1.2990127123\H,0.3062190566,
 3.6043085736,1.3319002071\H,0.068310046,2.0686706233,2.1823019388\H,1.
 6050368668,2.3988340142,1.3365181744\C,1.6022728478,-2.0635576277,-0.0
 501390164\H,2.063647216,-1.5918285269,0.8226873723\H,1.8748768383,-3.1
 240439169,-0.0482890884\H,2.0050695992,-1.6104351962,-0.961055531
```


Fragment ion m/z 57


```
1\1\GINC-MS12\Freq\RB3LYP\6-31+G(d)\C4H9(1+)\RABAEV\17-Dec-2007\0\\#N
 GEOM=ALLCHECK GUESS=TCHECK RB3LYP/6-31+G(D) FREQ\\F57-3\\1,1\C,0.00023
 14578,-0.0009942374,0.0002670085\C,0.703702493,0.9365186194,0.88151029
 23\H,0.7748356061,1.9072475346,0.3577355829\H,0.0713818974,1.162480806
 5,1.7563301635\H,1.6956510531,0.6084864383,1.1952014485\C,0.6703071579
 ,-1.22147812,-0.4587501728\H,1.1036846342,-1.756738862,0.40111678\H,0.
 0448415055,-1.8833501435,-1.0595741632\H,1.555938759,-0.9139990804,-1.
 0463911314\C,-1.3741371123,0.2838341024,-0.422736893\H,-1.7445365479,1
 .2674968904,-0.1298829455\H,-1.4859541968,0.1182426839,-1.5051419817\H
 ,-2.0164666889,-0.4971484549,0.0288648372
```


Fragment ion m/z 85


```
1\1\GINC-HPCVL5\Freq\RB3LYP\6-31+G(d)\C4H9N2(1+)\HPC1728\25-Apr-2008\0
 \\#B3LYP/6-31+G(D) OPT=CALCALL GEOM=CHECK\\F85-8-qn-con\\1,1\N,-2.2911
 680612,0.121359008,0.0322073066\N,-3.3944888567,0.1164015059,-0.025523
 5128\C,1.2188317676,-0.0469946444,-0.0004784606\C,1.1718484612,-1.1642
 589526,-0.9476603395\H,0.6328761001,-0.9108621894,-1.8678583484\H,2.22
 60591054,-1.3103698602,-1.2646741676\H,0.827730206,-2.1051860862,-0.51
 23150291\C,1.2719519875,1.3301860259,-0.4981055625\H,1.5117329705,1.41
 03526704,-1.5608157645\H,0.243717699,1.7241604433,-0.3581399899\H,1.90
 96025668,1.9735092302,0.1190777821\C,1.1847068395,-0.3148238332,1.4409
 818334\H,1.7696246991,-1.2087789304,1.6970471689\H,1.4564105433,0.5374
 226894,2.0656905597\H,0.1378102008,-0.5992231387,1.6667764073
```

Fragment ion m/z 56

1\1\GINC-MS6\Freq\UB3LYP\6-31+G(d)\C4H8(1+,2)\RABAEV\18-Apr-2008\0\\#N
GEOM=ALLCHECK GUESS=TCHECK UB3LYP/6-31+G(D) FREQ\\F56-3\\1,2\C,-0.743
0396996,-1.285786904,0.0013845155\H,-0.2170262255,-2.2360659007,-0.055
3868939\H,-1.828960639,-1.3045885185,0.0591875504\C,-0.0298365034,-0.0
514040996,0.0000454557\C,-0.7652038291,1.2201048757,0.1278161814\H,-1.
7407922698,1.1168560508,0.6110866771\H,-0.1638792802,2.0029143441,0.60
29510994\H,-0.9578744005,1.5830217832,-0.9039370553\C,1.4389526168,-0.
0539679784,-0.1290760646\H,1.8506148582,-0.0469132373,0.9022989266\H,1
.8351174714,-0.9487686511,-0.6175560844\H,1.8175649774,0.8598687667,-0
.599664748

Neutral fragment 57 amu

1\1\GINC-MS12\Freq\UB3LYP\6-31+G(d)\C4H9(2)\RABAEV\17-Apr-2008\0\\#N G
EOM=ALLCHECK GUESS=TCHECK UB3LYP/6-31+G(D) FREQ\\N57-3\\0,2\C,0.054103
3664,0.0764236176,-0.1327131486\C,0.695956825,0.98396801,0.8715431473\
H,0.336570318,2.0163642998,0.7767843587\H,0.4774692264,0.6710655138,1.
9118803236\H,1.7888472145,0.9922079448,0.7738993395\C,0.695286835,-1.2
47377004,-0.4154338935\H,0.4722938696,-1.9920798482,0.3742154907\H,0.3
393831153,-1.6802583414,-1.3588463259\H,1.7885139526,-1.1682774164,-0.
4665947395\C,-1.4075841791,0.2404097832,-0.4162101093\H,-1.6967326785,
1.2975713713,-0.4691384207\H,-1.6966871813,-0.2407063155,-1.3590380627
\H,-2.0362349205,-0.2164336492,0.3737220609

Neutral fragment 85 amu

1\1\GINC-HPCVL5\Freq\UB3LYP\6-31+G(d)\C4H9N2(2)\HPC2026\18-Jun-2008\0\
\#B3LYP/6-31+G(D) OPT=CALCALL SCF=QC\\N85-10\\0,2\N,-3.5966406922,0.17
00641594,0.4842413924\C,1.6585577136,-0.2274016014,-0.3923692672\C,1.4
038525561,-1.4366857468,-1.2395046418\H,1.7912166711,-1.30961125,-2.25
88265817\H,1.8593881096,-2.3387400768,-0.8107538894\H,0.3208608782,-1.
6491886133,-1.3400431603\C,1.4704457953,1.1285835486,-1.0010269134\H,1
.8552605718,1.1716864272,-2.0282748908\H,0.4005179729,1.4123367463,-1.
0552804484\H,1.969898312,1.9116461706,-0.4158704002\C,1.5828714997,-0.
3642419661,1.0975880842\H,2.0433875402,-1.2980937139,1.4455321397\H,2.
0764139969,0.4718635832,1.6098112526\H,0.5353084511,-0.3781664411,1.45
90130105\N,-3.4814475781,0.8877560923,1.3166970929

Neutral fragment 86 amu

1\1\GINC-MS6\Freq\RB3LYP\6-31+G(d)\C4H10N2\RABAEV\27-Mar-2008\0\\#N GE
OM=ALLCHECK GUESS=TCHECK RB3LYP/6-31+G(D) FREQ\\N86-3\\0,1\N,-1.990119
7757,-0.0226987693,0.\N,-0.9712827979,-0.7331600567,0.\C,0.3213662379,
0.0156148145,0.\C,1.0594592603,-0.4692749807,1.2626894894\H,1.13099424
53,-1.5621322462,1.2769997493\H,2.0731096981,-0.0529171895,1.286324430
1\H,0.5350528792,-0.1466634532,2.1696726244\C,1.0594592603,-0.46927498
07,-1.2626894894\H,0.5350528792,-0.1466634532,-2.1696726244\H,2.073109
6981,-0.0529171895,-1.2863244301\H,1.1309942453,-1.5621322462,-1.27699
97493\C,0.167708414,1.5399987161,0.\H,-0.3784771863,1.8871225811,0.882
8757535\H,1.1602157185,2.0053524508,0.\H,-0.3784771863,1.8871225811,-0
.8828757535\H,-2.7997160104,-0.6675414672,0.

N_2

```
1\1\GINC-MS10\Freq\RB3LYP\6-31+G(d)\N2\RABAEV\20-Aug-2008\0\\#N GEOM=A
 LLCHECK GUESS=TCHECK RB3LYP/6-31+G(D) FREQ\\N2-1\\0,1\N,0.5525629774,0
 .,0.\N,-0.5525629774,0.,0.
```

B. Acetone azine

Neutral acetone azine

```
1\1\GINC-MS7\Freq\RB3LYP\6-31+G(d)\C6H12N2\RABAEV\16-Mar-2007\0\\#N GE
 OM=ALLCHECK GUESS=TCHECK RB3LYP/6-31+G(D) FREQ\\((CH3)2CN)2\\0,1\N,-0.
 0065755287,0.346383439,-0.6971523818\N,0.0065755287,0.346383439,0.6971
 523818\C,1.1365754136,0.0490724783,1.2394242354\C,2.3782838226,-0.3701
 058021,0.4903422871\C,1.2159640658,0.1045780477,2.7416935998\C,-1.1365
 754136,0.0490724783,-1.2394242354\C,-2.3782838226,-0.3701058021,-0.490
 3422871\C,-1.2159640658,0.1045780477,-2.7416935998\H,-0.2494476147,0.3
 821828978,-3.1697226655\H,-1.5251710272,-0.8669135406,-3.1516362021\H,
 -1.9724059278,0.8359881106,-3.0589084814\H,-3.2798278757,-0.0570658104
 ,-1.0289621314\H,-2.3793912181,0.0447886062,0.5203050414\H,-2.41636877
 23,-1.4649326801,-0.399850591\H,1.5251710272,-0.8669135406,3.151636202
 1\H,1.9724059278,0.8359881106,3.0589084814\H,0.2494476147,0.3821828978
 ,3.1697226655\H,3.2798278757,-0.0570658104,1.0289621314\H,2.4163687723
 ,-1.4649326801,0.399850591\H,2.3793912181,0.0447886062,-0.5203050414
```

Ionized acetone azine

```
1\1\GINC-MS7\Freq\UB3LYP\6-31+G(d)\C6H12N2(1+,2)\RABAEV\13-Feb-2007\0\
 \#N GEOM=ALLCHECK GUESS=TCHECK UB3LYP/6-31+G(D) FREQ\\((CH3)2CN)2\\1,2
 \N,-0.1024067503,0.0108557027,-0.6442698791\N,0.102343933,-0.010686507
 9,0.6442498897\C,1.1176129512,0.3935584686,1.3218424922\C,2.3311493388
 ,1.006332151,0.6819446712\C,1.0633144899,0.2354491149,2.8110649382\C,-
 1.1176690964,-0.3934589988,-1.3218285229\C,-2.3309313422,-1.0067468625
 ,-0.6819542003\C,-1.0634829238,-0.2351478922,-2.8110478116\H,-0.129511
 9019,0.2220280024,-3.1417954518\H,-1.1767943846,-1.217010049,-3.287056
 9398\H,-1.9082114948,0.3806808535,-3.1437636724\H,-2.4826550747,-2.012
 8095587,-1.0922035875\H,-3.2154732014,-0.416432162,-0.951295448\H,-2.2
 421363761,-1.0619050211,0.4037641013\H,1.9085439387,-0.3795003953,3.14
 41028951\H,1.1756418785,1.2175415907,3.2868633331\H,0.1297132199,-0.22
 25238993,3.1417641877\H,2.4852857281,2.0110899938,1.0944041963\H,3.214
 9049793,0.4136542186,0.948768343\H,2.2411719045,1.0640861765,-0.403541
 4312
```

Fragment ion m/z 97


```
1\1\GINC-MS7\Freq\RB3LYP\6-31+G(d)\C5H9N2(1+)\RABAEV\09-May-2007\0\\#N
  GEOM=ALLCHECK GUESS=TCHECK RB3LYP/6-31+G(D) FREQ\\Fragment97-2\\1,1\N
 ,0.8123498097,-0.3307660021,-0.0064565539\N,-0.4297531782,-0.812871549
 1,-0.0239552999\C,-1.4178294753,0.0389391907,0.0035396679\C,-1.2909669
 252,1.5280786752,0.0375271765\C,-2.7790797372,-0.5732521843,-0.0131487
 406\C,1.962868206,-0.2167331066,-0.0043181848\C,3.4046967475,-0.045074
 9344,-0.0004783047\H,3.7020487826,0.6229411385,-0.8167869483\H,3.88616
 43994,-1.0205787528,-0.1362369714\H,3.7235726808,0.3856253498,0.955645
 6494\H,-3.2964674902,-0.3362052894,0.9262470551\H,-3.3780837644,-0.133
 5506173,-0.8202644345\H,-2.7310820268,-1.6564839275,-0.1349168357\H,-1
 .6237117036,1.9346627879,-0.9275039191\H,-1.9644833562,1.9412321376,0.
 7965797948\H,-0.274266836,1.8760741869,0.2313899007
```


Fragment ion m/z 97 - 1,2 H-shift


```
1\1\GINC-MS7\Freq\UB3LYP\6-31+G(d)\C5H9N2(1+,3)\RABAEV\18-Jun-2008\0\\
 #N GEOM=ALLCHECK GUESS=TCHECK UB3LYP/6-31+G(D) FREQ\\Fragment97-10\\1,
 3\N,0.9339590331,0.0712774341,-0.0723954065\N,-0.2012592273,-0.4976720
 853,-0.0271593904\C,-1.4017326643,-0.0096091691,0.1115615067\C,-1.6465
 710267,1.4598604345,0.2753780994\C,-2.5403185835,-0.9755395892,0.11633
 0238\C,2.1418187237,-0.4972911286,-0.2220283291\C,3.2757441395,0.27765
 52597,-0.2486936296\H,4.2459211463,-0.1907662815,-0.3700386254\H,3.227
 5098066,1.3576593649,-0.1505338426\H,-3.1548179068,-0.8164845589,1.011
 5137049\H,-3.1880000136,-0.7755943653,-0.7483000206\H,-2.2033141279,-2
 .0127276346,0.0809304399\H,-2.4719566625,1.7689656449,-0.3760052718\H,
 -1.9696314225,1.6491619038,1.3090201124\H,-0.7579338135,2.0565352077,0
 .0637480464\H,2.1696808208,-1.582441566,-0.3187382766
```


Fragment ion m/z 97 - 1,3 H-shift


```
1\1\GINC-MS7\Freq\RB3LYP\6-31+G(d)\C5H9N2(1+)\RABAEV\18-Aug-2008\0\\#N
  GEOM=ALLCHECK GUESS=TCHECK RB3LYP/6-31+G(D) FREQ\\Fragment97-12-co\\1
 ,1\C,-2.8729665275,0.2181765583,0.6844782734\H,-3.224089229,1.22386287
 77,0.4569636971\H,-3.3909547526,-0.3548990341,1.454058579\N,-0.8828368
 921,-0.8263649226,-0.5266750324\C,-1.8722672214,-0.3019570759,0.047318
 8334\N,0.4408615815,-0.9478393557,0.0282112165\H,-1.0223122622,-1.4228
 150784,-1.3490101296\C,1.2067874338,0.0893017492,-0.0549035195\C,2.573
 2637511,-0.095475285,0.5381526355\H,2.6729974045,-1.0723063567,1.01432
 59272\H,3.3298946814,0.0038966981,-0.2500491384\H,2.7690372719,0.69450
 57368,1.2734800382\C,0.8811377981,1.4232438083,-0.6636727074\H,-0.0039
 924587,1.4146311208,-1.3032619397\H,0.7311651671,2.1607379239,0.136001
 8743\H,1.736349947,1.7720775307,-1.2515032893
```

Fragment ion m/z 97 - 1,4 H-shift

```
1\1\GINC-MS7\Freq\RB3LYP\6-31+G(d)\C5H9N2(1+)\RABAEV\05-Aug-2008\0\\#N
  GEOM=ALLCHECK GUESS=TCHECK RB3LYP/6-31+G(D) FREQ\\Fragment97-11\\1,1\
 C,1.3520861004,0.0537711704,0.1149322223\C,1.7672252367,0.1738118436,-
 1.3103081852\H,1.3085490746,1.058840997,-1.7679245792\H,2.8530819382,0
 .2395409445,-1.3902195978\H,1.4074864598,-0.689244966,-1.8842479297\C,
 2.3576505922,0.0208790952,1.2112460618\H,2.9642379474,0.9351086635,1.1
 681863828\H,1.918435175,-0.0727290759,2.2080147771\H,3.0467953186,-0.8
 165679068,1.0399891735\N,0.0882530259,-0.0257343527,0.4254232005\N,-0.
 9051889103,-0.0000216081,-0.5639367179\H,-0.205741612,-0.1089661159,1.
 4031564405\C,-2.0837694748,-0.0832685145,-0.1633807071\C,-3.3562382833
 ,-0.1612746176,0.1056062104\H,-3.9408549581,0.737609514,0.2895304397\H
 ,-3.8551631796,-1.1268141918,0.1545359013
```

Fragment ion m/z 97 - 1,5 H-shift

```
1\1\GINC-MS10\Freq\RB3LYP\6-31+G(d)\C5H9N2(1+)\RABAEV\15-Aug-2008\0\\#
 N GEOM=ALLCHECK GUESS=TCHECK RB3LYP/6-31+G(D) FREQ\\F97-13\\1,1\C,0.12
 81944351,-2.7328632969,-0.2610684035\H,0.6752362834,-3.455773955,-0.85
 80012265\H,-0.6674962274,-3.0950911775,0.3825552423\C,0.4287002061,-1.
 4152694746,-0.3158539688\C,1.4905529856,-0.7534404969,-1.1426129914\H,
 1.0565801546,-0.0222506147,-1.835980152\H,2.2177243439,-0.230246868,-0
 .5093395967\H,2.0297991936,-1.4982008262,-1.7316934591\N,-0.3950657661
 ,-0.6463762301,0.5318965609\N,-0.2638604848,0.5542413708,0.6126508071\
 C,-0.3305007063,1.7898593687,0.849323616\C,-1.1870767375,2.743464477,0
 .0699260861\H,-1.8558685973,3.2578218752,0.7714637607\H,-0.5507677483,
 3.5064477194,-0.3942716852\H,-1.7773998134,2.2361830863,-0.6952395272\
 H,0.3054550701,2.1555513123,1.6603890373
```

Fragment ion m/z 97 - two 1,3-H shift

```
1\1\GINC-MS7\Freq\RB3LYP\6-31+G(d)\C5H9N2(1+)\RABAEV\19-Aug-2008\0\\#N
  GEOM=ALLCHECK GUESS=TCHECK RB3LYP/6-31+G(D) FREQ\\Fragment97-14\\1,1\
 C,1.4808479552,-1.4503377898,0.3151212945\H,2.4435520832,-1.9424125282
 ,0.3864841707\H,0.6464463103,-1.951550736,0.7983910532\C,1.3588768746,
 -0.3220771217,-0.3989105276\C,2.442955594,0.3357736403,-1.205811384\H,
 2.6786719784,1.3391865086,-0.8277507437\H,3.3536665631,-0.2651864807,-
 1.1719791978\H,2.1439681783,0.4308349726,-2.2574905026\N,0.1069319004,
 0.3612976027,-0.4893976715\N,-0.6953678824,0.2507513507,0.6556384727\C
 ,-1.9557136704,0.3250366484,0.6397182409\C,-3.2460550022,0.4157875598,
 0.6340769561\H,-3.7415135772,1.3808475705,0.7435962294\H,-3.8630787686
 ,-0.4763345085,0.5201745458\H,0.154148876,1.3327215098,-0.7892992685\H
 ,-0.1822802776,0.0424533971,1.5290206261
```

Neutral fragment 15 amu

```
1\1\GINC-MS7\Freq\UB3LYP\6-31+G(d)\C1H3(2)\RABAEV\14-May-2007\0\\#N GE
 OM=ALLCHECK GUESS=TCHECK UB3LYP/6-31+G(D) FREQ\\Neutral-15-1\\0,2\C,0.
 0000029985,0.,0.\H,-0.0000191812,-1.0840505809,0.0000000056\H,0.000000
 5951,0.5420252954,0.9388153394\H,0.0000005951,0.5420252857,-0.93881534
 5
```